Die approbierte Originalversion dieser Dissertation ist an der Hauptbibliothek der Technischen Universität Wien aufgestellt (http://www.ub.tuwien.ac.at).

The approved original version of this thesis is available at the main library of the Vienna University of Technology (http://www.ub.tuwien.ac.at/englweb/).

DISSERTATION

Coarse-graining in Micromagnetics

ausgeführt zum Zwecke der Erlangung des akademischen Grades
eines Doktors der technischen Wissenschaften unter der Leitung von

Univ.Prof. Dipl.-Ing. Dr.techn. Thomas Schrefl
E138
Institut für Festkörperphysik

eingereicht an der Technischen Universität Wien
Fakultät für Physik

von

Dipl.-Ing. Markus Kirschner
Matr.Nr. 9525261
Angergasse 61, 7123 Mönchhof

Wien, am 18. Dezember 2005

Abstract

Micromagnetism is a continuum theory to describe magnetization processes on a characteristic length scale of several atomic distances. For realistic geometries the micromagnetic equations have to be solved numerically. Therefore, the magnetic material is subdivided into smaller computational cells. To resolve domain walls or high frequency spin waves the computational cell size has to be in the order of a few nanometers. Then, the temperature dependent intrinsic magnetic properties which have to be assigned to the magnetic moment of each cell also depend on the number of atoms within a cell. As a consequence, the intrinsic material parameters have to be scaled accordingly to find cell size independent results of micromagnetic simulations at nonzero-temperatures.

In this thesis, a coarse-graining procedure for the material parameters is suggested. Scaling laws for the spontaneous magnetization, the anisotropy constant, and the exchange constant are calculated by Metropolis Monte Carlo simulations of atomistic exchange coupled Heisenberg spins in the classical approximation. Bloch-like scaling laws for the spontaneous magnetization are found for simple cubic, body-centered cubic, and face-centered cubic lattices.

The cell size dependent intrinsic magnetic parameters are used for non-atomistic Monte Carlo and Langevin simulations. The method is successfully applied for both simulations of equilibrium properties and simulations of thermally driven magnetization reversal processes. It is shown that a proper scaling of the material parameters leads to numerical results which are almost independent of the computational cell size.

Kurzfassung

Als Kontinuumstheorie beschreibt der Mikromagnetismus magnetische Prozesse auf einer Längenskala von einigen Atomdurchmessern. Die mikromagnetischen Gleichungen müssen für realistische Geometrien numerisch gelöst werden. Dazu ist eine Diskretisierung des magnetischen Materials in kleine Volumina notwendig. Um Domänenwände oder hochfrequente Spinwellen auflösen zu können, müssen Diskretisierungslängen im Nanometerbereich verwendet werden. Die intrinsischen magnetischen Materialparameter, die jedem Diskretisierungsvolumen zugeordnet werden, hängen dann nicht nur von der Temperatur, sondern auch von der Zahl der Atome innerhalb dieser Volumina ab. Damit ist eine entsprechende Skalierung der Materialparameter unumgänglich, um diskretisierungsunabhängige Resultate mit mikromagnetischen Simulationen bei endlichen Temperaturen zu erzielen.

In dieser Arbeit wird eine Methode präsentiert, die die Abhängigkeit der magnetischen Parameter von der Diskretisierungslänge beschreibt. Mit Hilfe von Metropolis-Monte-Carlo-Simulationen von austauschgekoppelten klassischen Heisenbergspins auf atomarer Ebene werden Skalierungsgesetze für die spontane Magnetisierung, die magnetokristalline Anisotropiekonstante und die Austauschkonstante abgeleitet. Die Simulationsergebnisse zeigen, dass sich die spontane Magnetisierung als Funktion der Diskretisierungslänge für einfach kubische, raumzentriert kubische und flächenzentriert kubische Gitter mit einem dem Blochschen Gesetz für die Temperaturabhängigkeit ähnlichen Skalierungsgesetz beschreiben lässt.

Die skalierten intrinsischen Materialparameter werden für nichtatomare Monte-Carlo- und Langevin-Simulationen verwendet. Die vorgestellte Methode erweist sich sowohl bei Berechnungen von Gleichgewichtsgrößen als auch bei Simulationen von Ummagnetisierungsprozessen aufgrund thermischer Fluktuationen als erfolgreich. Die Ergebnisse zeigen, dass die skalierten Materialparameter zu numerischen Resultaten führen, deren Abhängigkeit von der Größe der Diskretisierungsvolumina vernachlässigbar ist.

Wenn jemand sucht, dann geschieht es leicht, daß sein Auge nur noch das Ding sieht, das er sucht, daß er nichts zu finden, nichts in sich einzulassen vermag, weil er nur an das Gesuchte denkt, weil er ein Ziel hat, weil er vom Ziel besessen ist. Finden aber heißt: frei sein, offen stehen, kein Ziel haben.

Hermann Hesse

Danksagung

Allen voran möchte ich meinen Eltern für die vorgelebten Werte und ihre bedingungslose Liebe danken. Menschen zu wissen, bei denen man unter allen Umständen willkommen ist, betrachte ich keineswegs als selbstverständlich. Meiner Freundin Regina danke ich für die vielen gemeinsamen Momente, die mein Leben ungemein bereichern.

Den Professoren Thomas Schrefl und Josef Fidler und allen anderen Mitgliedern der Arbeitsgruppe für Mikromagnetismus möchte ich für die zahlreichen interessanten Diskussionen, das angenehme Arbeitsklima und den freundschaftlichen Umgang miteinander danken. Mein Betreuer Thomas Schrefl hat mir viele Möglichkeiten geboten, an internationalen Konferenzen teilzunehmen und mit Menschen aus den verschiedensten Ländern in Kontakt zu treten. Florian Dorfbauer, Werner Scholz, Gino Hrkac und Dieter Süss haben mir sehr bei der Korrektur meiner Dissertation geholfen. Werner war mir und der Arbeitsgruppe auch stets eine große Hilfe, wenn es wieder einmal galt, technische Probleme zu lösen.

Schlussendlich möchte ich dem FWF für seine finanzielle Unterstützung danken (Projektnr.: Y132-N02).

Contents

Abstract 2

Kurzfassung 3

Danksagung 5

1 Introduction 13

2 Magnetostatics 19

3 Atomistic System 21

3.1 Magnetic Moments and Magnetization 21
3.2 Classical Hamiltonian 23
3.2.1 Exchange Energy 24
3.2.2 Magnetocrystalline Anisotropy Energy 25
3.2.3 Strayfield Energy 27
3.2.4 Zeeman Energy 28

4 Micromagnetics 29

4.1 Gibbs Free Energy 30
4.1.1 Exchange Energy 31
4.1.2 Magnetocrystalline Anisotropy Energy 34
4.1.3 Strayfield Energy 35
4.1.4 Zeeman Energy 36
4.2 Energy Minimization and Effective Field 37

5 Metropolis Monte Carlo **43**
5.1 Method of Importance Sampling 44
5.2 Simulating Magnetic Systems 45
5.2.1 Restrictions to the Transition Probability 47
5.2.2 Heat Bath Algorithm 48

6 The Dynamic Equation **52**
6.1 Dynamics at Zero Temperature 52
6.2 Stochastic Dynamics 54
6.3 The Fokker-Planck Equation 57
6.3.1 Classification of Random Processes 58
6.3.2 Interpretation of Stochastic Integrals 60
6.3.3 Kramers-Moyal Expansion 62
6.3.4 Markov Processes and Fokker-Planck Equation 64
6.4 Thermal Field Strength 65
6.5 Heun Method 67

7 Influence of Discretization **70**
7.1 Geometry and Material Parameters 71
7.2 Results and Discussion 72

8 Coarse-graining **75**
8.1 Atomistic Monte Carlo Simulations 76
8.1.1 Equilibrium Magnetization 78
8.1.2 Anisotropy Constant 81
8.2 Non-atomistic Simulations 82
8.2.1 Exchange Constant 84
8.3 Summary 86

9 Relaxation Times **87**
9.1 Geometry and Material Parameters 87
9.2 Results and Discussion 88

10 Cubic Crystal Lattices **91**
10.1 General Aspects 92
10.2 Geometry and Material Parameters 93
10.3 Results and Discussion 95
10.4 Summary 97

A Dirac Delta Function **99**

B Kramers-Moyal Coefficients **100**

C Algorithm Tests **103**
C.1 Paramagnetism 103
C.2 Stoner-Wohlfarth Particle 104
C.3 Exchange Coupled Moments 105

D Monte Carlo Program **107**

List of Figures **110**

List of Tables **112**

Bibliography **113**

Presentations and Publications **120**

Curriculum Vitæ **125**

Lebenslauf **126**

Conventions and Nomenclature

Although Gaussian (or cgs) units are widespread in the scientific community of magnetism, we exclusively use SI units (Système International d'Unités) in the entire thesis with the definition of the magnetic induction (in T)

$$\boldsymbol{B} = \mu_0(\boldsymbol{H} + \boldsymbol{M}) = \mu_0 \boldsymbol{H} + \boldsymbol{J} \quad . \tag{1}$$

$\boldsymbol{H}$ denotes the magnetic field (in A/m), $\boldsymbol{J}$ the magnetic polarization (in T), $\boldsymbol{M}$ the magnetization (in A/m), and μ_0 the permeability of free space. In this work, both, the polarization $\boldsymbol{J} = \mu_0 \boldsymbol{M}$ and the magnetization $\boldsymbol{M}$ are used.

Variables in calligraphic style indicate quantum mechanical operators (e.g. the Hamiltonian $\mathcal{H}$), whereas bold letters represent vectors. Greek indices (always superscripts) will be consistently used to label atomistic lattice sites or nodes in the continuum model, respectively. Einstein's summation convention is used only for Latin indices (always subscripts), which indicate the Cartesian components.

In the following, important variables and symbols together with their units are given. Useful constants are listed at the end of this chapter (taken from Ref. [37]).

Important Variables and Symbols

a	[m]	Edge length of cubic atomistic unit cells
$\boldsymbol{a}$	[1]	Unit vector parallel to the easy axis
A	[J/m]	Exchange constant
A_0	[J/m]	Exchange constant at an atomistic level
A_{cell}	[J/m]	Cell size dependent exchange constant
$\boldsymbol{B}$	[T]	Magnetic induction or flux density
c	[1]	Number of atoms in the cubic atomistic unit cell
D	[$\mathrm{A^2\,s/m^2}$]	Strength of thermal field
E	[J]	Total energy
E_{exch}	[J]	Exchange energy
E_{ani}	[J]	Anisotropy energy
E_{stray}	[J]	Strayfield energy
E_{ext}	[J]	Zeeman energy
g_{L}	[1]	Landé factor or spectroscopic splitting factor
$\boldsymbol{H}$	[A/m]	Magnetic field
$\boldsymbol{H}_{\mathrm{ani}}$	[A/m]	Anisotropy field
$\boldsymbol{H}_{\mathrm{eff}}$	[A/m]	Effective field
$\boldsymbol{H}_{\mathrm{exch}}$	[A/m]	Exchange field
$\boldsymbol{H}_{\mathrm{ext}}$	[A/m]	External field
$\boldsymbol{H}_{\mathrm{stray}}$	[A/m]	Strayfield or Dipole field
$\boldsymbol{H}_{\mathrm{th}}$	[A/m]	Thermal field
J	[J]	Exchange integral
J_{S}	[T]	Spontaneous polarization
$J_{\mathrm{S,0}}$	[T]	Spontaneous polarization at zero temperature
$J_{\mathrm{S,cell}}$	[T]	Cell size dependent spontaneous polarization
$J_{\mathrm{S},\infty}$	[T]	Spontaneous polarization for large cells
$\boldsymbol{J}$	[T]	Magnetic polarization

K_1	[J/m^3]	Uniaxial anisotropy constant
$K_{1,0}$	[J/m^3]	Uniaxial anisotropy constant at an atomistic level
$K_{1,\mathrm{cell}}$	[J/m^3]	Cell size dependent uniaxial anisotropy constant
$K_{1,\infty}$	[J/m^3]	Uniaxial anisotropy constant for large cells
l_exch	[m]	Exchange length
l_thex	[m]	Thermal exchange length
$\boldsymbol{m}$	[Am^2]	Magnetic moment
M_S	[A/m]	Spontaneous magnetization
$M_{\mathrm{S},0}$	[A/m]	Spontaneous magnetization at zero temperature
$M_{\mathrm{S,cell}}$	[A/m]	Cell size dependent spontaneous magnetization
$M_{\mathrm{S},\infty}$	[A/m]	Spontaneous magnetization for large cells
$\boldsymbol{M}$	[A/m]	Magnetization
n, N	[1]	Number of atoms or magnetic moments
q	[1]	Exponent in the scaling law for $M_{\mathrm{S,cell}}$
$\boldsymbol{r}$	[m]	Position vector
S	[1]	Modulus of $\boldsymbol{S}$
$\boldsymbol{S}$	[1]	Classical total angular momentum
t	[s]	Time
T	[K]	Temperature
T_C	[K]	Curie temperature
T_C^mf	[K]	Mean field critical temperature
$\boldsymbol{u}$	[1]	Unit vector of the magnetization or the total angular momentum, respectively
v	[m^3]	Volume
v_at	[m^3]	Volume per atomistic spin (volume of primitive unit cell)
V	[m^3]	Total volume of a magnetic body
$\hat{\boldsymbol{x}}$	[1]	Unit vector in $+x$-direction
$\hat{\boldsymbol{y}}$	[1]	Unit vector in $+y$-direction

z	[1]	Number of nearest neighbors
$\hat{\boldsymbol{z}}$	[1]	Unit vector in $+z$-direction
α	[1]	Damping constant in Langevin dynamics
β	[1/J]	$\beta = (k_\mathrm{B}T)^{-1}$
γ	[m/As]	Gyromagnetic ratio
γ'	[m/As]	$\gamma' = \gamma/(1+\alpha^2)$
ε	[J/m^3]	Energy density
ε_ani	[J/m^3]	Energy density of magnetocrystalline anisotropy
$\varepsilon_\mathrm{exch}$	[J/m^3]	Energy density of exchange interaction
ε_ext	[J/m^3]	Energy density of Zeeman interaction
$\varepsilon_\mathrm{stray}$	[J/m^3]	Energy density of strayfield interaction
Δt	[s]	Time step
Δx	[m]	Spatial discretization in x-direction
Δx_at	[m]	Edge length of a cube with $v = v_\mathrm{at}$
Δy	[m]	Spatial discretization in y-direction
Δz	[m]	Spatial discretization in z-direction

Constants

e	$=$	$-1.6022 \cdot 10^{-19}$	C	Electron charge
$\hbar$	$=$	$1.0545 \cdot 10^{-34}$	Js	Planck constant
k_B	$=$	$1.3806 \cdot 10^{-23}$	J/K	Boltzmann constant
m_e	$=$	$9.1094 \cdot 10^{-31}$	kg	Electron mass
μ_0	$=$	$4\pi \cdot 10^{-7}$	Vs/Am	Permeability of free space
μ_B	$=$	$9.2740 \cdot 10^{-24}$	J/T	Bohr magneton (Ampère's definition)

Chapter 1

Introduction

The development and application of modern magnetic materials with specific magnetic properties require a basic understanding of the underlying physics. The theory of micromagnetics relates the microscopic magnetization distribution to the physical and chemical microstructure of a magnetic material and has turned out to be a proper and efficient way of describing and predicting the static and dynamic properties. Recently, micromagnetic modeling has become an important tool to characterize the magnetic behavior of such different magnetic systems as thin film heads, recording media, patterned magnetic elements, and nanocrystalline permanent magnets. Micromagnetism highly promotes the design of new materials, where a detailed knowledge of the magnetic response to external fields and temperature as function of time is essential.

A typical field where micromagnetic simulations help research and development greatly is magnetic recording. Nowadays, information in commercial hard disks is stored by aligning the magnetization of grains parallel to the surface (longitudinal recording). The areal density (in bits/in^2) defines the amount of information, which can be stored on a given area of a hard disk and is almost doubled every year. However, the superparamagnetic limit determines an upper bound for the areal density. In the year 1997, Charap *et al.* quoted a limit of about 40 GBits/in^2 [13]. New methods like antiferromagnetically-coupled (AFC) media have been developed and allow higher areal densities in longitudinal recording [23]. In perpendicular recording, where the magnetization of each bit is perpendicular to the surface, much higher areal densities can be achieved. This technology lead to the world record in areal density of 230 GBits/in^2 [32] in spring 2005.

Numerical micromagnetics is a suitable method to treat magnetization dynamics on the nanometer scale. A description of the magnetization in the framework of a continuum approach goes back to Landau and Lifshitz [39]. The continuum theory of micromagnetics assumes the magnetization to be a continuous function of space, $\boldsymbol{M}(\boldsymbol{r})$, and allows for the calculation of the magnetization configuration on a mesoscopic length scale. Brown used the continuum expression for the Gibbs free energy of a ferromagnetic body to calculate the critical external field at which the magnetization of a uniform body becomes unstable [11]. The variation of the total Gibbs free energy shows that the equilibrium magnetization is parallel to a total effective field. The Landau-Lifshitz-Gilbert (LLG) equation describes the time evolution of the magnetization in the effective field and is the basis for many micromagnetic simulations.

Most such simulations have been performed at zero temperature. However, the decreasing dimensions of magnetic devices make the use of nonzero-temperature micromagnetics essential. Heinonen and Cho [30] investigated thermal magnetic noise in TMR (tunneling magnetoresistance) sensors and claim that thermal magnetic noise becomes essential as device sizes shrink. Since the noise contains important information about the performance and stability of the sensors, a stochastic description is highly required. Weller and Moser [61] showed that magnetization reversal due to thermal fluctuations has become important in magnetic recording and calls for temperature dependent simulations.

Brown [12] added a stochastic, thermal field to the effective field in the LLG equation allowing for stochastic simulations. The thermal field describes the interaction of the magnetization with the microscopic degrees of freedom and ensures that the system finally achieves the stationary Boltzmann distribution. The strength of the thermal field, derived via the Fokker-Planck equation, is strictly speaking only valid for noninteracting magnetic moments. However, for small fluctuations around equilibrium, Chubykalo *et al.* [15] and also Lyberatos *et al.* [40] showed that it is still valid for interacting moments.

To solve a micromagnetic problem numerically, it is necessary to use a discretization of space. The finite difference method is a possibility to simulate magnetization processes in regularly shaped elements [50]. For arbitrarily shaped magnetic bodies the finite element method is more suitable [22]. Normally, the intrinsic magnetic parameters of materials in micromagnetics, such as the spontaneous magnetization and the magneto-crystalline anisotropy constant, are supposed to be independent of the computational cell size. This common assumption is valid only if the computational cell contains enough atomistic spins to justify the use of statistics and the laws of thermodynamics [8]. Then, one can use the experimentally measured, only temperature dependent values for the material parameters. However, in order to resolve domain walls or high frequency spin waves the computational cell size has to be small. Then the intrinsic magnetic properties which have to be assigned to the magnetic moment of each cell depend both on temperature and on the number of atoms within the cell. As a consequence, the intrinsic magnetic properties have to be scaled accordingly if the number of atoms within a computational cell becomes too small (less than about 20 000 atoms per cell or 10 nm cell size). For instance, Fig. 1.1 depicts the situation for the spontaneous magnetization, which decreases with increasing discretization length and finally approaches the experimental value $M_{\mathrm{S},\infty}$. Between the atomistic level and the thermodynamic region the use of cell size-independent parameters leads to wrong numerical results even at temperatures far below the Curie temperature T_{C}. Several groups, for instance Tsiantos *et al.* [57] or Feng and Visscher [21] reported on cell size dependencies in nonzero-temperature micromagnetics when cell size independent parameters are used. The knowledge of temperature- and cell size-dependent corrections of the system parameters has become crucial, since Igarashi *et al.* pointed out that small computational cells

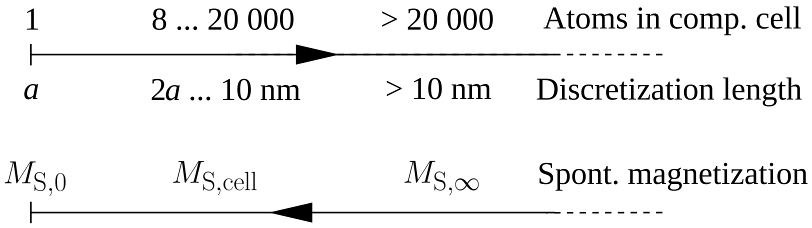

Figure 1.1: Number of atoms in the computational cell and the required spontaneous magnetization M_S for micromagnetic simulations as function of the discretization length. a denotes the atomistic lattice constant and $M_{S,0}$ the spontaneous magnetization at zero temperature, $M_S(T=0)$. A cell size-independent spontaneous magnetization $M_{S,\infty}$ is valid only for large computational cells. Between the atomistic level with $M_{S,0}$ and the thermodynamic region with $M_{S,\infty}$, the spontaneous magnetization $M_{S,\text{cell}}$ depends on the cell size.

are necessary to find correct results due to the importance of high-frequency spin waves [35].

Dobrovitski *et al.* faced the problem of cell size dependencies by applying the ideas of coarse graining [18, 19]. Starting at an atomistic level, they introduced large-scale variables as averages of the atomistic parameters by using appropriate weighting functions. However, the proper choice of the weighting functions is mathematically expensive even for simple one-dimensional systems. It is not clear, how their method can be applied to more complex systems.

Grinstein and Koch suggested a mathematical coarse-graining method to describe systems near the Curie point [27]. They pointed out that the effective exchange constant of the system undergoes a temperature-dependent renormalization. The basic assumption in continuum micromagnetics that the angle between neighboring moments have to be small is, however, violated near T_C.

In this work, we propose an approximate coarse-graining procedure. We suggest to use the experimentally measured, only temperature dependent material parameters for large computational cells and apply corrections to these

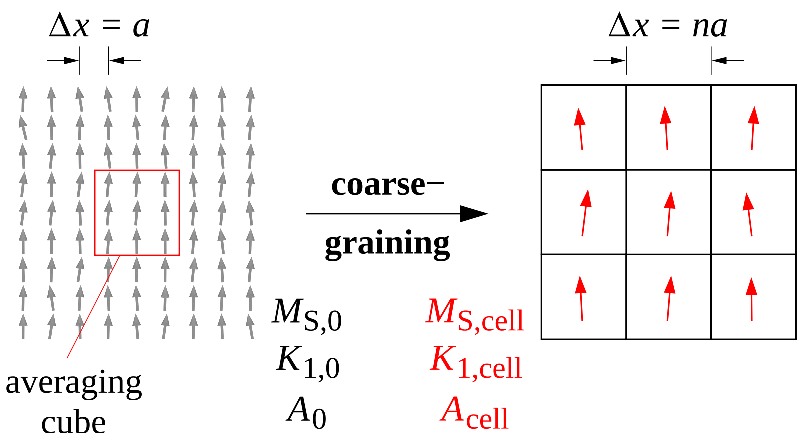

Figure 1.2: Illustration of the coarse-graining procedure. Δx denotes the discretization length, a the atomistic lattice constant. Starting with MC simulations at an atomistic level (left hand side) with the so-defined parameters $M_{\mathrm{S},0}$, $K_{1,0}$, and A_0, the cell size dependent values $M_{\mathrm{S,cell}}$, $K_{1,\mathrm{cell}}$, and A_{cell} can be extracted. The cell size dependent material parameters are then used for non-atomistic simulations (right hand side).

parameters at least if the computational cell size approaches the exchange length [57]. We perform atomistic and non-atomistic Monte Carlo (MC) simulations of exchange-coupled anisotropic Heisenberg spins at finite temperatures and extract a cell size dependent spontaneous magnetization $M_{\mathrm{S,cell}}$, anisotropy constant $K_{1,\mathrm{cell}}$, and exchange constant A_{cell} after equilibration, see Fig. 1.2. The so-obtained material parameters can then be used for any kind of non-atomistic stochastic LLG and MC simulations. We will show that our method can be applied successfully for both, simulations of equilibrium properties and simulations of thermally driven magnetization reversal processes.

The combination of MC calculations at an atomistic level and non-atomistic stochastic LLG simulations proposed in this thesis is an easy way to treat coarse-graining in micromagnetics. The method is applicable for a variety of micromagnetic problems, such as the calculation of thermal magnetic noise in spin valve heads [56, 63] or transition rates of thermally induced decay in perpendicular recording [59]. Due to the shrinking head dimensions, thermal fluctuations strongly influence the performance of write heads and have to be considered in micromagnetic modeling [4, 53]. Magnetization switching due to spin-polarized current injection is one of the most intensively studied magnetic phenomena at present and promises interesting applications, such as fast switching of nanoelements [6, 45]. A fundamental understanding of the complicated switching processes in small elements requires simulations at finite temperatures.

After a short introduction to Maxwell's equations of magnetostatics in chapter 2, the atomistic energy contributions are discussed in chapter 3. The continuum theory of micromagnetics and the discretization of the different energy terms in the context of the finite difference method are outlined in chapter 4. The Metropolis Monte Carlo method for magnetic systems is explained in chapter 5. Micromagnetic simulations at zero and finite temperatures based on the Landau-Lifshitz-Gilbert equation are described in chapter 6. Chapter 7 verifies the influence of the discretization length on the simulation results. In chapter 8, our coarse-graining procedure is introduced and applied to calculate equilibrium properties of magnetic systems. Chapter 9 points out that the cell size dependent parameters can also be used for highly dynamic processes. Finally, chapter 10 shows how the coarse-graining procedure can be applied for different crystal lattices, such as body-centered and face-centered cubic lattices. This thesis is completed by an appendix including algorithm tests of the MC and LLG programs and a description of the MC parameter file.

Chapter 2

Magnetostatics

The theory of magnetostatics is a restriction of the general form of Maxwell's equations and is valid for static magnetic fields, i.e. the currents as physical sources of the fields are static. However, it is still a good approximation for non-static currents as long as current variations are slow enough, that one can still assume stationary conditions at each time step [8].

Maxwell's equations of magnetostatics in SI units reads

$$\nabla \cdot \boldsymbol{B} = 0 \tag{2.1}$$

$$\nabla \times \boldsymbol{B} = \mu_0 \boldsymbol{j} \quad , \tag{2.2}$$

where $\boldsymbol{B}$ is the magnetic induction (or flux density) in T, $\boldsymbol{j}$ the current density (in $\mathrm{A/m^2}$), and $\mu_0 = 4\pi \cdot 10^{-7}$ Vs/Am is the permeability of free space.

In the presence of matter we have to distinguish between the magnetic induction $\boldsymbol{B}_{\mathrm{free}}$ due to free current densities $\boldsymbol{j}_{\mathrm{free}}$ and $\langle \boldsymbol{B}_{\mathrm{mat}} \rangle$ due to bound current densities $\langle \boldsymbol{j}_{\mathrm{mat}} \rangle$. Since quantities in $\langle \cdot \rangle$ represent spatial averages over many atomic unit cells, Maxwell's equations in matter do not account for fluctuations on an atomic length scale. Those quantities satisfy the relations

$$\nabla \cdot \boldsymbol{B}_{\mathrm{free}} = 0 \tag{2.3}$$

$$\nabla \times \boldsymbol{B}_{\mathrm{free}} = \mu_0 \boldsymbol{j}_{\mathrm{free}} \tag{2.4}$$

and

$$\begin{aligned} \boldsymbol{\nabla} \cdot \langle \boldsymbol{B}_{\mathrm{mat}} \rangle &= 0 && (2.5) \\ \boldsymbol{\nabla} \times \langle \boldsymbol{B}_{\mathrm{mat}} \rangle &= \mu_0 \langle \boldsymbol{j}_{\mathrm{mat}} \rangle \quad . && (2.6) \end{aligned}$$

The total field $\boldsymbol{B} = \boldsymbol{B}_{\mathrm{free}} + \langle \boldsymbol{B}_{\mathrm{mat}} \rangle$ fulfills the equations

$$\begin{aligned} \boldsymbol{\nabla} \cdot \boldsymbol{B} &= 0 && (2.7) \\ \boldsymbol{\nabla} \times \boldsymbol{B} &= \mu_0 \boldsymbol{j}_{\mathrm{free}} + \mu_0 \langle \boldsymbol{j}_{\mathrm{mat}} \rangle \quad . && (2.8) \end{aligned}$$

$\langle \boldsymbol{j}_{\mathrm{mat}} \rangle$ generates the magnetization $\boldsymbol{M}$ (in A/m) within the body,

$$\boldsymbol{\nabla} \times \boldsymbol{M} = \langle \boldsymbol{j}_{\mathrm{mat}} \rangle \quad . \tag{2.9}$$

Per definition, $\boldsymbol{M}$ vanishes outside the material.

If we define the so-called magnetic field $\boldsymbol{H}$ (in A/m) via the relation

$$\boldsymbol{B} = \mu_0 (\boldsymbol{H} + \boldsymbol{M}) = \mu_0 \boldsymbol{H} + \boldsymbol{J} \quad , \tag{2.10}$$

where $\boldsymbol{J}$ denotes the magnetic polarization (in T), we obtain Maxwell's macroscopic or phenomenological equations of magnetostatics,

$$\begin{aligned} \boldsymbol{\nabla} \cdot \boldsymbol{B} &= 0 && (2.11) \\ \boldsymbol{\nabla} \times \boldsymbol{H} &= \mu_0 \boldsymbol{j}_{\mathrm{free}} \quad , && (2.12) \end{aligned}$$

where bound current densities do not appear anymore.

For the important case of vanishing free current densities, the remaining Maxwell's equations read

$$\begin{aligned} \boldsymbol{\nabla} \cdot \boldsymbol{B} &= 0 && (2.13) \\ \boldsymbol{\nabla} \times \boldsymbol{H} &= 0 \quad . && (2.14) \end{aligned}$$

Chapter 3

Atomistic System

3.1 Magnetic Moments and Magnetization

We start with an ensemble of atoms or ions (like a solid), each of them having the total angular momentum $\hbar\boldsymbol{\mathcal{S}}$, which is the sum of the total orbital momentum and the spin momentum of electrons. In the scope of this work we always assume that it is valid to replace the quantum mechanical operators $\boldsymbol{\mathcal{S}}$ by classical vectors $\boldsymbol{S}$ with $|\boldsymbol{S}| = S$ (S is dimensionless).

The magnetic moment $\boldsymbol{m}$ (in Am^2) associated with $\boldsymbol{S}$ reads

$$\boldsymbol{m} = -\gamma\hbar\boldsymbol{S} = -g_{\mathrm{L}}\mu_{\mathrm{B}}\boldsymbol{S} = g_{\mathrm{L}}\mu_{\mathrm{B}}S\boldsymbol{u} \tag{3.1}$$

and is thus *antiparallel* to $\boldsymbol{S}$. $\gamma = \mu_0 g_{\mathrm{L}}|e|/2m_{\mathrm{e}} = g_{\mathrm{L}} \cdot 1,105 \cdot 10^5$ m/As is the gyromagnetic ratio ($\gamma > 0$), $\mu_{\mathrm{B}} = |e|\hbar/2m_{\mathrm{e}} = 9.2740 \cdot 10^{-24}$ J/T is the Bohr magneton, and g_{L} denotes the Landé factor or spectroscopic splitting factor. g_{L} is close to 2 for many ferromagnetic materials (quenching of the orbital momentum [44]). $\boldsymbol{u}$ denotes a unit vector in the direction of $\boldsymbol{m}$.

In ferromagnetic materials, the magnetic moments line up parallel to each other due to exchange interaction, leading to the macroscopic effect of magnetization even for vanishing external fields. The magnetization $\boldsymbol{M}$ is defined as the total magnetic moment per volume v,

$$\boldsymbol{M} = \boldsymbol{m}_{\mathrm{tot}}/v \quad . \tag{3.2}$$

In this work, the magnetic polarization $\boldsymbol{J} = \mu_0 \boldsymbol{M}$ is often used instead of the magnetization $\boldsymbol{M}$.

The norm of $\boldsymbol{M}$ is defined by the temperature dependent *spontaneous magnetization* M_{S},

$$\boldsymbol{M} = M_{\mathrm{S}} \boldsymbol{u} \quad , \tag{3.3}$$

with $|\boldsymbol{u}| = 1$.

It was first suggested by Weiss in 1907 that in ferromagnetic materials a molecular field due to exchange interactions of the elementary magnetic moments gives rise to long range order and a substantial spontaneous magnetization below the Curie temperature T_{C} [8]. For instance, iron shows a spontaneous magnetization of about 2 T at room temperature. However, Weiss postulated this field arbitrarily. The first successful attempt to approach ferromagnetism theoretically was in terms of mean field theory, which can be regarded as a justification of the molecular field of Weiss.

The mean field approximation is described in many textbooks, for instance in Ref. [3, 44]. Here, the problem of ferromagnetism is reduced to the problem of isolated spins interacting with a field $\boldsymbol{H} = \boldsymbol{H}_{\mathrm{mf}} + \boldsymbol{H}_{\mathrm{ext}}$, which is actually the problem of paramagnetism. $\boldsymbol{H}_{\mathrm{mf}}$ denotes the molecular or Weiss field generated by the neighboring spins and is proportional to the mean value $\langle \boldsymbol{\mathcal{S}} \rangle$. Due to the internal molecular field, the magnetization parallel to the external field is nonzero even if the applied field vanishes. For zero temperature all ferromagnetic moments are parallel, and the maximum spontaneous magnetization

$$M_{\mathrm{S},0} = g_{\mathrm{L}} \mu_{\mathrm{B}} v_{\mathrm{at}}^{-1} S \tag{3.4}$$

is achieved. v_at is the volume per atomistic spin (volume per atom),

$$v_\mathrm{at} = \begin{cases} a^3 & \text{for simple cubic,} \\ a^3/2 & \text{for body centered cubic, and} \\ a^3/4 & \text{for face centered cubic lattices.} \end{cases} \tag{3.5}$$

The edge of the atomistic *cubic* unit cell is denoted by a. For finite temperatures, thermal fluctuations lead to a temperature dependent spontaneous magnetization $M_\mathrm{S}(T)$, which vanishes at the Curie temperature T_C. In the framework of mean field theory of exchange coupled spins with quantized states, the Curie temperature reads

$$T_\mathrm{C}^\mathrm{mf} = \frac{S(S+1)Jz}{3k_\mathrm{B}} \tag{3.6}$$

and is sometimes used as a reference temperature. z denotes the coordination number (number of nearest neighbors), $k_\mathrm{B} = 1.3807 \cdot 10^{-23}$ J/K is Boltzmann's constant, and J is the isotropic exchange integral between nearest neighbors, see Sec. 3.2.1. However, T_C^mf gives only a hint of the real Curie temperature and has to be handled with care since the approximation of the exchange interaction by the molecular field is valid only for small fluctuations around equilibrium, i.e. far away from criticality. In particular, T_C^mf always overestimates the actual critical temperature though the agreement improves as the coordination number z increases [3].

3.2 Classical Hamiltonian

We now assume magnetic moments localized on an atomistic lattice with lattice sites $\boldsymbol{r}^\mu$, $\boldsymbol{m}^\mu \equiv \boldsymbol{m}(\boldsymbol{r}^\mu)$, coupled via strayfield and isotropic exchange interactions. The crystalline symmetry with its preferred directions is described by an additional anisotropy term, and we suppose a homogeneous external field $\boldsymbol{H}_\mathrm{ext}$. Then, the classical Hamiltonian, which can be obtained from quantum mechanical expressions by replacing operators with their expectation values (classical limit), reads

$$E = E_{\mathrm{exch}} + E_{\mathrm{ani}} + E_{\mathrm{stray}} + E_{\mathrm{ext}} \quad . \tag{3.7}$$

E is a sum of the exchange energy, anisotropy energy, strayfield energy, and Zeeman energy and represents the total energy of the system. Both, strayfield energy and Zeeman energy are magnetostatic energy contributions: the dipolar or strayfield energy arises from dipole-dipole interaction and the Zeeman energy from the interaction with an external field.

Throughout this work, Greek indices (always superscripts) will be consistently used to label atomistic lattice sites or nodes in the continuum model, respectively. Einstein's summation convention is used only for Latin indices (always subscripts), which indicate the Cartesian components.

3.2.1 Exchange Energy

The exchange energy is minimized by aligning the magnetic moments parallel or antiparallel, respectively, and is responsible for long range order of the moments. It has no classical analogue and is caused by the overlap of electronic wave functions and the Pauli principle in quantum mechanics. The Hamiltonian of the exchange interaction in the Heisenberg model (direct exchange coupling) is usually written in the form [37]

$$\mathcal{H}_{\mathrm{exch}} = -\sum_{\mu} \sum_{\nu \neq \mu} J^{\mu\nu}(\boldsymbol{r}^{\mu} - \boldsymbol{r}^{\nu})\, \boldsymbol{\mathcal{S}}^{\mu} \cdot \boldsymbol{\mathcal{S}}^{\nu} \quad . \tag{3.8}$$

$J^{\mu\nu}(\boldsymbol{r}^{\mu} - \boldsymbol{r}^{\nu})$ denotes the exchange integral between the quantum mechanical spin operators of the total angular momenta $\hbar\boldsymbol{\mathcal{S}}^{\mu}$ at lattice site $\boldsymbol{r}^{\mu}$ and $\hbar\boldsymbol{\mathcal{S}}^{\nu}$ at $\boldsymbol{r}^{\nu}$ and can be derived using quantum mechanics. For ferromagnetic ordering the exchange integrals are positive, whereas negative integrals lead to antiferromagnetic ordering. The exchange integrals decrease rapidly with increasing distance between the atoms. Thus, it is usually a good approximation to take the inner sum only for nearest neighbors.

Replacing the quantum mechanical operators by classical spin vectors $\boldsymbol{S} = -S\boldsymbol{u}$ (Eq. (3.1)) and supposing an isotropic exchange constant J, we arrive at the classical atomistic exchange energy

$$E_{\mathrm{exch}} = -JS^2 \sum_{\mu} \sum_{\nu \in \mathrm{nn}} \boldsymbol{u}^{\mu} \cdot \boldsymbol{u}^{\nu} \quad , \tag{3.9}$$

where the inner sum is carried out only for the nearest neighbors (nn) of μ.

Since we used $S^{\mu} = S^{\nu} = S$, we have restricted ourselves to *homogeneous materials* in the sense that material parameters are independent of $\boldsymbol{r}^{\mu}$.

3.2.2 Magnetocrystalline Anisotropy Energy

The assumption of an isotropic exchange integral between neighboring spins resulted in the isotropic exchange energy of Eq. (3.9). However, the energy depends on the angles between the spins and the crystal axes, as can be observed via hysteresis measurements on single crystals and magnetic domain patterns. Consequently, a more realistic model requires an additional energy term which takes into account anisotropy effects. The most common type of anisotropy is the magnetocrystalline anisotropy, which is caused by the asymmetric overlap of electron density distributions of neighboring lattice sites. Due to spin-orbit coupling the charge density of the electrons is not spherical but reflects the crystal structure of the lattice. This asymmetry and the direction of the magnetic moment are tied together by spin-orbit coupling. Hence, if one changes the spin direction, the overlap energy changes as well. Therefore, many ferro- and ferrimagnetic materials exhibit easy and hard directions in space. More energy (or a higher external field) is required to saturate the crystal in a hard direction compared to an easy one. Though spin-orbit coupling can be evaluated from basic principles, it is easier to use phenomenological expressions (power series) according to the crystal structure and take the coefficients from experiments [2].

For crystals with *uniaxial anisotropy* (e.g. hexagonal crystals such as Co) the phenomenological expression of the anisotropy energy of a single moment has the form

$$E_{\mathrm{ani}} = K_0 v + K_1 v \sin^2\theta + \text{higher order terms} \quad . \tag{3.10}$$

K_0 and K_1 are the anisotropy constants (in $\mathrm{J/m^3}$), v the associated volume and θ the angle between the easy direction and the magnetization vector. The higher order terms (a series of even powers of $\sin\theta$) are often small and thus negligible.

The magnetocrystalline anisotropy energy for *cubic crystals* (e.g. Fe, Ni) is given by

$$\begin{aligned} E_{\mathrm{ani}} &= K_{\mathrm{c0}} v + K_{\mathrm{c1}} v \big(\alpha_1^2\alpha_2^2 + \alpha_2^2\alpha_3^2 + \alpha_1^2\alpha_3^2\big) + K_{\mathrm{c2}} v\, \alpha_1^2\alpha_2^2\alpha_3^2 + \\ &\quad + \text{higher order terms} \quad , \end{aligned} \tag{3.11}$$

where α_1, α_2 and α_3 designate the direction cosines of the direction of magnetization with respect to the cubic lattice vectors. Analogously, K_{c2} and higher order terms can be neglected in most cases. Naturally, uniaxial anisotropies are much stronger than cubic ones.

Since $K_0 v$ and $K_{\mathrm{c0}} v$ are only constant offsets of the anisotropy energy, they are usually omitted. The remaining first anisotropy constants cover several orders of magnitude (10^2 - 10^7 $\mathrm{J/m^3}$) and are temperature dependent.

In this work we restrict ourselves to uniaxial anisotropies. The anisotropy energy of a single atomistic spin $\boldsymbol{S} = -S\boldsymbol{u}$ then reads

$$E_{\mathrm{ani}} = K_1 v \left(1 - (\boldsymbol{a} \cdot \boldsymbol{u})^2\right) \quad , \tag{3.12}$$

where $\boldsymbol{a}$ is a unit vector parallel to the easy axis of the crystal and v the volume associated with the spin $\boldsymbol{S}$.

3.2.3 Strayfield Energy

The strayfield energy (also called magnetic self energy, demagnetizing energy, or even just magnetostatic energy) is connected with the magnetic field generated by the magnetic moments themselves. Each lattice site is occupied by a magnetic dipole $\boldsymbol{m} = g\mu_\mathrm{B}S\boldsymbol{u}$ (Eq. (3.1)). Let us consider a magnetic body, successively built up by adding N magnetic dipoles [36]. $E(\mu|\nu)$ denotes the required energy to put the dipole μ into the field of dipole ν. Since no energy is needed for the positioning of the first dipole, the magnetic self energy follows as

$$\begin{aligned} E_\mathrm{stray} = & \quad E(2|1) + \\ & + E(3|1) + E(3|2) + \\ & \ \vdots \\ & + E(N|1) + E(N|2) + \ldots + E(N|N-1) \quad . \end{aligned} \tag{3.13}$$

However, one can also put together the magnet in reversed order, obtaining

$$\begin{aligned} E_\mathrm{stray} = & \quad E(N-1|N) + \\ & + E(N-2|N) + E(N-2|N-1) + \\ & \ \vdots \\ & + E(1|N) + E(1|N-1) + \ldots + E(1|2) \quad . \end{aligned} \tag{3.14}$$

Hence, we find

$$\begin{aligned} 2E_\mathrm{stray} = & \quad 0 \quad + E(1|2) \quad + \ldots + E(1|N-1) + E(1|N) + \\ & + E(2|1) \quad 0 \quad + \ldots + E(2|N-1) + E(2|N) + \\ & \ \vdots \\ & + E(N|1) + E(N|2) + \ldots + E(N|N-1) + \ 0 \quad . \end{aligned} \tag{3.15}$$

Rewriting Eq. (3.15), we obtain for the magnetic strayfield energy

$$E_{\mathrm{stray}} = \frac{1}{2}\sum_{\mu} E^{\mu} \quad , \tag{3.16}$$

where $E^{\mu} \equiv E(\boldsymbol{r}^{\mu})$ designates the energy of dipole $\boldsymbol{m}^{\mu}$ in the field generated by all the other dipoles. The factor 1/2 in Eq. (3.16) is typical for self energies. The energy of dipole interaction, E^{μ}, can be found in Ref. [2] and reads

$$E^{\mu} = \frac{\mu_0}{4\pi}(g_{\mathrm{L}}\mu_{\mathrm{B}}S)^2 \sum_{\nu\neq\mu}\left(\frac{\boldsymbol{u}^{\mu}\cdot\boldsymbol{u}^{\nu}}{(r^{\mu\nu})^3} - \frac{3(\boldsymbol{u}^{\mu}\cdot\boldsymbol{r}^{\mu\nu})(\boldsymbol{u}^{\nu}\cdot\boldsymbol{r}^{\mu\nu})}{(r^{\mu\nu})^5}\right) \quad , \tag{3.17}$$

where $\boldsymbol{r}^{\mu\nu} = \boldsymbol{r}^{\nu} - \boldsymbol{r}^{\mu}$ points from μ to ν.

3.2.4 Zeeman Energy

The Zeeman energy of a dipole $\boldsymbol{m}$ in an external field $\boldsymbol{H}_{\mathrm{ext}}$ simply reads

$$E_{\mathrm{ext}} = -\mu_0\,\boldsymbol{m}\cdot\boldsymbol{H}_{\mathrm{ext}} = -\mu_0 g_{\mathrm{L}}\mu_{\mathrm{B}}S\,\boldsymbol{u}\cdot\boldsymbol{H}_{\mathrm{ext}} \quad . \tag{3.18}$$

Chapter 4

Micromagnetics

Micromagnetics is a phenomenological theory based on the work of Landau and Lifshitz about magnetic domains in the year 1935 [39], as well as Brown [11], who named it *micromagnetism*. Quantum mechanical spin operators are replaced by classical vector fields, which has already been done in the previous chapter. Those classical discrete magnetic moments $\boldsymbol{m}^{\mu}$ at the positions of the atoms, $\boldsymbol{r}^{\mu}$, are then replaced by the continuous function of magnetization, $\boldsymbol{M}(\boldsymbol{r})$. A proper classical description of the exchange interaction in the continuum limit together with the phenomenological Maxwell equations lead to a theory of *continuous* magnetic materials.

The theory of micromagnetics is a suitable framework to investigate magnetic phenomena in the nanometer regime. As long as the underlying assumptions, such as slow variations of the magnetic polarization in space and regions much larger than the atomic distance, are not violated, micromagnetics proofed to be very successfully in the analysis of domain structures in small particles and thin films, nucleation problems and interaction between defects and domain walls [37].

4.1 Gibbs Free Energy

The basis of a micromagnetic description of a magnetic material is the total energy of the system in the continuum limit, given by the Gibbs free energy [2, 11]

$$E = \int_V \mathrm{d}^3 r \, (\varepsilon_{\mathrm{exch}} + \varepsilon_{\mathrm{ani}} + \varepsilon_{\mathrm{stray}} + \varepsilon_{\mathrm{ext}}) \quad , \tag{4.1}$$

with the energy densities of the exchange interaction $\varepsilon_{\mathrm{exch}}$, magnetocrystalline anisotropy $\varepsilon_{\mathrm{ani}}$, of the strayfield contribution $\varepsilon_{\mathrm{stray}}$, and the Zeeman interaction $\varepsilon_{\mathrm{ext}}$, respectively. V denotes the volume of the magnetic body. Magnetostrictive terms are omitted since the effect is usually small and we are not interested in mechanical deformations due to magnetization (cases which can be written in the same form as the appropriate magnetocrystalline anisotropy are, however, included anyway since the anisotropy coefficients come from experiments and include different contributions to the anisotropy energy). Also ignored are surface anisotropy terms, which are discussed for instance in Ref. [2]. Thermodynamics tells us that the most probable state of a magnetic system for a fixed temperature T is given by the minimum of E.

Gibbs free energy is a function of the magnetic polarization, where the vector field

$$\boldsymbol{J}(\boldsymbol{r}, t) = J_{\mathrm{S}}(\boldsymbol{r}) \boldsymbol{u}(\boldsymbol{r}, t) \quad \text{with} \quad |\boldsymbol{u}| = 1 \tag{4.2}$$

is constrained by $|\boldsymbol{J}| = J_{\mathrm{S}} = \text{const.}$ for every point $\boldsymbol{r} \in V$, disregarding the Holstein-Primakoff effect (dependence of J_{S} on the external field) [33]. Of course, the spontaneous polarization depends on the temperature of the sample, $J_{\mathrm{S}} = J_{\mathrm{S}}(T)$. Although we deal with homogeneous materials in this work, we let the spontaneous polarization depend on $\boldsymbol{r}$ just for generality reasons, because no difficulties occur in the discussion.

In the following sections the energy contributions in the continuum limit are given. However, to solve a micromagnetic problem numerically, we have to use a discretization of space, either by using finite differences or finite elements. At least at this point the material parameters may depend on the position

$\boldsymbol{r}^\mu$ or, to be more precise, on the associated volume v^μ, which is obvious for the spontaneous magnetization (see Eq. (3.2)). Then, for instance, $\boldsymbol{J}^\mu(t) \equiv \boldsymbol{J}(\boldsymbol{r}^\mu, t) = J_\mathrm{S}^\mu \boldsymbol{u}^\mu(t)$ denotes the value of the *continuous* vector field $\boldsymbol{J}$ at node μ. The assumption of isotropic exchange is then still valid, since the same exchange constant is used for all interactions between the moment at node μ with its nearest neighbors. We present the energy terms in Eq. (4.1) in a form suitable for *regular cubic lattices* (method of finite differences) with lattice sites $\boldsymbol{r}^\mu$ and lattice spacing Δx in any direction. By assuming a homogeneous material, the material parameters then generally depend on Δx (even though not explicitly written) but not on the position $\boldsymbol{r}^\mu$.

4.1.1 Exchange Energy

The dot product in the isotropic exchange energy Eq. (3.9) can be written in terms of the angles $\varphi^{\mu\nu}$ between the interacting moments,

$$E_\mathrm{exch} = -JS^2 \sum_\mu \sum_{\nu \in \mathrm{nn}} \cos \varphi^{\mu\nu} \quad . \tag{4.3}$$

After subtracting the energy of the state where all spins are aligned, which only redefines the zero level of the exchange energy, we arrive at [2]

$$E_\mathrm{exch} = -JS^2 \sum_\mu \sum_{\nu \in \mathrm{nn}} (\cos \varphi^{\mu\nu} - 1) = 2JS^2 \sum_\mu \sum_{\nu \in \mathrm{nn}} \sin^2(\varphi^{\mu\nu}/2) \quad . \tag{4.4}$$

We now assume small angles between neighboring magnetic moments due to the strong exchange interaction and use $\sin x \approx x$ for small x, which brings us to

$$E_\mathrm{exch} = \frac{1}{2} JS^2 \sum_\mu \sum_{\nu \in \mathrm{nn}} \varphi^{\mu\nu 2} \quad . \tag{4.5}$$

For small angles $\varphi^{\mu\nu}$, the approximation $|\varphi^{\mu\nu}| \approx |\boldsymbol{u}^\mu - \boldsymbol{u}^\nu|$ is also valid, where we used the *continuous* unit vector $\boldsymbol{u} = \boldsymbol{M}/M_\mathrm{S}$. In general, the spontaneous magnetization M_S is also a function of space, $M_\mathrm{S} = M_\mathrm{S}(\boldsymbol{r})$. Using the Taylor expansion

$$|\boldsymbol{u}^{\mu} - \boldsymbol{u}^{\nu}| \approx |(\boldsymbol{s}^{\mu} \cdot \boldsymbol{\nabla})\boldsymbol{u}|^2 \tag{4.6}$$

with $\boldsymbol{s}^{\mu} = \boldsymbol{r}^{\nu} - \boldsymbol{r}^{\mu}$ yields

$$E_{\text{exch}} = \frac{1}{2} J S^2 \sum_{\mu} \sum_{\boldsymbol{s}^{\mu}} |(\boldsymbol{s}^{\mu} \cdot \boldsymbol{\nabla})\boldsymbol{u}|^2 \quad . \tag{4.7}$$

The second sum is carried out over all vectors $\boldsymbol{s}^{\mu}$ pointing to the nearest neighbors of lattice site μ. For instance, for primitive (or simple) cubic lattices with lattice constant a the sum has to be carried out over $\boldsymbol{s} \in \{\pm a\hat{\boldsymbol{x}}, \pm a\hat{\boldsymbol{y}}, \pm a\hat{\boldsymbol{z}}\}$.

After changing the first sum in Eq. (4.7) to an integral over the magnetic body, we finally obtain the continuum representation of the exchange energy,

$$E_{\text{exch}} = \int_V \mathrm{d}^3 r \, A \left[(\boldsymbol{\nabla} u_x)^2 + (\boldsymbol{\nabla} u_y)^2 + (\boldsymbol{\nabla} u_z)^2 \right] \quad . \tag{4.8}$$

The *exchange constant* A for cubic lattices is given by

$$A = \frac{J S^2}{a} c \quad , \tag{4.9}$$

where a denotes the edge of the *cubic* atomistic unit cell and c the number of atoms in the cubic atomistic unit cell. $c = 1, 2, 4$ for a simple cubic, body centered cubic (bcc), and face centered cubic (fcc) crystal structure, respectively. The same result for the exchange energy in Eq. (4.8) is found for hexagonal close-packed crystals (e.g. Co), but then a is the distance between nearest neighbors and $c = 2\sqrt{2}$ [2, 37].

The value of the exchange constant A can be measured experimentally by determining the domain wall width or measuring the correlation of spins near the Curie point T_C and is found to be of the order of 10^{-12} to 10^{-11} J/m [34].

Discretization of the Exchange Energy

The partial derivatives in Eq. (4.8) of the continuous vector field $\boldsymbol{u}$ can be approximated by finite differences. For instance, the approximation of the first term reads

$$(\boldsymbol{\nabla} u_x)^2 \approx \left(\frac{\Delta_x u_x}{\Delta x}\right)^2 + \left(\frac{\Delta_y u_x}{\Delta y}\right)^2 + \left(\frac{\Delta_z u_x}{\Delta z}\right)^2 \quad , \tag{4.10}$$

where Δx, Δy, and Δz are the lattice spacings in the three dimensions of space, and Δ_x, Δ_y, Δ_z denote finite difference operators [51]. In this work we only use regular cubic lattices and we simply write Δx for the lattice spacing in all directions.

If $\boldsymbol{u}^\mu$ denotes the magnetization vector at lattice site μ, $\boldsymbol{u}^{\mu+1}$ is the neighbor of $\boldsymbol{u}^\mu$ in $+x$-direction and $\boldsymbol{u}^{\mu-1}$ the neighbor in $-x$-direction. Thus, we can write the first term in Eq. (4.10) as the arithmetic mean of the two opposite nearest neighbors,

$$\left(\frac{\Delta_x u_x}{\Delta x}\right)^2_{\boldsymbol{r}^\mu} = \frac{1}{2\Delta x^2}\left((u_x^{\mu-1} - u_x^\mu)^2 + (u_x^{\mu+1} - u_x^\mu)^2\right) \quad . \tag{4.11}$$

Doing so analogously for the second and third term in Eq. (4.10) with the nearest neighbors in y- and z-direction, we arrive at

$$(\boldsymbol{\nabla} u_x)^2_{\boldsymbol{r}^\mu} \approx \frac{1}{2\Delta x^2}\sum_{\nu\in\mathrm{nn}}(u_x^\nu - u_x^\mu)^2 \quad , \tag{4.12}$$

where the sum is evaluated for the 6 nearest neighbors (nn) of the magnetic moment at $\boldsymbol{r}^\mu$. Summing up all contributions in Eq. (4.8), utilizing $|\boldsymbol{u}| = 1$, and changing $\int \mathrm{d}^3 r \rightarrow \Delta x^3 \sum_\mu$, our final result for the exchange energy in discretized form reads

$$E_{\mathrm{exch}} = A\Delta x \sum_\mu \sum_{\nu\in\mathrm{nn}} (1 - \boldsymbol{u}^\mu \cdot \boldsymbol{u}^\nu) \quad . \tag{4.13}$$

Eq. (4.13) is probably the most common representation of the exchange energy in discrete form and is only valid for small deviations between neighboring moments, $\boldsymbol{u}^\mu$ and $\boldsymbol{u}^\nu$. However, other approximations are possible, leading to different representations and properties, as reported in Ref. [20].

Omitting the constant term in Eq. (4.13), the discretized expression of the exchange energy looks very similar to the atomistic version Eq. (3.9). However, in Eq. (4.13) the unit vector $\boldsymbol{u}$ is a *continuous* vector field, evaluated on the lattice sites μ. The derivation of Eq. (4.13) supposed small angles between neighboring spins whereas the angle between neighboring spins in Eq. (3.9) is arbitrary. The exchange constant A is a phenomenological constant, determined via macroscopic measurements. Last but not least, the dependence on the lattice spacing, Δx, does not occur in Eq. (3.9) and is a typical relict of discretizing a continuum formulation.

4.1.2 Magnetocrystalline Anisotropy Energy

The continuum formulation of the magnetocrystalline anisotropy energy for the most important case of uniaxial anisotropies, Eq. (3.12), is straightforward and reads

$$E_{\text{ani}} = \int_V \mathrm{d}^3 r\, K_1 \left(1 - (\boldsymbol{a} \cdot \boldsymbol{u})^2\right) \quad . \tag{4.14}$$

K_1 is the first magnetocrystalline anisotropy constant, $\boldsymbol{a}$ is a unit vector parallel to the easy axis, and $\boldsymbol{u}$ is now a continuous vector field, $\boldsymbol{u} = \boldsymbol{J}/J_{\mathrm{S}}$.

Discretization of the Anisotropy Energy

For the method of finite differences with a regular cubic lattice of lattice spacings Δx in all directions, the discretized form of Eq. (4.14) reads

$$E_{\text{ani}} = K_1 \Delta x^3 \sum_{\mu} \left(1 - (\boldsymbol{a} \cdot \boldsymbol{u}^{\mu})^2\right) \quad . \tag{4.15}$$

The sum is carried out over all lattice sites μ, and the anisotropy constant may depend on Δx but not on the lattice site (homogeneous material).

4.1.3 Strayfield Energy

The strayfield energy in the limit of a continuous material is given by [1, 37]

$$E_{\mathrm{stray}} = -\frac{1}{2}\int_V \mathrm{d}^3r\, \boldsymbol{J} \cdot \boldsymbol{H}_{\mathrm{stray}} \quad . \tag{4.16}$$

The factor 1/2 again points out that E_{stray} is a self energy. The strayfield or demagnetizing field $\boldsymbol{H}_{\mathrm{stray}}$ only appears if $\boldsymbol{J}$ is spatially inhomogeneous, either in orientation or in the absolute value $|\boldsymbol{J}| = J_{\mathrm{S}}$, and has to fulfill Maxwell's phenomenological equation of magnetostatics (Eq. (2.14)),

$$\boldsymbol{\nabla} \times \boldsymbol{H}_{\mathrm{stray}} = 0 \quad . \tag{4.17}$$

The general solution reads

$$\boldsymbol{H}_{\mathrm{stray}} = -\boldsymbol{\nabla} U \quad , \tag{4.18}$$

where U is a scalar magnetic potential. Using Eq. (2.10) and Eq. (2.13), we get the Poisson equation for U,

$$\boldsymbol{\nabla}^2 U = \frac{1}{\mu_0}\boldsymbol{\nabla} \cdot \boldsymbol{J} \quad . \tag{4.19}$$

These equations have to be solved together with the appropriate boundary conditions to obtain $\boldsymbol{H}_{\mathrm{stray}}$ and finally the strayfield energy E_{stray}.

In a ferromagnetic material, the exchange energy E_{exch} competes with the strayfield energy E_{stray}. This is the reason why large domains break up into a number of smaller domains when magnetic particles become larger than the critical size of a single-domain particle [37]. Above the critical diameter, flux closure configurations (i.e. multi-domain configurations) are energetically more favorable.

Discretization of the Magnetostatic Energy

For regular cubic lattices Schabes and Aharoni [49] presented an exact analytic formula for the magnetostatic interaction energy. However, the expressions obtained are complex and computationally expensive. For the method of finite differences it is normally sufficient to approximate each cubic cell μ with volume Δx^3 by a magnetic dipole $\boldsymbol{m}^\mu = \boldsymbol{M}^\mu \Delta x^3$ and to use the energy expression for dipole-dipole interaction (see Eq. (3.16) and Eq. (3.17)),

$$E_{\text{stray}} = -\frac{\Delta x^3}{2} \sum_{\mu} \boldsymbol{J}^\mu \cdot \boldsymbol{H}^\mu_{\text{stray}} \quad . \tag{4.20}$$

The strayfield $\boldsymbol{H}^\mu_{\text{stray}}$ at lattice site $\boldsymbol{r}^\mu$ is given by

$$\boldsymbol{H}^\mu_{\text{stray}} = -\frac{1}{4\pi\mu_0} \sum_{\nu \neq \mu} \left(\frac{\boldsymbol{J}^\nu}{(r^{\mu\nu})^3} - 3\,\frac{\boldsymbol{r}^{\mu\nu}(\boldsymbol{J}^\nu \cdot \boldsymbol{r}^{\mu\nu})}{(r^{\mu\nu})^5} \right) \quad , \tag{4.21}$$

where $\boldsymbol{r}^{\mu\nu} = \boldsymbol{r}^\nu - \boldsymbol{r}^\mu$ points from μ to ν.

The difference between the exact formula and the dipole approximation is negligible for small volumes Δx^3 [1].

4.1.4 Zeeman Energy

The Zeeman energy, Eq. (3.18), in the continuum theory of micromagnetism reads

$$E_{\text{ext}} = -\int_V \mathrm{d}^3 r\, \boldsymbol{J} \cdot \boldsymbol{H}_{\text{ext}} \quad . \tag{4.22}$$

Discretization of the Zeeman Energy

The discretized form of Eq. (4.22) for a regular cubic lattice with lattice spacing Δx and lattice sites $\boldsymbol{r}^\mu$ is

$$E_{\text{ext}} = -\Delta x^3 \sum_{\mu} \boldsymbol{J}^\mu \cdot \boldsymbol{H}_{\text{ext}} \quad . \tag{4.23}$$

4.2 Energy Minimization and Effective Field

The minimum of the total Gibbs free energy of a magnetic body V with continuous polarization $\boldsymbol{J}(\boldsymbol{r}) = J_\mathrm{S}(\boldsymbol{r})\boldsymbol{u}(\boldsymbol{r})$ (with $|\boldsymbol{u}(\boldsymbol{r})| = 1$),

$$\begin{aligned} E &= \int_V \mathrm{d}^3 r \left\{ A\left[(\boldsymbol{\nabla} u_x)^2 + (\boldsymbol{\nabla} u_y)^2 + (\boldsymbol{\nabla} u_z)^2\right] + \right. \\ & \left. + K_1\left(1 - (\boldsymbol{a}\cdot\boldsymbol{u})^2\right) - \frac{1}{2}\boldsymbol{J}\cdot\boldsymbol{H}_\mathrm{stray} - \boldsymbol{J}\cdot\boldsymbol{H}_\mathrm{ext}\right\} \quad , \qquad (4.24) \end{aligned}$$

is the most probable state of the magnetic system. Brown suggested a variational method to find the magnetization distribution which minimizes the energy (originally, the name *micromagnetics* only denoted this theory before it was extended later on and now includes any sort of magnetic calculation ignoring the atomic structure of the material in the energy contributions explicitly) [11].

Let us consider small variations of $\boldsymbol{J}$ around the polarization distribution $\boldsymbol{J}_0 = J_\mathrm{S}\boldsymbol{u}_0$ with the constraint $|\boldsymbol{u}| = 1$ everywhere. Though, the spontaneous polarization J_S is, for generality reasons, a function of space, it is chosen once and then assumed to be constant at any point $\boldsymbol{r} \in V$. Therefore, variations $\delta\boldsymbol{J} = \boldsymbol{J} - \boldsymbol{J}_0$ only apply for the vector field $\boldsymbol{u}$ and let J_S unaffected, $\delta\boldsymbol{J} = J_\mathrm{S}\,\delta\boldsymbol{u}$. A spontaneous magnetization depending on $\boldsymbol{r}$ but constant at any point is thus in agreement with the original constraint of Brown, $\boldsymbol{M}^2 = M_\mathrm{S}^2 = \mathrm{const.}$ (In the context of this section, we can actually extend this assumption and let all material parameters be functions of $\boldsymbol{r}$ but inalterable for any $\boldsymbol{r} \in V$, even though not explicitly written.)

We set

$$u_x = u_{0,x} + \zeta w_x \quad \text{and} \quad u_y = u_{0,y} + \zeta w_y \quad , \qquad (4.25)$$

where ζ is small and w_x and w_y are arbitrary functions of space [2]. u_z is determined by the constraint $|\boldsymbol{u}| = 1$ and reads to first order of ζ

$$u_z = u_{0,z} - \zeta\lambda \quad , \qquad (4.26)$$

where

$$\lambda = \frac{u_{0,x} w_x + u_{0,y} w_y}{u_{0,z}} \quad . \tag{4.27}$$

At a minimum, the variation of the total Gibbs free energy,

$$\delta E = \int_V \mathrm{d}^3 r \; (\varepsilon(\boldsymbol{u}) - \varepsilon(\boldsymbol{u}_0)) \quad , \tag{4.28}$$

should vanish for *any choice* of w_x and w_y.

We start with the variation of the exchange energy, which is (to a first order in ζ)

$$\delta E_{\mathrm{exch}} = 2\zeta \int_V \mathrm{d}^3 r \, A \left[(\partial_i u_{0,x})(\partial_i w_x) + (\partial_i u_{0,y})(\partial_i w_y) - (\partial_i u_{0,z})(\partial_i \lambda) \right] \quad , \tag{4.29}$$

where we used Einstein's summation convention, and ∂_i is the i-th component of the nabla operator $\boldsymbol{\nabla}$. With the first Green's identity

$$\int_V \mathrm{d}^3 r \; \left[(\partial_i g)(\partial_i h) + g \partial_i^2 h \right] = \oint_{\partial V} \mathrm{d}^2 f_i \, g \partial_i h \quad , \tag{4.30}$$

where g and h are any two functions and ∂V denotes the surface of V, we obtain

$$\begin{aligned} \delta E_{\mathrm{exch}} \quad = \quad & 2\zeta \oint_{\partial V} \mathrm{d}^2 f_i \, A \left[w_x \partial_i u_{0,x} + w_y \partial_i u_{0,y} - \lambda \partial_i u_{0,z} \right] - \\ & -2\zeta \int_V \mathrm{d}^3 r \, A \left[w_x \partial_i^2 u_{0,x} + w_y \partial_i^2 u_{0,y} - \lambda \partial_i^2 u_{0,z} \right] \quad . \end{aligned} \tag{4.31}$$

A variation of the uniaxial anisotropy energy yields

$$\begin{aligned} \delta E_{\mathrm{ani}} \quad = \quad & 2\zeta \int_V \mathrm{d}^3 r \, K_1 (- a_x u_{0,x} a_x w_x - a_x u_{0,x} a_y w_y + a_x u_{0,x} a_z \lambda - \\ & \qquad - a_y u_{0,y} a_x w_x - a_y u_{0,y} a_y w_y + a_y u_{0,y} a_z \lambda - \\ & \qquad - a_z u_{0,z} a_x w_x - a_z u_{0,z} a_y w_y + a_z u_{0,z} a_z \lambda) = \\ = \quad & -2\zeta \int_V \mathrm{d}^3 r \, K_1 (a_i u_{0,i} a_x w_x + a_i u_{0,i} a_y w_y - a_i u_{0,i} a_z \lambda) \quad , \end{aligned} \tag{4.32}$$

again to first order in ζ.

For the variation of the strayfield energy we obtain

$$\begin{aligned}\delta E_{\text{stray}} &= -\frac{1}{2}\int_V \mathrm{d}^3r\ [(\boldsymbol{J}_0 + \delta\boldsymbol{J})\cdot(\boldsymbol{H}_{\text{stray},0} + \delta\boldsymbol{H}_{\text{stray}}) - \boldsymbol{J}\cdot\boldsymbol{H}_{\text{stray}}] = \\ &= -\frac{1}{2}\int_V \mathrm{d}^3r\ [\boldsymbol{J}_0\cdot\delta\boldsymbol{H}_{\text{stray}} + \boldsymbol{H}_{\text{stray},0}\cdot\delta\boldsymbol{J}] \quad , \qquad (4.33)\end{aligned}$$

which is true to first order for small variations δ. Since $\boldsymbol{H}_{\text{stray},0}$ is the field generated by $\boldsymbol{J}_0$ and $\delta\boldsymbol{H}_{\text{stray}}$ stems from the small polarization $\delta\boldsymbol{J}$, we can use the *reciprocity theorem* [11]

$$\int_V \mathrm{d}^3r\,\boldsymbol{J}_0\cdot\delta\boldsymbol{H}_{\text{stray}} = \int_V \mathrm{d}^3r\,\boldsymbol{H}_{\text{stray},0}\cdot\delta\boldsymbol{J} \qquad (4.34)$$

and obtain

$$\delta E_{\text{stray}} = -\int_V \mathrm{d}^3r\ J_{\mathrm{S}}\boldsymbol{H}_{\text{stray},0}\cdot\delta\boldsymbol{u} \quad . \qquad (4.35)$$

A variation of the Zeeman energy leads to a similar result as for the strayfield energy in Eq. (4.35) since $\boldsymbol{H}_{\text{ext}}$ does not depend on the magnetization distribution. With the definition

$$\boldsymbol{H}_0 = \boldsymbol{H}_{\text{stray},0} + \boldsymbol{H}_{\text{ext}} \qquad (4.36)$$

we can summarize both energy terms and end up with

$$\delta E_{\text{stray}} + \delta E_{\text{ext}} = -\zeta\int_V \mathrm{d}^3r\ J_{\mathrm{S}}(H_{0,x}w_x + H_{0,y}w_y - H_{0,z}\lambda) \quad . \qquad (4.37)$$

The variation δE must vanish for any choice of w_x and w_y. Thus, the integrand of the surface integral in Eq. (4.31) must be zero and also the sum of the volume integrands. Omitting the index 0 (it is not necessary anymore) and using

$$\mathrm{d}^2f_i\,\partial_i = \mathrm{d}^2f\,\frac{\partial}{\partial n} \quad , \qquad (4.38)$$

where $\boldsymbol{n}$ is the normal vector to the surface ($|\boldsymbol{n}| = 1$), the first condition leads to the boundary conditions on the surface,

$$A\left(\frac{\partial u_x}{\partial n}-\frac{u_x}{u_z}\frac{\partial u_z}{\partial n}\right) = 0 \quad , \tag{4.39}$$

$$A\left(\frac{\partial u_y}{\partial n}-\frac{u_y}{u_z}\frac{\partial u_z}{\partial n}\right) = 0 \quad . \tag{4.40}$$

Multiplying Eq. (4.39) by u_y and Eq. (4.40) by u_x and subtracting both equations leads to

$$A\left(u_x\frac{\partial u_y}{\partial n}-u_y\frac{\partial u_x}{\partial n}\right)=0 \quad . \tag{4.41}$$

The boundary conditions can now be written in vector notation,

$$\boldsymbol{u}\times\frac{\partial \boldsymbol{u}}{\partial n}=0 \quad , \tag{4.42}$$

but one has to bear in mind that there are only two independent equations.

The second condition that the integrand of the volume integral should vanish also leads to two differential equations (we omitted the index 0 and multiplied both equations by u_z),

$$\begin{aligned}2A(u_z\partial_i^2 u_x-u_x\partial_i^2 u_z)+2K_1(a_iu_ia_xu_z-a_iu_ia_zu_x)+&\\+J_\mathrm{S}(u_zH_x-u_xH_z)=0&\end{aligned} \tag{4.43}$$

and

$$\begin{aligned}2A(u_z\partial_i^2 u_y-u_y\partial_i^2 u_z)+2K_1(a_iu_ia_yu_z-a_iu_ia_zu_y)+&\\+J_\mathrm{S}(u_zH_y-u_yH_z)=0 \quad .&\end{aligned} \tag{4.44}$$

Again, we can build a third equation by multiplying Eq. (4.43) by u_y and Eq. (4.44) by u_x and subtracting both equations. After dividing the result by u_z, we obtain

$$\begin{aligned}2A(u_y\partial_i^2 u_x-u_x\partial_i^2 u_y)+2K_1(a_iu_ia_xu_y-a_iu_ia_yu_x)+&\\+J_\mathrm{S}(u_yH_x-u_xH_y)=0 \quad .&\end{aligned} \tag{4.45}$$

These three equations read in vector notation

$$\boldsymbol{u} \times \left(2A\boldsymbol{\nabla}^2\boldsymbol{u} + 2K_1(\boldsymbol{a}\cdot\boldsymbol{u})\boldsymbol{a} + J_\mathrm{S}\boldsymbol{H}_\mathrm{stray} + J_\mathrm{S}\boldsymbol{H}_\mathrm{ext}\right) = 0 \quad . \tag{4.46}$$

Brown's equations thus mean that the magnetic polarization $\boldsymbol{J} = J_\mathrm{S}\boldsymbol{u}$ in equilibrium is parallel to an *effective field*

$$\boldsymbol{H}_\mathrm{eff} = \boldsymbol{H}_\mathrm{exch} + \boldsymbol{H}_\mathrm{ani} + \boldsymbol{H}_\mathrm{stray} + \boldsymbol{H}_\mathrm{ext} \tag{4.47}$$

at any point $\boldsymbol{r} \in V$, and the torque vanishes, $\boldsymbol{J} \times \boldsymbol{H}_\mathrm{eff} = 0$. The effective field is composed of the exchange field

$$\boldsymbol{H}_\mathrm{exch} = \frac{2A}{J_\mathrm{S}}\boldsymbol{\nabla}^2\boldsymbol{u} \quad , \tag{4.48}$$

the anisotropy field

$$\boldsymbol{H}_\mathrm{ani} = \frac{2K_1}{J_\mathrm{S}}(\boldsymbol{a}\cdot\boldsymbol{u})\boldsymbol{a} \quad , \tag{4.49}$$

the strayfield $\boldsymbol{H}_\mathrm{stray}$, and the external field $\boldsymbol{H}_\mathrm{ext}$.

Brown's equations have to be solved together with Maxwell's equations of magnetostatics (see Chap. 2) and the boundary conditions (4.42). Since the condition that the variation of the energy E vanishes is also fulfilled for maxima of E, it is necessary to check whether a solution is a maximum or a minimum.

In a discretized form (finite differences or finite elements), the effective field at node $\boldsymbol{r}^\mu$ can be approximated using the box scheme [25],

$$\boldsymbol{H}^\mu_\mathrm{eff} = -\frac{1}{v^\mu J^\mu_\mathrm{S}}\frac{\partial E}{\partial \boldsymbol{u}^\mu} \quad . \tag{4.50}$$

At this point we restrict ourselves again to homogeneous materials. For the method of finite differences with a regular cubic lattice ($v^\mu = \Delta x^3$) we end up with

$$\boldsymbol{H}^{\mu}_{\mathrm{eff}} = \frac{2A}{J_{\mathrm{S}}\Delta x^2} \sum_{\nu \in \mathrm{nn}} \boldsymbol{u}^{\nu} + \frac{2K_1}{J_{\mathrm{S}}} (\boldsymbol{a} \cdot \boldsymbol{u}^{\mu}) \boldsymbol{a} + \boldsymbol{H}^{\mu}_{\mathrm{stray}} + \boldsymbol{H}_{\mathrm{ext}} \quad , \tag{4.51}$$

where the material parameters J_{S}, A, and K_1 may depend on Δx. Eq. (4.13) and Eq. (4.15) were used to calculate the exchange field and the anisotropy field, respectively. The stray field for the method of finite differences, $\boldsymbol{H}^{\mu}_{\mathrm{stray}}$, is given by Eq. (4.21).

Chapter 5

Metropolis Monte Carlo

The Monte Carlo method provides approximate solutions to numerous mathematical and physical problems of many degrees of freedom by performing statistical sampling experiments on a computer. Ultimately, it is used to calculate quantities appearing as results of high-dimensional integrals by using a random sequence of numbers. The method applies to problems with non-probabilistic structure as well as to those with probabilistic behavior, for instance physical systems in contact with a heat bath.

For problems in physics, the Monte Carlo method starts with a description of the physical system by a (classical) Hamiltonian and by choosing the appropriate ensemble. All mean values of the observables of interest are then computable via the associated distribution function and the partition function. Normally, *importance sampling* Monte Carlo (like the Metropolis Monte Carlo method) is used instead of *simple sampling* to sample the main contributions in phase space in order to get estimates for the observables more quickly [9, 38].

In the framework of Monte Carlo simulations it is a priori not possible to describe physical systems dynamically. However, only recently, a Monte Carlo method with a quantified time step was introduced to systems of interacting magnetic moments, see for instance Ref. [14, 31]. The authors claim that the interpretation of a Monte Carlo step as a physical time interval is possible by comparing this step with a time interval of the corresponding Langevin equation (in our case of magnetic moments, the stochastic Landau-Lifshitz-Gilbert equation (6.6)).

5.1 Method of Importance Sampling

To get an idea, how importance sampling works, we look at the simple one-dimensional integration problem [29]

$$I = \int_a^b \mathrm{d}x\, f(x) \quad . \tag{5.1}$$

According to the mean value theorem of analytical calculus, the integral I can be calculated via the mean value $\langle f(x) \rangle$ within $[a, b]$,

$$I = (b-a)\langle f \rangle \approx \frac{b-a}{n} \sum_{i=1}^{n} f(x_i) \quad , \tag{5.2}$$

where x_i are n randomly distributed numbers in $[a, b]$. The approach given above is usually called *direct sampling* or *simple sampling.* The error of the result is

$$\sigma_{\mathrm{I}} \approx \frac{1}{\sqrt{n}} \sigma_{\mathrm{f}} \quad , \tag{5.3}$$

where σ_{f} denotes the maximum range of $f(x)$ between a and b. If the function $f(x)$ has a large variation in $[a, b]$, the convergence will be very slow. On the other hand, if the function is more or less uniform, the estimate will be very efficient.

In the method of *importance sampling* we use a probability density function $W(x)$ with $W(x) \geq 0$, $\forall x \in [a, b]$, and the analytically solvable integral

$$\int_a^b \mathrm{d}x\, W(x) = 1 \quad , \tag{5.4}$$

and rewrite the integral I,

$$I = \int_a^b \mathrm{d}x\, f(x) = \int_a^b \mathrm{d}x\, W(x) \frac{f(x)}{W(x)} = \left\langle \frac{f}{W} \right\rangle_{\mathrm{W}} \approx \frac{1}{n} \sum_{\{x_i\}_{\mathrm{W}}} \frac{f(x_i)}{W(x_i)} \quad . \tag{5.5}$$

$\langle \cdot \rangle_{\mathrm{W}}$ denotes the mean value with respect to the distribution function $W(x)$, and $\{x_i\}_{\mathrm{W}}$ is a sequence of random numbers in $[a, b]$ distributed according to $W(x)$. The method is most efficient for

$$W(x) \approx \frac{f(x)}{\int_a^b \mathrm{d}x\, f(x)} \quad , \tag{5.6}$$

i.e. for $f(x)/W(x) \approx$ const., where the statistical error reduces enormously without increasing sample size (variance reduction [29]). Here, we arrived at the idea of importance sampling, where we preferably choose points x_i with dominant contributions to the integral.

5.2 Simulating Magnetic Systems

Now, let us consider a system of interacting magnetic moments, either atomistic or non-atomistic (finite differences), described by the classical Hamiltonian

$$E = E_{\mathrm{exch}} + E_{\mathrm{ani}} + E_{\mathrm{stray}} + E_{\mathrm{ext}} \quad , \tag{5.7}$$

which represents the total energy. The energy is a function of all unit vectors, $E = E(\boldsymbol{u}^1, \ldots, \boldsymbol{u}^N) = E(\underline{\boldsymbol{u}})$, where we defined the $3N$-dimensional vector $\underline{\boldsymbol{u}} = (u_x^1, u_y^1, \ldots, u_z^N)^{\mathrm{T}}$. The magnetic system is in contact with a heat bath, and the appropriate ensemble is the *canonical* one. We want to compute the mean value of an observable $O(\underline{\boldsymbol{u}})$, given by the ensemble average

$$\langle O \rangle = \frac{1}{Z} \int_{\Pi} \mathrm{d}\underline{\boldsymbol{u}}\, f(E(\underline{\boldsymbol{u}}))\, O(\underline{\boldsymbol{u}}) \quad , \tag{5.8}$$

with the canonical distribution function

$$f(E(\underline{\boldsymbol{u}})) \propto \exp\left(-\frac{E(\underline{\boldsymbol{u}})}{k_{\mathrm{B}}T}\right) \tag{5.9}$$

and the partition function

$$Z = \int_{\Pi} \mathrm{d}\underline{\boldsymbol{u}}\, f(E(\underline{\boldsymbol{u}})) \quad . \tag{5.10}$$

Π denotes the phase space with all possible states $\underline{\boldsymbol{u}}$ of the magnetic system. All vectors $\underline{\boldsymbol{u}}$ corresponding to states with high energies give only small contributions to the integral in Eq. (5.8). Since we use the ensemble average (5.8), we have implicitly assumed ergodicity, which allows for the replacement of time averages by ensemble averages [29].

Proceeding analogously to the last section, we can rewrite Eq. (5.8) as

$$\langle O \rangle = \int_{\Pi} \mathrm{d}\underline{\boldsymbol{u}}\, \underbrace{Z^{-1} f(E(\underline{\boldsymbol{u}}))}_{W(\underline{\boldsymbol{u}})} O(\underline{\boldsymbol{u}}) \approx \frac{1}{n} \sum_{\{\underline{\boldsymbol{u}}_i\}_{\mathrm{W}}} O(\underline{\boldsymbol{u}}_i) \quad , \tag{5.11}$$

with Metropolis' choice of the variance reduction function $W(\underline{\boldsymbol{u}})$ [43] and the states $\{\underline{\boldsymbol{u}}_i\}_{\mathrm{W}}$, randomly distributed according to $W(\underline{\boldsymbol{u}})$. With the probability density $W(\underline{\boldsymbol{u}})$ equal to the equilibrium distribution, the variance is almost zero since primarily the thermodynamic equilibrium states of the system are sampled and the observable O only fluctuates around its mean value. Eq. (5.11) means that in Metropolis Monte Carlo simulations the calculation of $\langle O \rangle$ has been reduced to simple arithmetic averaging.

The problem at hand now is to randomly generate states $\underline{\boldsymbol{u}}$ which are distributed according to $W(\underline{\boldsymbol{u}})$. Metropolis *et al.* [43] suggested to build a Markov chain with a well-defined correlation between subsequent states, starting from an arbitrary initial state $\underline{\boldsymbol{u}}_0$ (for more details about Markov processes, see Sec. 6.3.1). To ensure that these states $\underline{\boldsymbol{u}}$ are finally distributed according to $W(\underline{\boldsymbol{u}})$, restrictions must be addressed to the transition probability $P(\underline{\boldsymbol{u}}'|\underline{\boldsymbol{u}})$ from the state $\underline{\boldsymbol{u}}$ to the state $\underline{\boldsymbol{u}}'$.

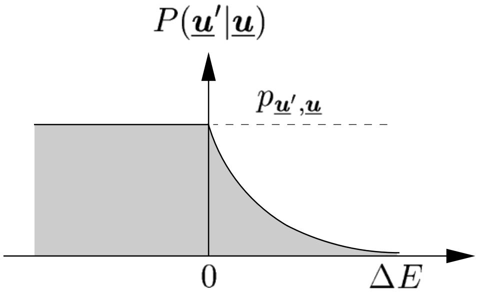

Figure 5.1: Transition probability for the heat bath algorithm according to Eq. (5.16).

5.2.1 Restrictions to the Transition Probability

As a probability function, $P(\underline{\boldsymbol{u}}'|\underline{\boldsymbol{u}})$ has to fulfill

$$P(\underline{\boldsymbol{u}}'|\underline{\boldsymbol{u}}) \geq 0 \quad , \qquad \forall \underline{\boldsymbol{u}}, \underline{\boldsymbol{u}}' \tag{5.12}$$

and

$$\sum_{\underline{\boldsymbol{u}}} P(\underline{\boldsymbol{u}}'|\underline{\boldsymbol{u}}) = 1 \quad , \qquad \forall \underline{\boldsymbol{u}}' \quad . \tag{5.13}$$

Furthermore, the choice of $P(\underline{\boldsymbol{u}}'|\underline{\boldsymbol{u}})$ has to guarantee ergodicity, which means that any state of the system must be accessible from any other state in a finite number of transitions. And, finally, to ensure that the states $\underline{\boldsymbol{u}}$ are ultimately randomly distributed according to the thermodynamic equilibrium distribution $W(\underline{\boldsymbol{u}})$, it is sufficient (but not necessary) to impose the condition of *detailed balance* [9],

$$P(\underline{\boldsymbol{u}}'|\underline{\boldsymbol{u}})W(\underline{\boldsymbol{u}}) = P(\underline{\boldsymbol{u}}|\underline{\boldsymbol{u}}')W(\underline{\boldsymbol{u}}') \quad . \tag{5.14}$$

Note that it does not matter how many intermediate states $\underline{\boldsymbol{u}}''$ are realized until the system actually reaches $\underline{\boldsymbol{u}}'$, starting from $\underline{\boldsymbol{u}}$. This follows from the Chapman-Kolmogorov equation (6.25), which is valid for Markov processes.

5.2.2 Heat Bath Algorithm

For our canonical ensemble, Eq. (5.14) means that in thermodynamic equilibrium the ratio of transition probabilities only depends on the change in energy $\Delta E = E(\underline{\boldsymbol{u}}') - E(\underline{\boldsymbol{u}})$ between state $\underline{\boldsymbol{u}}$ and successor $\underline{\boldsymbol{u}}'$,

$$\frac{P(\underline{\boldsymbol{u}}'|\underline{\boldsymbol{u}})}{P(\underline{\boldsymbol{u}}|\underline{\boldsymbol{u}}')} = \frac{W(\underline{\boldsymbol{u}}')}{W(\underline{\boldsymbol{u}})} = \exp\left(-\frac{\Delta E}{k_{\mathrm{B}}T}\right) \quad . \tag{5.15}$$

A possible and physically obvious form to specify the transition probability for the Metropolis Monte Carlo method is

$$P(\underline{\boldsymbol{u}}'|\underline{\boldsymbol{u}}) = \begin{cases} p_{\underline{\boldsymbol{u}}',\underline{\boldsymbol{u}}} \exp(-\Delta E/k_{\mathrm{B}}T) & , \text{ if } \Delta E > 0, \\ p_{\underline{\boldsymbol{u}}',\underline{\boldsymbol{u}}} \quad , & \text{ else.} \end{cases} \tag{5.16}$$

That is, the transition probability from state $\underline{\boldsymbol{u}}$ to state $\underline{\boldsymbol{u}}'$ is proportional to the Boltzmann factor if the energy increases and does not depend on the energy difference if the energy decreases. The numbers $p_{\underline{\boldsymbol{u}}',\underline{\boldsymbol{u}}} \geq 0$ are arbitrary but have to fulfill

$$p_{\underline{\boldsymbol{u}}',\underline{\boldsymbol{u}}} = p_{\underline{\boldsymbol{u}},\underline{\boldsymbol{u}}'} \qquad \text{and} \qquad \sum_{\underline{\boldsymbol{u}}} p_{\underline{\boldsymbol{u}}',\underline{\boldsymbol{u}}} = 1 \quad . \tag{5.17}$$

The first relation directly follows from Eq. (5.15) together with Eq. (5.16). To make the second relation plausible, consider $\underline{\boldsymbol{u}}'$ to be the state with the maximum possible energy $E(\underline{\boldsymbol{u}}') = E_{\mathrm{max}}$. With this, we find for the energy differences $\Delta E = E(\underline{\boldsymbol{u}}') - E(\underline{\boldsymbol{u}}) > 0$ for all states $\underline{\boldsymbol{u}}$ and therefore $P(\underline{\boldsymbol{u}}'|\underline{\boldsymbol{u}}) = p_{\underline{\boldsymbol{u}}',\underline{\boldsymbol{u}}}$, $\forall \underline{\boldsymbol{u}}$. Then, the second relation in Eq. (5.17) follows from Eq. (5.13).

Fig. 5.1 depicts the transition probability of Eq. (5.16). For an implementation of the transition probability, a random variable $\xi \in [0, p_{\underline{\boldsymbol{u}}',\underline{\boldsymbol{u}}}]$ is required which decides whether a new state $\underline{\boldsymbol{u}}'$ is accepted or not: if ξ lies within the gray area in Fig. 5.1 for a certain energy difference ΔE, the new state is accepted, otherwise rejected. To make life easier, $p_{\underline{\boldsymbol{u}}',\underline{\boldsymbol{u}}} = 1$ and $\xi \in [0, 1]$ can always be chosen in a computer program.

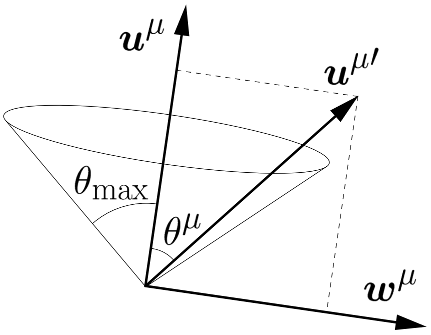

Figure 5.2: Trial step in the heat bath algorithm. The new spin direction $\boldsymbol{u}^{\mu\prime}$ is generated within a cone of opening angle $2\theta_{\max}$ around the old direction $\boldsymbol{u}^\mu$. The random unit vector $\boldsymbol{w}^\mu$ is perpendicular to $\boldsymbol{u}^\mu$.

In our Monte Carlo (MC) simulations of interacting moments in an external field $\boldsymbol{H}_{\text{ext}}$, we use the following heat bath algorithm:

1. Initial configuration parallel to $\boldsymbol{H}_{\text{ext}}$.
2. Randomly pick a spin $\boldsymbol{u}^\mu$.
3. Generate a new spin direction $\boldsymbol{u}^{\mu\prime}$ within a cone around $\boldsymbol{u}^\mu$ (trial step).
4. Compute the energy difference ΔE.
5. If $\Delta E < 0$, accept $\boldsymbol{u}^{\mu\prime}$ and return to step 2.
6. Else, compute $\exp(-\Delta E/k_{\text{B}}T)$.
7. Generate a random number $\xi \in [0, 1]$.
8. If $\xi < \exp(-\Delta E/k_{\text{B}}T)$, accept $\boldsymbol{u}^{\mu\prime}$ and return to step 2.
9. Else, the old spin direction is also the new one.

Since each loop (steps 2–9) is performed with just one magnetic moment, this method is called single spin update mechanism. The algorithm starts with a completely ordered ferromagnetic configuration parallel to the external field. However, to be sure that the results are independent of the starting configuration, we verified our calculations with initially frustrated moments.

We define one MC step as N trial steps as described above, where N is the number of magnetic moments. That is, on average every spin is considered once per MC step. For our simulations at temperatures well below the critical temperature T_C (Eq. (3.6)), the single spin update method is sufficient. Around T_C, the correlation length diverges and almost all single spin trial steps are rejected (critical slowing down). Then, cluster flipping methods are much more efficient, for instance the Wolff method which can be applied for continuous-spin models [38, 62]. However, this method fails for spin systems with anisotropy terms in the total energy. De Meo and Oh [17] solved this problem by modifying Wolff's algorithm. The remaining disadvantage of saving all spins of the cluster can be avoided by introducing interactions between the physical spins with a so-called ghost spin [58].

The rate of accepted trial steps strongly depends on the opening angle $2\theta_\mathrm{max}$ of the cone around $\boldsymbol{u}^\mu$. Particularly at low temperatures the major part of the trial steps may be rejected because ΔE is large compared to $k_\mathrm{B}T$. So, we start with $\theta_\mathrm{max} = 180^\circ$ (trial directions are chosen randomly on a sphere) and then adapt the "cone" to achieve maximum performance. After each MC step, θ_max is increased (decreased) by 2° whenever the acceptance rate exceeds (falls below) 50%. The new directions within the cone have to be chosen carefully in order to avoid artificial anisotropies. Otherwise, mean values of magnetization components which should be zero for symmetry reasons do not vanish due to an incorrect drift of the magnetization. We follow the suggestions of Serena *et al.* [55] to achieve an isotropic and homogeneous sampling probability inside the cone and calculate the new spin direction at site μ via

$$\boldsymbol{u}^{\mu\prime} = \boldsymbol{u}^\mu \cos\theta^\mu + \boldsymbol{w}^\mu \sin\theta^\mu \quad , \tag{5.18}$$

where $\boldsymbol{w}^\mu$ denotes a unit vector perpendicular to the original direction $\boldsymbol{u}^\mu$, see Fig. 5.2. A unit vector $\boldsymbol{\zeta}^\mu \neq \boldsymbol{u}^\mu$ is randomly chosen first, and then $\boldsymbol{w}^\mu$ is calculated via

$$\boldsymbol{w}^\mu = \frac{\boldsymbol{u}^\mu \times \boldsymbol{\zeta}^\mu}{|\boldsymbol{u}^\mu \times \boldsymbol{\zeta}^\mu|} \quad . \tag{5.19}$$

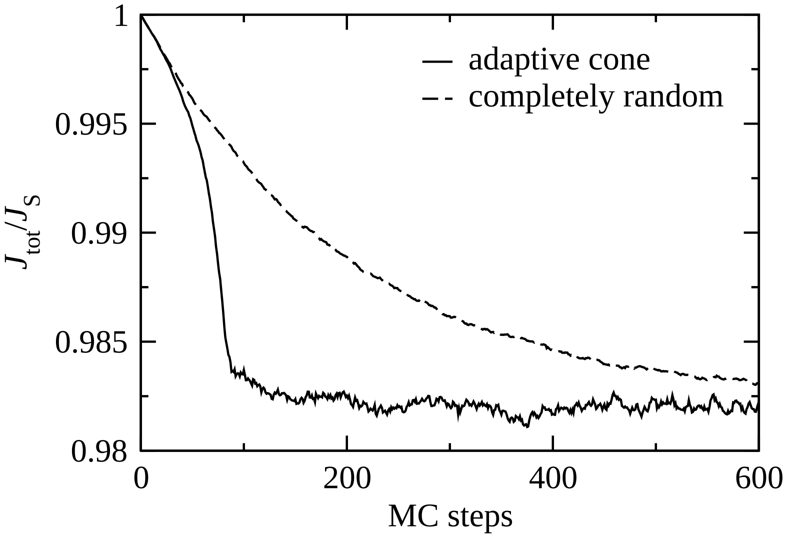

Figure 5.3: Comparison between adaptive cone method and completely random trial steps. The equilibration takes about 150 MC steps for the adaptive cone method, whereas approximately 1500 MC steps are required for trial steps randomly chosen on a sphere. The feedback algorithm of the adaptive method yielded an optimal angle of $\theta_{\max} \approx 13°$.

The rotation angle θ^μ is obtained from

$$\cos\theta^\mu = 1 + \xi^\mu \left(\cos\theta_{\max} - 1\right) \quad , \tag{5.20}$$

with the random number $\xi^\mu \in [0, 1]$.

In Fig. 5.3 we simulated a cube of 40 nm edge length with periodic boundary conditions and without strayfield interactions. The material parameters were chosen as $J_S = 1.76$ T, $K_1 = 4.5 \cdot 10^5$ J/m^3 (easy axis parallel z-axis), and $A = 1.3 \cdot 10^{-11}$ J/m. We subdivided the cube into 20^3 subcubes, each with 2 nm edge length, and started with a ferromagnetic configuration parallel to the z-axis. The results clearly show the advantage of the adaptive cone method. After about 150 MC steps the total magnetization already fluctuates around its equilibrium value whereas for completely random trial directions the equilibration takes about 1500 MC steps. For the chosen parameters, the feedback algorithm resulted in an optimal angle of $\theta_{\max} \approx 13°$.

Chapter 6

The Dynamic Equation

Brown [11] proposed a variational method to minimize the energy in continuous form (4.24), yielding the magnetization distribution in equilibrium, where the torque on the magnetization vanishes (see Sec. 4.2). A more physical description also accounts for the *dynamics* of the system, i.e. for the Larmor precession around the local magnetic field.

6.1 Dynamics at Zero Temperature

The starting point of any dynamic description of micromagnetic processes is the equation

$$\frac{\partial \boldsymbol{J}}{\partial t} = -\gamma\, \boldsymbol{J} \times \boldsymbol{H}_{\mathrm{eff}} \quad , \tag{6.1}$$

which can be obtained directly from the quantum mechanical expression for the precession of a magnetic moment around a magnetic field which is considered here to be the effective field, $\boldsymbol{H}_{\mathrm{eff}}$, of Eq. (4.47). $\boldsymbol{J}$ denotes the magnetic polarization vector, $\boldsymbol{J} = \mu_0 \boldsymbol{M}$, and is presumed to be a continuous function in space and time, $\boldsymbol{J} = \boldsymbol{J}(\boldsymbol{r}, t)$. $\gamma = \mu_0 g_{\mathrm{L}} |e| / 2 m_{\mathrm{e}} = g_{\mathrm{L}} \cdot 1,105 \cdot 10^5$ m/As is the gyromagnetic ratio ($\gamma > 0$).

Eq. (6.1) describes the undamped Larmor precession of the magnetization around the effective field with the Larmor frequency $\omega = \gamma H_{\mathrm{eff}}$ (usually in the GHz range). Since no losses have been taken into account the angle between

$\boldsymbol{J}$ and $\boldsymbol{H}_{\text{eff}}$ does not change. However, experiments show a relaxation of the magnetization towards equilibrium in a finite time due to damping processes. In the *Gilbert equation* [26]

$$\frac{\partial \boldsymbol{J}}{\partial t} = -\gamma\, \boldsymbol{J} \times \boldsymbol{H}_{\text{eff}} + \frac{\alpha}{J_{\text{S}}}\, \boldsymbol{J} \times \frac{\partial \boldsymbol{J}}{\partial t} \tag{6.2}$$

an additional term with the dimensionless damping factor α is introduced to describe dissipative phenomena. The phenomenological factor α combines all damping effects, like magnon-magnon and magnon-phonon interactions, interactions between localized and itinerant electrons, eddy currents and macroscopic discontinuities [52]. J_{S} denotes the spontaneous polarization.

Obviously, the dot product of $\boldsymbol{J}$ with the right hand side of Eq. (6.2) vanishes, and therefore

$$\boldsymbol{J} \cdot \frac{\partial \boldsymbol{J}}{\partial t} = \frac{1}{2}\frac{\partial \boldsymbol{J}^2}{\partial t} = 0 \quad . \tag{6.3}$$

Thus, $|\boldsymbol{J}| = J_{\text{S}} = \text{const.}$ for any point in the magnetic body is ensured during time evolution according to the Gilbert equation.

The Gilbert equation can be transformed into the older and mathematically equivalent *Landau-Lifshitz-Gilbert (LLG) equation* [2]

$$\frac{\partial \boldsymbol{J}}{\partial t} = -\gamma' \boldsymbol{J} \times \boldsymbol{H}_{\text{eff}} - \frac{\alpha\gamma'}{J_{\text{S}}}\, \boldsymbol{J} \times (\boldsymbol{J} \times \boldsymbol{H}_{\text{eff}}) \quad , \tag{6.4}$$

with

$$\gamma' = \frac{\gamma}{1+\alpha^2} \quad . \tag{6.5}$$

Eq. (6.4) has the general form of an ordinary differential equation (ODE), $\dot{\boldsymbol{y}} = f(\boldsymbol{y}, t)$. The damping term introduced by Landau and Lifshitz drives $\boldsymbol{J}$ towards the direction of the effective field until both vectors align parallel (see Fig. 6.1).

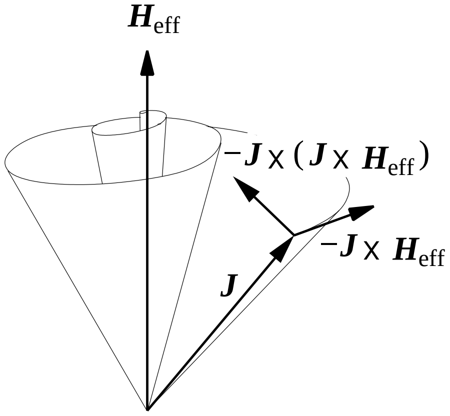
H_{eff}
$-J \times (J \times H_{\text{eff}})$
$-J \times H_{\text{eff}}$
J

Figure 6.1: Illustration of the Landau-Lifshitz-Gilbert-Eq. (6.4).

6.2 Stochastic Dynamics

Dynamic approaches based on the LLG Eq. (6.4) are probably the most common method for the simulation of magnetization processes at zero temperature. However, temperature effects in magnetic systems are often not negligible. For example, thermally activated magnetization reversal has become an important issue in magnetic recording due to rapidly increasing recording density and decreasing bit size [61]. In order to treat thermally activated processes in the framework of micromagnetics, Brown added a stochastic, thermal field, $\boldsymbol{H}_{\text{th}}$, to the effective field, $\boldsymbol{H}_{\text{eff}}$ [12]. It accounts for the interaction of the magnetic polarization $\boldsymbol{J}$ with the microscopic degrees of freedom (phonons, conducting electrons, nuclear spins, etc.) which causes fluctuations of the magnetic moments [24]. Those interactions are also responsible for the damping of the precession around the effective field, since dissipation and fluctuation are related via the fluctuation–dissipation theorem.

After adding the thermal field, we obtain the *stochastic Landau-Lifshitz-Gilbert (LLG) equation*

$$\frac{\partial \boldsymbol{J}}{\partial t} = -\gamma' \boldsymbol{J} \times (\boldsymbol{H}_{\text{eff}} + \boldsymbol{H}_{\text{th}}) - \frac{\alpha\gamma'}{J_{\text{S}}} \boldsymbol{J} \times (\boldsymbol{J} \times (\boldsymbol{H}_{\text{eff}} + \boldsymbol{H}_{\text{th}})) \quad , \tag{6.6}$$

which is a Langevin type stochastic differential equation with *multiplicative noise* and is similar to the Langevin equation of a Brownian particle in a viscous liquid [16]. The constraint $|\boldsymbol{J}| = J_\mathrm{S} = \text{const.}$ is still fulfilled. However, in reality the moment of a particle also fluctuates in its magnitude J_S, but the exchange interaction keeps fluctuations of J_S very small, and it can be neglected normally [12].

In order to solve the stochastic problem numerically, we have to replace the continuous solution in space by a discrete set of lattice points of a finite difference lattice (or nodes of a finite element mesh, respectively). Indicating lattice points by Greek indices and Cartesian components by Latin indices, we get

$$\frac{\partial \boldsymbol{J}^\mu}{\partial t} = -\gamma' \boldsymbol{J}^\mu \times (\boldsymbol{H}^\mu_\mathrm{eff} + \boldsymbol{H}^\mu_\mathrm{th}) - \frac{\alpha\gamma'}{J^\mu_\mathrm{S}}\, \boldsymbol{J}^\mu \times (\boldsymbol{J}^\mu \times (\boldsymbol{H}^\mu_\mathrm{eff} + \boldsymbol{H}^\mu_\mathrm{th})) \quad . \tag{6.7}$$

The effective field can be approximated using the box scheme [25],

$$\boldsymbol{H}^\mu_\mathrm{eff} = -\frac{1}{v^\mu}\frac{\partial E}{\partial \boldsymbol{J}^\mu} \quad , \tag{6.8}$$

and is given in Eq. (4.51) for finite differences with a regular cubic lattice.

In general, the spontaneous polarization (as well as the other parameters) may depend on $\boldsymbol{r}^\mu$. However, even for homogeneous materials a spatial discretization at finite temperatures lets the material parameters depend on the associated volume v^μ and therefore on the node position.

It is assumed that a large number of independent random variables (microscopic degrees of freedom) contribute to the thermal field. The *central limit theorem* [16] states that the sum of many such independent stochastic processes, each having arbitrary distribution functions, approaches a normally distributed random variable and thus validates the assumption that the thermal field is a *Gaussian random process.* Therefore, the thermal field is completely defined by its mean value

$$\left\langle H^\mu_{\mathrm{th},i}(t) \right\rangle = 0 \tag{6.9}$$

and its second moment or variance

$$\left\langle H^{\mu}_{\mathrm{th},i}(t) H^{\nu}_{\mathrm{th},j}(t')\right\rangle = 2D^{\mu}\delta_{ij}\delta^{\mu\nu}\delta(t-t') \quad . \tag{6.10}$$

Several assumptions are summarized in Eq. (6.10): The variance of the thermal field is isotropic in space, and the strength is given by the constant D^{μ}. Different components of the thermal field are uncorrelated, expressed by the Kronecker δ_{ij}. Usually, thermal fields acting on different magnetic moments are supposed to be uncorrelated, too, given by $\delta^{\mu\nu}$. The most important assumption is that the stochastic field is uncorrelated in time (Dirac δ in time), or – more precisely – has autocorrelation times much shorter than the rotational-response time of the system (factor ≈ 1000) and thus can be treated as *white noise*. (As the Fourier transform of $\exp(-i\omega t)$, $\delta(t)$ has the unit of an inverse time.) So, the spectral density of the stochastic field is independent of the frequency ω, leading to interesting consequences as discussed in the next section.

The strength of the thermal field, D^{μ}, is calculated in Sec. 6.4 via the Fokker-Planck equation. We will find the relation

$$D^{\mu} = \frac{\alpha k_{\mathrm{B}} T}{\gamma v^{\mu} J^{\mu}_{\mathrm{S}}} \quad , \tag{6.11}$$

which is a manifestation of the *fluctuation-dissipation theorem.*

It is convenient to split the stochastic LLG Eq. (6.6) into a deterministic part, governed by $\boldsymbol{H}_{\mathrm{eff}}$, and a stochastic one, driven by $\boldsymbol{H}_{\mathrm{th}}$ [54]:

$$\frac{\partial J^{\mu}_{i}}{\partial t} = B^{\mu}_{ik}(\boldsymbol{J}^{\mu}, t)\big(H^{\mu}_{\mathrm{eff},k}(\boldsymbol{J}^{\nu}, t) + H^{\mu}_{\mathrm{th},k}(t)\big) \quad , \tag{6.12}$$

where the matrix elements B^{μ}_{ik} read

$$\begin{aligned} B^{\mu}_{ik}(\boldsymbol{J}^{\mu}, t) &= -\gamma' \varepsilon_{ijk} J^{\mu}_{j} - \frac{\alpha\gamma'}{J^{\mu}_{\mathrm{S}}} \varepsilon_{ijk}\varepsilon_{klm} J^{\mu}_{j} J^{\mu}_{l} = \\ &= -\gamma' \varepsilon_{ijk} J^{\mu}_{j} - \frac{\alpha\gamma'}{J^{\mu}_{\mathrm{S}}} (J^{\mu}_{i} J^{\mu}_{k} - \delta_{ik} J^{\mu 2}_{\mathrm{S}}) \quad . \end{aligned} \tag{6.13}$$

With the definition

$$A_i^\mu(\boldsymbol{J}^\nu, t) = B_{ik}^\mu H_{\mathrm{eff},k}^\mu \quad , \tag{6.14}$$

we find the stochastic LLG equation in the form of a general Langevin equation,

$$\frac{\partial J_i^\mu}{\partial t} = A_i^\mu(\boldsymbol{J}^\nu, t) + B_{ik}^\mu(\boldsymbol{J}^\mu, t) H_{\mathrm{th},k}^\mu(t) \quad . \tag{6.15}$$

$A_i^\mu(\boldsymbol{J}^\nu, t)$ generally depends on the magnetization at all lattice sites $\boldsymbol{r}^\nu$ since exchange and dipole interactions enter in the effective field as non-local contributions.

6.3 The Fokker-Planck Equation

The stochastic Landau-Lifshitz-Gilbert equation (6.15) has the form of the general nonlinear Langevin equation for d time dependent stochastic variables $\boldsymbol{\xi}(t) = (\xi_1, \ldots, \xi_d)^{\mathrm{T}}$,

$$\dot{\xi}_i = h_i(\boldsymbol{\xi}, t) + g_{ij}(\boldsymbol{\xi}, t)\, \eta_j(t) \quad , \tag{6.16}$$

with the Langevin forces $\eta_j(t)$. If g_{ij} does not depend on $\boldsymbol{\xi}$, Eq. (6.16) is called a Langevin equation with additive noise. Otherwise one speaks of multiplicative noise.

$\eta_i(t)$ are Gaussian random forces with the mean values

$$\langle \eta_i(t) \rangle = 0 \tag{6.17}$$

and the correlation functions

$$\langle \eta_i(t) \eta_j(t') \rangle = 2\, \delta_{ij}\, \delta(t - t') \quad . \tag{6.18}$$

Since the Langevin forces $\eta_i(t)$ are uncorrelated in time, this kind of noise is called white noise, i.e. the spectral density of the Langevin forces, which for stationary processes is the Fourier transform of the correlation function

(Wiener-Khintchine theorem [48]), does not depend on the frequency ω.

It is convenient to use different symbols for random variables and their values. We use ξ_i for the stochastic variables and x_i for the values or realizations of ξ_i (for a certain time t the identity $\xi_i = x_i$ is valid). Any statistical property of $\boldsymbol{\xi}$ can be obtained from the probability density $W(\boldsymbol{x}, t)$ ($W(\boldsymbol{x}, t)\,\mathrm{d}\boldsymbol{x}$ denotes the probability that $\boldsymbol{\xi}$ takes a value within $[\boldsymbol{x}, \boldsymbol{x} + \mathrm{d}\boldsymbol{x}]$ at time t). Thus, the knowledge of $W(\boldsymbol{x}, t)$ completely determines the statistical properties of $\boldsymbol{\xi}$. A differential equation for the probability density $W(\boldsymbol{x}, t)$ can be derived via the Kramers-Moyal expansion, which will be carried out later on. We will see that this expansion with an infinite number of terms stops after the second term since Eq. (6.16) with δ-correlated Langevin forces η_i describes a Markov process [48]. This equation for the time evolution of the probability density $W(\boldsymbol{x}, t)$ is the Fokker-Planck equation.

Before dealing with the Kramers-Moyal expansion, we have a look at the classification of random processes and the different interpretations of stochastic differential equations.

6.3.1 Classification of Random Processes

A realization of $\boldsymbol{\xi}(t)$ for a certain time interval is a curve in a $\boldsymbol{\xi}(t)$-t space. Now we can ask for the conditional probability density of $\boldsymbol{\xi}$ at time t_n, $P(\boldsymbol{x}_n, t_n|\boldsymbol{x}_{n-1}, t_{n-1}; \ldots; \boldsymbol{x}_1, t_1)$, under the conditions that $\boldsymbol{\xi}$ has the values $\boldsymbol{x}_{n-1}$ at t_{n-1}, and $\boldsymbol{x}_{n-2}$ at t_{n-2}, ..., and $\boldsymbol{x}_1$ at the time t_1 (with $t_n > t_{n-1} > \ldots > t_1$) [25, 48]. In other words, $P(\boldsymbol{x}_n, t_n|\boldsymbol{x}_{n-1}, t_{n-1}; \ldots; \boldsymbol{x}_1, t_1)\,\mathrm{d}\boldsymbol{x}_n$ gives the probability that the random variable $\boldsymbol{\xi}$ has a value within $[\boldsymbol{x}_n, \boldsymbol{x}_n + \mathrm{d}\boldsymbol{x}_n]$ at t_n under the condition that the stochastic variable has the sharp value $\boldsymbol{\xi}(t_{n-1}) = \boldsymbol{x}_{n-1}$ and met $\boldsymbol{\xi}(t_i) = \boldsymbol{x}_i$, with $t_i = t_1, \ldots, t_{n-2}$, in the past. Therefore, the conditional probability density is also often called transition probability density.

The conditional probability density can be expressed by the probability densities W according to

$$P(\boldsymbol{x}_n, t_n | \boldsymbol{x}_{n-1}, t_{n-1}; \dots; \boldsymbol{x}_1, t_1) = \frac{W_n(\boldsymbol{x}_n, t_n; \dots; \boldsymbol{x}_1, t_1)}{W_{n-1}(\boldsymbol{x}_{n-1}, t_{n-1}; \dots; \boldsymbol{x}_1, t_1)} \quad . \tag{6.19}$$

This relation becomes clearer in the form

$$\begin{aligned} & W_n(\boldsymbol{x}_n, t_n; \dots; \boldsymbol{x}_1, t_1) = \\ & \quad = W_{n-1}(\boldsymbol{x}_{n-1}, t_{n-1}; \dots; \boldsymbol{x}_1, t_1)\, P(\boldsymbol{x}_n, t_n | \boldsymbol{x}_{n-1}, t_{n-1}; \dots; \boldsymbol{x}_1, t_1) = \\ & \quad = W_1(\boldsymbol{x}_1, t_1)\, P(\boldsymbol{x}_2, t_2 | \boldsymbol{x}_1, t_1)\, P(\boldsymbol{x}_3, t_3 | \boldsymbol{x}_2, t_2; \boldsymbol{x}_1, t_1) \dots \\ & \qquad \dots P(\boldsymbol{x}_n, t_n | \boldsymbol{x}_{n-1}, t_{n-1}; \dots; \boldsymbol{x}_1, t_1) \quad . \end{aligned} \tag{6.20}$$

With the conditional probability density, two equations can be built which are valid for all stochastic processes ($t_3 > t_2 > t_1$) [25]:

$$\begin{aligned} W(\boldsymbol{x}_2, t_2) &= \int \mathrm{d}\boldsymbol{x}_1\, P(\boldsymbol{x}_2, t_2 | \boldsymbol{x}_1, t_1)\, W(\boldsymbol{x}_1, t_1) \quad , & (6.21) \\ P(\boldsymbol{x}_3, t_3 | \boldsymbol{x}_1, t_1) &= \int \mathrm{d}\boldsymbol{x}_2\, P(\boldsymbol{x}_3, t_3 | \boldsymbol{x}_2, t_2; \boldsymbol{x}_1, t_1)\, P(\boldsymbol{x}_2, t_2 | \boldsymbol{x}_1, t_1) \quad . & (6.22) \end{aligned}$$

Wang and Uhlenbeck [60] classified three types of stochastic processes: Purely random processes, Markov processes, and general processes.

Purely random processes fulfill

$$P(\boldsymbol{x}_n, t_n | \boldsymbol{x}_{n-1}, t_{n-1}; \dots; \boldsymbol{x}_1, t_1) = P(\boldsymbol{x}_n, t_n) \quad , \tag{6.23}$$

i.e. the conditional probability density does not depend on the history of the stochastic variable $\boldsymbol{\xi}$.

For physical systems with continuous time t, the random variable $\boldsymbol{\xi}(t)$ has to be a continuous function of t. Thus, $\boldsymbol{\xi}(t_{n-1})$ and $\boldsymbol{\xi}(t_n)$ have to be correlated for small time intervals $t_n - t_{n-1}$. This is the reason why purely random processes can describe physical systems with continuous stochastic variables only in a limiting sense.

Markov processes are the next more complicated case. Here, the conditional probability density depends (besides on $\boldsymbol{\xi}(t_n) = \boldsymbol{x}_n$) only on the value of $\boldsymbol{\xi}$ at the previous time t_{n-1},

$$P(\boldsymbol{x}_n, t_n | \boldsymbol{x}_{n-1}, t_{n-1}; \ldots ; \boldsymbol{x}_1, t_1) = P(\boldsymbol{x}_n, t_n | \boldsymbol{x}_{n-1}, t_{n-1}) \quad . \tag{6.24}$$

The time interval $t_n - t_{n-1}$ is arbitrary. For small time intervals the transition probability strongly depends on the value $\boldsymbol{x}_{n-1}$ of the previous time step, whereas large time differences lead to a weak dependence on the history of $\boldsymbol{\xi}$.

For Markov processes, Eq. (6.22) reduces to the *Chapman-Kolmogorov equation* [48]

$$P(\boldsymbol{x}_3, t_3 | \boldsymbol{x}_1, t_1) = \int \mathrm{d}\boldsymbol{x}_2 \; P(\boldsymbol{x}_3, t_3 | \boldsymbol{x}_2, t_2) \, P(\boldsymbol{x}_2, t_2 | \boldsymbol{x}_1, t_1) \quad . \tag{6.25}$$

In reality Markov processes do not exist. But there are numerous physical processes with memory times small enough to validate the mathematical approximation of Markov as long as the typical response time of the system is much larger than the intrinsic memory time. The Langevin equation (6.16) with δ-correlated forces in time (Eq. (6.18)) describes such a Markov process since a first-order differential equation is uniquely determined by an initial value, and because a δ-correlated noise term at time t_{n-1} cannot change the transition probability at time t_n [48].

General processes have conditional probability densities at least depending also on $\boldsymbol{x}_2$ at t_2. However, a lot of non-Markovian processes can be considered as a projection of a higher-dimensional Markov process, i.e. taking into account additional random variables yields a more complex Markov process.

6.3.2 Interpretation of Stochastic Integrals

The system of Langevin equations (6.16) with δ correlated noise in time (Eq. (6.18)) is not completely defined mathematically. To see this, let us write Eq. (6.16) in the integral form

$$\xi_i(t+\tau) - x_i(t) = \int_t^{t+\tau} \mathrm{d}t' h_i(\boldsymbol{\xi}(t'), t') + \int_t^{t+\tau} \mathrm{d}t' g_{ij}(\boldsymbol{\xi}(t'), t')\, \eta_j(t') \qquad (6.26)$$

with the infinitesimal time interval τ and the sharp value $\boldsymbol{\xi}(t) = \boldsymbol{x}(t)$ [54, 42]. The first integral is a Riemann integral and becomes $h_i(\boldsymbol{x}(t), t)\,\tau$ for infinitesimal τ. The second one is a stochastic integral. Since each jump in the Langevin noise causes the stochastic variable to jump, it is not clear which value of $\boldsymbol{\xi}$ one should use in the function g_{ij}.

In the *Itô* interpretation of the stochastic integral the value of $\boldsymbol{\xi}$ at the beginning of the time interval is used [16]:

$$\xi_i(t+\tau) - x_i(t) = h_i(\boldsymbol{x}(t), t)\,\tau + g_{ij}(\boldsymbol{x}(t), t) \int_t^{t+\tau} \mathrm{d}t' \eta_j(t') \quad . \qquad (6.27)$$

Stratonovich's definition of the stochastic integral in Eq. (6.26) takes the mean of the values $\boldsymbol{\xi}(t) = \boldsymbol{x}(t)$ and $\boldsymbol{\xi}(t+\tau)$ – the value in the future:

$$\begin{aligned} \xi_i(t+\tau) - x_i(t) &= h_i(\boldsymbol{x}(t), t)\,\tau + \\ &+ g_{ij}\left(\frac{1}{2}(\boldsymbol{x}(t) + \boldsymbol{\xi}(t+\tau)), t + \frac{\tau}{2}\right) \int_t^{t+\tau} \mathrm{d}t' \eta_j(t') \quad . \end{aligned} \qquad (6.28)$$

From a mathematical point of view it is not clear whether Itô's or Stratonovich's or some other interpretation should be used. However, in physics the δ function for the noise correlation in time is usually replaced by the limit of a narrow function *symmetric* around the origin (white noise as a limit of colored noise with short autocorrelation time [54]), automatically leading to Stratonovich's interpretation of the stochastic problem (see also App. B).

In thermal equilibrium the magnetization vector as a solution of the stochastic LLG equation (6.15) has to fulfill the Maxwell-Boltzmann distribution. We will see, that the Maxwell-Boltzmann distribution is a stationary solution of the Stratonovich Fokker-Planck equation in Cartesian coordinates.

This is not the case for the Fokker-Planck equation in Itô interpretation [42].

For these reasons we use the Stratonovich interpretation of stochastic integrals throughout this work.

6.3.3 Kramers-Moyal Expansion

In this section we carry out the Kramers-Moyal forward expansion, using the general expression (6.21), and closely follow Risken [48]. (The Kramers-Moyal backward expansion starts from the Chapman-Kolmogorov equation (6.25). In Ref. [48] the equivalence of both ways is shown.) For simplicity reasons we first consider the one-dimensional case with the stochastic variable $\xi(t)$ and generalize the results afterwards.

Let us write Eq. (6.21) in the form

$$W(x,t+\tau) = \int \mathrm{d}x'\, P(x,t+\tau|x',t)\, W(x',t) \quad , \tag{6.29}$$

with $\tau \geq 0$. With $x'' = x - x'$ and the Taylor expansion of the integrand of Eq. (6.29),

$$\begin{aligned} P(x,t+\tau|x',t)\, W(x',t) &= P(x+x''-x'',t+\tau|x-x'',t)\, W(x-x'',t) = \\ &= \sum_{n=0}^{\infty} \frac{x''^n}{n!} (-\partial_x)^n P(x+x'',t+\tau|x,t)\, W(x,t) \end{aligned} \tag{6.30}$$

(∂_x means the derivative $\partial/\partial x$), we can write Eq. (6.29) in the form

$$\begin{aligned} &W(x,t+\tau) = \\ &\quad = \sum_{n=0}^{\infty} \frac{(-\partial_x)^n}{n!}\, W(x,t) \int \mathrm{d}x'\, (x-x')^n P(2x-x',t+\tau|x,t) \quad . \end{aligned} \tag{6.31}$$

Finally, with $y = 2x - x'$ we get the expression

$$W(x,t+\tau) = \sum_{n=0}^{\infty} \frac{(-\partial_x)^n}{n!}\, W(x,t) \underbrace{\int \mathrm{d}y\,(y-x)^n P(y,t+\tau|x,t)}_{=\langle(\xi(t+\tau)-\xi(t))^n\rangle\big|_{\xi(t)=x}} \quad . \tag{6.32}$$

The integral in Eq. (6.32) is the n-th moment $M^{(n)}(x,t,\tau)$ of $(\xi(t+\tau)-\xi(t))$ under the condition $\xi(t) = x$.

Let us assume the existence of the Taylor expansion with respect to τ,

$$M^{(n)}(x,t,\tau) = M^{(n)}(x,t,0) + \tau \frac{\partial}{\partial\tau} M^{(n)}(x,t,\tau)\big|_{\tau=0} + \mathcal{O}(\tau^2) \quad . \tag{6.33}$$

Using the definition of the Kramers-Moyal coefficients

$$\begin{aligned} K^{(n)}(x,t) &= \frac{1}{n!}\frac{\partial}{\partial\tau} M^{(n)}(x,t,\tau)\big|_{\tau=0} = \\ &= \frac{1}{n!}\lim_{\tau\to 0}\frac{1}{\tau}\Big\langle\, (\xi(t+\tau)-\xi(t))^n \,\Big\rangle\Big|_{\xi(t)=x} \end{aligned} \tag{6.34}$$

and the fact that the first term in Eq. (6.33) vanishes due to the initial value $P(x,t|x',t) = \delta(x-x')$, we arrive at

$$\begin{aligned} &W(x,t+\tau) - W(x,t) = \\ &= \sum_{n=1}^{\infty}\frac{(-\partial_x)^n}{n!}\left(K^{(n)}(x,t)\,\tau + \mathcal{O}(\tau^2)\right) W(x,t) \quad . \end{aligned} \tag{6.35}$$

With $\tau \to 0$ we finally obtain a differential equation for the time evolution of the probability density – the *Kramers-Moyal expansion*:

$$\frac{\partial}{\partial t} W(x,t) = \underbrace{\sum_{n=1}^{\infty}(-\partial_x)^n K^{(n)}(x,t)}_{=L_{\mathrm{KM}}(x,t)}\; W(x,t) = L_{\mathrm{KM}}(x,t)\, W(x,t) \quad , \tag{6.36}$$

where $L_{\mathrm{KM}}(x,t)$ denotes the Kramers-Moyal operator.

For d dimensions with $\boldsymbol{\xi}(t) = (\xi_1,\ldots,\xi_d)^{\mathrm{T}}$, the derivation of the Kramers-

Moyal expansion is very similar to the one-dimensional case and yields

$$\begin{aligned}\frac{\partial}{\partial t}W(\boldsymbol{x},t) &= \underbrace{\sum_{n=1}^{\infty}(-1)^n\partial_{i_1}\dots\partial_{i_n}K^{(n)}_{i_1\dots i_n}(\boldsymbol{x},t)}_{=L_{\mathrm{KM}}(\boldsymbol{x},t)}\,W(\boldsymbol{x},t) = \\ &= L_{\mathrm{KM}}(\boldsymbol{x},t)\,W(\boldsymbol{x},t) \quad , \qquad (6.37)\end{aligned}$$

where we used $\partial_k = \partial/\partial x_k$. The Kramers-Moyal coefficients are given by

$$K^{(n)}_{i_1\dots i_n}(\boldsymbol{x},t) = \frac{1}{n!}\lim_{\tau\to 0}\frac{1}{\tau}\Big\langle \prod_{j=1}^{n}\big(\xi_{i_j}(t+\tau)-\xi_{i_j}(t)\big)\Big\rangle\Big|_{\boldsymbol{\xi}(t)=\boldsymbol{x}} \quad . \qquad (6.38)$$

6.3.4 Markov Processes and Fokker-Planck Equation

The process described by the Langevin equations (6.16) with the δ-correlated forces in time (Eq. (6.18)) is a Markov process, and the associated Kramers-Moyal expansion (6.37) stops after the second term. A derivation of the Kramers-Moyal coefficients for the one-dimensional case is given in App. B. For the general d dimensional process the calculation is very similar to the one-dimensional case. The additional condition that different degrees of freedom of the Langevin forces are uncorrelated (δ_{ij} in Eq. (6.18)) enters in the calculation wherever the variance of the noise occurs (see Eq. (B.8) and Eq. (B.11)). The Kramers-Moyal coefficients (6.38) in *Stratonovich* interpretation then read [48]

$$\begin{aligned}K^{(1)}_{i}(\boldsymbol{x},t) &= h_i(\boldsymbol{x},t) + g_{kj}(\boldsymbol{x},t)\partial_k g_{ij}(\boldsymbol{x},t) \qquad (6.39)\\ K^{(2)}_{ij}(\boldsymbol{x},t) &= g_{ik}(\boldsymbol{x},t)\,g_{jk}(\boldsymbol{x},t) = K^{(2)}_{ji}(\boldsymbol{x},t) \qquad (6.40)\\ K^{(n)}_{i_1\dots i_n}(\boldsymbol{x},t) &= 0 \ , \quad \forall n \geq 3 \quad . \qquad (6.41)\end{aligned}$$

In this case the, Kramers-Moyal expansion for the time evolution of the probability density function is called the *Fokker-Planck equation*,

$$\frac{\partial}{\partial t}W(\boldsymbol{x},t) = \Big(-\partial_i K^{(1)}_{i}(\boldsymbol{x},t) + \partial_i\partial_j K^{(2)}_{ij}(\boldsymbol{x},t)\Big)\,W(\boldsymbol{x},t) \quad , \qquad (6.42)$$

with the *drift vector* $K_i^{(1)}(\boldsymbol{x},t)$ and the *diffusion matrix* $K_{ij}^{(2)}(\boldsymbol{x},t)$.

6.4 Thermal Field Strength

The Fokker-Planck equation in Stratonovich interpretation associated with the stochastic Landau-Lifshitz-Gilbert equation (6.15) was originally derived by Brown [12] for an *isolated* single domain particle (single magnetic moment without interactions). It describes the time evolution of the non-equilibrium probability density distribution $W(\boldsymbol{J},t)$ of the orientation of a single magnetic polarization vector $\boldsymbol{J}$.

By comparing the set of general Langevin equations (6.16) and their noise terms given by Eq. (6.17) and (6.18) with the stochastic LLG equation (6.15) together with Eq. (6.9) and (6.10), we obtain the required substitutions

$$\begin{aligned} \boldsymbol{\xi},\, \boldsymbol{x} &\hat{=} \boldsymbol{J} && (6.43)\\ h_i(\boldsymbol{\xi},t) &\hat{=} A_i(\boldsymbol{J},t) && (6.44)\\ g_{ij}(\boldsymbol{\xi},t) &\hat{=} \sqrt{D}\, B_{ij}(\boldsymbol{J},t) && (6.45) \end{aligned}$$

for the Kramers-Moyal coefficients (6.39) and (6.40) for a *single magnetic moment*. Using $\partial_k = \partial/\partial J_k$, the Fokker-Planck equation in Stratonovich interpretation reads

$$\begin{aligned} \frac{\partial}{\partial t} W &= -\partial_i(A_i + D \underbrace{B_{kj}\partial_k B_{ij}}_{=B_{jk}\partial_j B_{ik}} - D \underbrace{\partial_j B_{ik} B_{jk}}_{\substack{=B_{ik}\partial_j B_{jk}- \\ -B_{jk}\partial_j B_{ik}}})W = \\ &= -\partial_i(A_i W - D W B_{ik}\partial_j B_{jk} - D B_{ik} B_{jk}\partial_j W) \quad . \qquad (6.46) \end{aligned}$$

After some vector algebra and applying Eq. (6.13), we easily obtain

$$B_{ik}\partial_j B_{jk} = 0 \qquad (6.47)$$

and thus arrive at

$$\frac{\partial}{\partial t} W = -\partial_i (A_i - D B_{ik} B_{jk} \partial_j) W \quad , \tag{6.48}$$

with

$$B_{ik} B_{jk} = \gamma'^2 (1 + \alpha^2)(J_\mathrm{S}^2 \delta_{ij} - J_i J_j) \quad . \tag{6.49}$$

For a given initial distribution function $W_\mathrm{init}(\boldsymbol{J})$, the Fokker-Planck equation (6.48) describes the time evolution of W (on the surface of a sphere, since $|\boldsymbol{J}| = J_\mathrm{S} = \mathrm{const.}$) until it reaches the equilibrium distribution density $W_0(\boldsymbol{J})$ with $\partial W_0 / \partial t = 0$. For physical reasons, this stationary solution of Eq. (6.48) has to be the Maxwell-Boltzmann distribution [24]

$$W_0(\boldsymbol{J}) \propto \exp(-\beta E(\boldsymbol{J})) \quad , \tag{6.50}$$

with $\beta = (k_\mathrm{B} T)^{-1}$, leading to a condition for the variance D of the thermal field $\boldsymbol{H}_\mathrm{th}$.

Utilizing Eq. (6.14) and $v H_{\mathrm{eff},i} = -\partial_i E$ (Eq. (4.50)), the first term in Eq. (6.48) reads for $W = W_0$:

$$\begin{aligned} -\partial_i A_i W_0 \;&=\; \gamma' \varepsilon_{ijk} \underbrace{\Big(H_{\mathrm{eff},k} W_0 \underbrace{\partial_i J_j}_{=\delta_{ij}} + J_j W_0 \partial_i \underbrace{H_{\mathrm{eff},k}}_{=-v^{-1}\partial_k E} + J_j H_{\mathrm{eff},k} \underbrace{\partial_i W_0}_{=\beta v H_{\mathrm{eff},i} W_0}\Big)}_{=0} + \\ &\quad + \partial_i \frac{\alpha \gamma'}{J_\mathrm{S}} (J_i J_k - \delta_{ik} J_\mathrm{S}^2) H_{\mathrm{eff},k} W_0 \quad . \end{aligned} \tag{6.51}$$

Finally, we use Eq. (6.49) and obtain

$$\frac{\partial}{\partial t} W_0 = 0 = \underbrace{\left(\frac{\alpha \gamma'}{J_\mathrm{S}} - D \beta v \gamma'^2 (1 + \alpha^2) \right)}_{=0} \partial_i (J_i J_k - \delta_{ik} J_\mathrm{S}^2) H_{\mathrm{eff},k} W_0 \quad , \tag{6.52}$$

with the solution

$$D = \frac{\alpha k_\mathrm{B} T}{\gamma v J_\mathrm{S}} \quad . \tag{6.53}$$

Eq. (6.53) is a special form of the *fluctuation-dissipation theorem*, which relates the variance of thermal fluctuations and the damping parameter.

The strength of the thermal noise, Eq. (6.53), was derived for an *isolated* magnetic moment. Nevertheless, the generalized form

$$D^{\mu} = \frac{\alpha k_{\mathrm{B}} T}{\gamma v^{\mu} J_{\mathrm{S}}^{\mu}} \quad , \tag{6.54}$$

is used in every temperature dependent computation of magnetization dynamics, with or without interactions between magnetic moments on different lattice sites $\boldsymbol{r}^{\mu}$. It is still a topic of discussion whether interactions between magnetic moments introduce correlations in the thermal field between different lattice sites or not. For example, Chubykalo *et al.* [15] took into account interactions in the effective field and linearized the stochastic LLG equation near equilibrium under the assumption of small fluctuations. They found that interactions of magnetic moments do not lead to correlations in the thermal field and that the fluctuation-dissipation theorem (6.54) is valid for interacting moments. Lyberatos *et al.* obtained the same result in the limit of small fluctuations [40]. However, Berkov and Gorn [5, 7] claimed that thermal bath correlations for ultrafast processes introduce correlations of the thermal field, which originate from the discretization of the physical problem. They found correlations in space and time with alternating sign as discretization changes.

6.5 Heun Method

For the time integration of the Langevin Eq. (6.15) we use the Heun scheme, which is a predictor-corrector method with second order accuracy in time [24, 54]. The stochastic Heun algorithm converges in quadratic mean to the solution of the system of stochastic differential equations (6.15) in *Stratonovich interpretation.*

The predictor $\bar{\boldsymbol{J}}^{\mu}$ for the polarization vector at lattice site $\boldsymbol{r}^{\mu}$ is given by an Euler type integration,

$$\bar{J}_i^\mu = J_i^\mu(t) + A_i^\mu(\boldsymbol{J}^\nu, t)\Delta t + B_{ik}^\mu(\boldsymbol{J}^\mu, t)\Delta W_k^\mu(t) \quad , \tag{6.55}$$

with the discretization time step Δt and the Gaussian random numbers

$$\Delta W_i^\mu = \int_t^{t+\Delta t} \mathrm{d}t' \, H_{\mathrm{th},i}^\mu(t') \quad . \tag{6.56}$$

The mean value of $\Delta W_i^\mu(t)$ is

$$\langle \Delta W_i^\mu(t) \rangle = 0 \quad , \tag{6.57}$$

and together with Eq. (6.10) and Eq. (A.4) we find for the variance

$$\langle \Delta W_i^\mu(t) \Delta W_j^\nu(t') \rangle = \int_t^{t+\Delta t} \mathrm{d}t'' \underbrace{\int_{t'}^{t'+\Delta t} \mathrm{d}t''' \left\langle H_{\mathrm{th},i}^\mu(t'') H_{\mathrm{th},j}^\nu(t''') \right\rangle}_{=2D^\mu \delta_{ij} \delta^{\mu\nu} [\Theta(t'+\Delta t - t'') - \Theta(t'-t'')]} \quad . \tag{6.58}$$

The Θ functions in square brackets demand for $t'' \in [t', t' + \Delta t]$. For successive time steps Δt the time intervals $[t, t + \Delta t]$ and $[t', t' + \Delta t]$ do not overlap for $t \neq t'$, and we thus arrive at

$$\langle \Delta W_i^\mu(t) \Delta W_j^\nu(t') \rangle = \begin{cases} 2D^\mu \Delta t \, \delta_{ij} \delta^{\mu\nu} & \text{for } t = t', \\ 0 & \text{else.} \end{cases} \tag{6.59}$$

The variance of the thermal field in the discretized form then reads for $t = t'$

$$\langle H_{\mathrm{th},i}^\mu H_{\mathrm{th},j}^\nu \rangle = 2D^\mu \Delta t^{-1} \, \delta_{ij} \delta^{\mu\nu} \quad , \tag{6.60}$$

which is consistent with an approximation of the Dirac δ in Eq. (6.10) for small Δt by a narrow rectangle (see Eq. (A.1)),

$$\delta(t) \approx \frac{1}{\Delta t} \big(\Theta\left(t + \Delta t/2\right) - \Theta\left(t - \Delta t/2\right) \big) \quad . \tag{6.61}$$

Finally, the corrector step reads

$$\begin{aligned} J_i^\mu(t+\Delta t) &= J_i^\mu(t) + \frac{1}{2}\left(A_i^\mu(\bar{\boldsymbol{J}}^\nu, t+\Delta t) + A_i^\mu(\boldsymbol{J}^\nu, t)\right)\Delta t + \\ &\quad + \frac{1}{2}\left(B_{ik}^\mu(\bar{\boldsymbol{J}}^\mu, t+\Delta t) + B_{ik}^\mu(\boldsymbol{J}^\mu, t)\right)\Delta W_k^\mu \quad , \qquad (6.62) \end{aligned}$$

with the same Gaussian random numbers ΔW_k^μ as used for the calculation of the predictor $\bar{\boldsymbol{J}}^\mu$.

The time step Δt for the Heun method should be at most 1/30th of the precession time $t_\mathrm{p} = 2\pi/\omega = 2\pi/\gamma H_\mathrm{eff}$ of the magnetization vector in the effective field [51]. Without strayfield, $\Delta t = 0.1$ ps turned out to be sufficient, whereas with strayfield the time step often has to be much smaller (0.01 ps or even 1 fs).

Chapter 7

Influence of Discretization

In Sec. 4.1 we derived expressions for the energy terms suitable for the method of finite differences assuming small deviations between neighboring moments. The lattice spacing Δx for a regular cubic lattice appears in all energy contributions and affects the simulation results. Small lattice spacings are necessary to resolve domain walls and high frequency spin waves. For instance, Igarashi *et al.* [35] performed simulations of perpendicular recording media and pointed out the necessity to use small computational cells in order to achieve correct results. Usually, discretization lengths below the exchange length

$$l_{\mathrm{exch}} = \sqrt{\frac{2\mu_0 A}{J_{\mathrm{S}}^2}} \tag{7.1}$$

are supposed to be sufficient [47]. Other authors, for instance Tsiantos *et al.* [57], claim that the discretization length Δx has to be smaller than the minimum of l_{exch} and the thermal exchange length

$$l_{\mathrm{thex}} = \sqrt{\frac{A}{J_{\mathrm{S}}\sigma_{\mathrm{th}}}} \quad , \tag{7.2}$$

where

$$\sigma_{\mathrm{th}} = \sqrt{\frac{2\alpha k_{\mathrm{B}} T}{\Delta t \gamma J_{\mathrm{S}} \Delta x^3}} \tag{7.3}$$

is the standard deviation of the thermal field (see Eq. (6.60)). However, the thermal exchange length often lies in the atomistic range and is thus beyond the micromagnetic regime.

In this chapter we perform Metropolis Monte Carlo and Langevin simulations of an array of N^3 non-atomistic magnetic moments and investigate the influence of the lattice spacing Δx on the equilibrium properties of the magnetic system. The results are compared in terms of the mean value of the total magnetization,

$$\langle u_i \rangle \equiv \frac{\langle M_i \rangle}{M_\mathrm{S}} = \frac{1}{N^3} \sum_{\mu=1}^{N^3} u_i^\mu \quad . \tag{7.4}$$

7.1 Geometry and Material Parameters

We simulate a cubic ensemble of interacting moments with a uniaxial anisotropy parallel to the z-axis. The material parameters are chosen as $K_1 = 4.5 \cdot 10^5$ J/m^3, $J_\mathrm{S} = 1.76$ T, and $A = 1.3 \cdot 10^{-11}$ J/m. The moments are exposed to an external field of $\mu_0 H_\mathrm{ext} = 0.1$ T in $+z$-direction. We start with a ferromagnetic configuration parallel to $\boldsymbol{H}_\mathrm{ext}$ and apply $T = 300$ K. Since the damping constant α in the stochastic LLG equation (6.12) does not affect the equilibrium properties of magnetic systems [14], the relatively large value of $\alpha = 1$ is used to reduce the equilibration time. A cube of 20 nm edge length is discretized into N^3 subcubes of size Δx. Open boundary conditions are applied in all directions.

For the MC simulations we discard the first 10^4 MC steps to ensure equilibration and fluctuation around equilibrium, although a much smaller number would also be sufficient for the simulations without strayfield interaction. The next 10^5 steps are then used for averaging. The Langevin simulations are performed with a time step of $\Delta t = 0.1$ ps. We execute $2 \cdot 10^6$ time steps and exclude the first 10^5 steps from averaging. For this particular set of parameters, smaller time steps had no influence on the results of the Langevin simulations with or without strayfield interaction. For instance, the difference

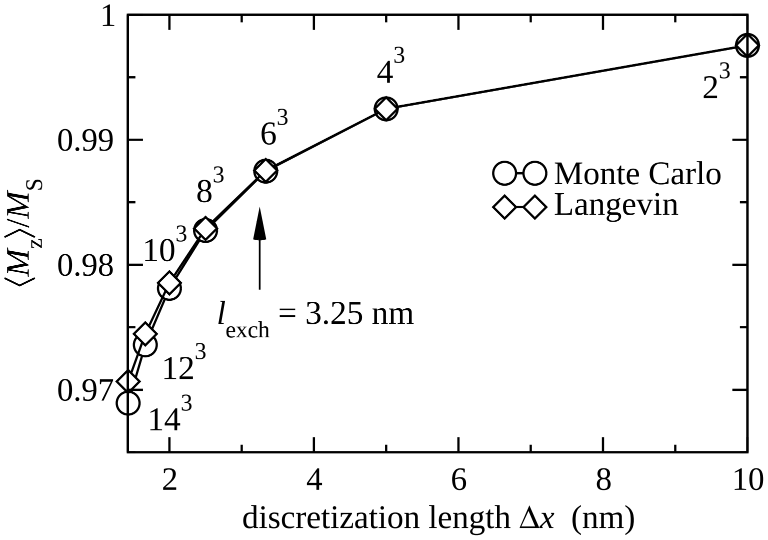

Figure 7.1: Magnetization parallel to the external field axis as a function of the discretization length Δx at $T = 300$ K without strayfield interaction. The numbers in the diagram indicate the number of subcubes. The difference between MC and stochastic LLG simulations is negligible for all cell sizes. $\langle M_z \rangle$ decreases with decreasing Δx which cannot be attributed to the thermal field in the Langevin simulations.

in $\langle M_z \rangle$ between simulations with $\Delta t = 0.1$ ps and $\Delta t = 0.01$ ps at $\Delta x = 5$ nm is only 0.004% when strayfield interaction is taken into account.

The chosen parameters lead to an exchange length of $l_{\mathrm{exch}} = 3.25$ nm. The condition that the discretization length fulfills at least $\Delta x = l_{\mathrm{thex}}$ yields $\Delta x = 0.26$ nm and is thus not applicable.

7.2 Results and Discussion

The mean value of the magnetization parallel to the z-axis as a function of Δx for the simulations without strayfield interaction is given in Fig. 7.1. With both simulation methods, $\langle u_x \rangle = \langle u_y \rangle = 0$ is found due to symmetry reasons in the case of lacking dipole interaction.

The results reveal an excellent agreement between MC and stochastic LLG

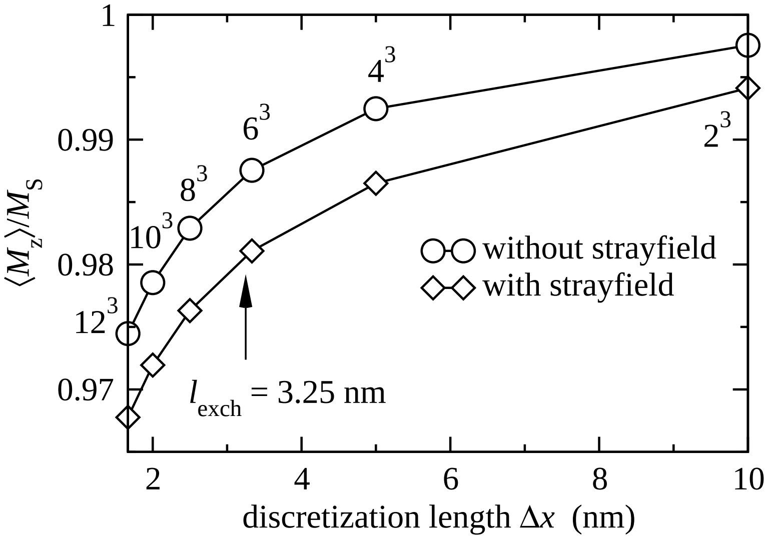

Figure 7.2: Comparison of the magnetization parallel to the external field axis as a function of the discretization length Δx between stochastic LLG simulations with and without strayfield interaction at $T = 300$ K. The numbers in the diagram indicate the number of subcubes. $\langle M_z \rangle$ obtained from simulations with dipole interaction decreases with respect to the results without strayfield interaction due to the principle of pole avoidance [2].

simulations for all cell sizes. Only for very small discretization lengths there are differences in the equilibrium property $\langle u_z \rangle$. However, at $\Delta x = 1.43$ nm (14^3 subcubes), the difference is only 0.2% and thus negligible.

The behavior of $\langle u_z \rangle$ as a function of Δx is, however, everything else but satisfying. The magnetization decreases with decreasing cell size and does not converge for small cell sizes. In particular, using cell sizes below the exchange length $l_{\text{exch}} = 3.25$ nm has no positive effect on the simulation results.

Fig. 7.2 compares the results of the Langevin simulations with and without strayfield interaction. The mean value $\langle u_z \rangle$ decreases when the strayfield interaction is turned on because the magnetic system tries to avoid free magnetic poles on the surface [2]. Apart from that, the general behavior of the magnetization as a function of cell size is the same with or without strayfield interaction. The MC calculations with strayfield again yielded only negligible differences (for instance 0.006% at $\Delta x = 5$ nm) and are not presented in this picture. In general, the mean values of the other components do not vanish anymore since asymmetric spin configurations are possibly more favorable in terms of total energy. Anyhow, since $\langle u_z \rangle$ is close to 1 for all discretization lengths, the deviations of $\langle u_x \rangle$ and $\langle u_y \rangle$ from zero, respectively, between simulations with and without dipole interaction are very small.

Using other material parameters and temperatures always results in an excellent agreement between MC and stochastic LLG simulations for all cell sizes and temperatures and point out that both methods coincide very well down to a cell size of at least 1.5 nm. The equilibrium magnetization parallel to the external field always decreases for decreasing discretization length, and no convergence can be found for $\Delta x < l_{\mathrm{exch}}$. The agreement between MC and Langevin simulations points out that the behavior of $\langle M_z \rangle$ cannot be attributed to the thermal field in the stochastic LLG simulations. In addition, Fig. 7.2 clearly shows that the temperature was relatively low, ensuring validity of the variance of $\boldsymbol{H}_{\mathrm{th}}$, since Eq. (6.10) is strictly speaking only valid in the linear regime of exchange coupled magnetic moments.

To obtain cell size independent results it is necessary to use a coarse-graining procedure for the material parameters, applicable for both MC and stochastic LLG simulations.

Chapter 8

Coarse-graining

In the last chapter we pointed out that micromagnetic simulations at nonzero temperatures depend on the computational cell size, introduced by the exchange coupling of the magnetic moments. The problem of cell size dependencies arises since the common assumption of micromagnetics that the computational cells contain enough magnetic moments to permit the use of statistics [8], is clearly violated for small cells. The experimentally measured, only temperature dependent values for the material parameters are valid unless the number of atoms within a computational cell becomes too small. Then, statistical averages over the cell volume will give parameters depending not only on the temperature, but also on the cell size, i.e. on the discretization length Δx.

In this chapter we propose a coarse-graining procedure for small computational cells to achieve cell size independent results. Starting on an atomistic level, we extract material parameters depending on the discretization length and suggest to use them for non-atomistic simulations. For physical reasons we first look at the spontaneous magnetization as function of cell size and consider anisotropy and exchange constants afterwards (however, the order of deriving scaling laws is not uniquely defined).

8.1 Atomistic Monte Carlo Simulations

To compute the material parameters as a function of temperature and cell size, we first perform Metropolis MC simulations of a cubic spin array on an atomistic level. We use a three-dimensional discrete Heisenberg model of exchange-coupled magnetic moments localized on a primitive cubic lattice in an isotropic external field $\boldsymbol{H}_{\text{ext}} = H_{\text{ext}}\hat{\boldsymbol{z}}$. The easy axis is also parallel to the z-axis. Periodic boundary conditions are applied in all directions, and dipole interactions are neglected. Thus, the total energy E of the magnetic system reads

$$E = E_{\text{exch}} + E_{\text{ani}} + E_{\text{ext}} \quad . \tag{8.1}$$

The different contributions to E are discussed in detail in Chap. 3.

Although the spontaneous magnetization and the exchange constant are only reasonable for volumes larger than the atomic unit cell, Eq. (3.4) and Eq. (4.9) can be used for the substitutions $JS^2 = A_0\, a$ and $g_{\text{L}}\mu_{\text{B}}S = M_{\text{S},0}\, a^3$ in the total energy. The index “0” indicates that the parameters are used for simulations on an atomistic level. Consistently, the atomistic anisotropy constant $K_{1,0}$ can be introduced, arriving at

$$\begin{aligned} E \;=\; & -A_0\, a \sum_{\mu=1}^{N^3} \sum_{\nu \in \text{nn}} \boldsymbol{u}^{\mu} \cdot \boldsymbol{u}^{\nu} + K_{1,0}\, a^3 \sum_{\mu=1}^{N^3} \left(1 - (\hat{\boldsymbol{z}} \cdot \boldsymbol{u})^2\right) \\ & -\mu_0 M_{\text{S},0}\, a^3 H_{\text{ext}} \hat{\boldsymbol{z}} \cdot \sum_{\mu=1}^{N^3} \boldsymbol{u}^{\mu} \quad . \end{aligned} \tag{8.2}$$

N denotes the number of spins in one direction, and the sum over ν is carried out over the 6 nearest neighbor moments.

In the center of the cubic spin array an averaging cube with n^3 atomistic spins and an edge length of $\Delta x = na$ is used to derive magnetic properties after equilibration. In particular, we extract the (normalized) spontaneous magnetization as a function of cell size [10],

$$M_{\mathrm{S,cell}} = \left\langle \sum_{i=1}^{3} {M_i}^2 \right\rangle^{1/2} \quad , \tag{8.3}$$

and $\langle M_z \rangle$, the averaged magnetization per moment parallel to the z-axis, for a given temperature T. M_i denotes the Cartesian components of the total magnetization within the averaging cube,

$$M_i = \frac{M_{\mathrm{S},0}}{n^3} \sum_{\mu=1}^{n^3} u_i^{\mu} \quad . \tag{8.4}$$

The mean values $\langle M_x \rangle$ and $\langle M_y \rangle$ vanish for symmetry reasons. Fig. 8.1 depicts the arrangement of the atomistic MC simulations.

To illustrate our coarse-graining method, the material parameters are chosen as $\mu_0 M_{\mathrm{S},0} = 1.76$ T, $A_0 = 1.3 \cdot 10^{-11}$ J/m, $K_{1,0} = 4.5 \cdot 10^5$ J/m^3, and $a = 0.376$ nm. With Eq. (3.6), a mean field critical temperature of $T_{\mathrm{C}}^{\mathrm{mf}} = 884.4$ K can be obtained. An external field of 0.1 T is applied to ensure that the whole system does not switch thermally to the negative z-direction. However, we will see that the external field strength only affects $\langle M_z \rangle$ and that the influence on the spontaneous magnetization is negligible. The system size is mainly based on the exchange length, Eq. (7.1), and thus on the exchange constant. For this particular set of parameters, we obtain $l_{\mathrm{exch}} = 3.25$ nm and use $N^3 = 60^3$, whereas the size of the central averaging cube is $n = 1, 2, 4, 6, \ldots, 30$. The properly chosen system size ensures that the equilibrium quantities within the averaging cube neither depend on the total number of moments, N^3, nor on the boundary conditions. The MC algorithm starts with a completely ordered ferromagnetic configuration parallel to the external field. For every temperature T we discard the first 10^4 MC steps and use the next 10^5 steps for averaging.

To summarize, the idea is to start at an atomistic level and evaluate rescaled material parameters for non-atomistic simulations with a discretization length

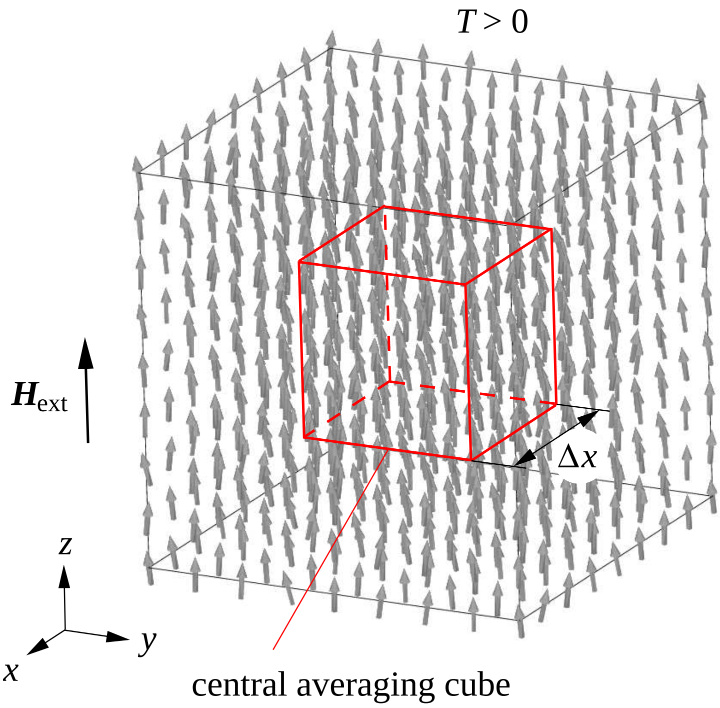

Figure 8.1: Setup of the atomistic MC simulations. After equilibration a central averaging cube of edge length Δx is used to extract the spontaneous magnetization and the magnetization parallel to the field axis as a function of Δx.

of $\Delta x = na$. The atomistic spins within an averaging cube can then be replaced by one non-atomistic moment per computational cell with the appropriate rescaled parameters. The aim is to find the same equilibrium properties of the central magnetic moment as for the mean values within the central averaging cell of same size obtained via atomistic MC simulations.

8.1.1 Equilibrium Magnetization

After equilibration, the atomistic MC simulations show a cell size independent mean value $\langle M_z \rangle$, since Eq. (8.4) is linear in the Cartesian components u_i^μ. Therefore, it does not matter if only one spin is considered for averaging or many, as long as the "averaging time" is sufficient. Fig. 8.2 summarizes the results for $\langle M_z \rangle$ for different temperatures. Taking the average over all cell

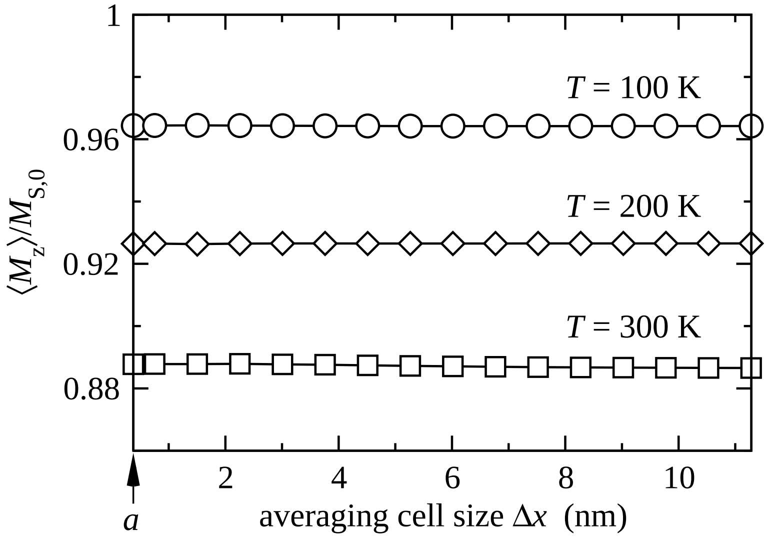

Figure 8.2: Mean value $\langle M_z \rangle$ of the magnetization parallel to the field axis as function of the averaging cube size Δx. In equilibrium, $\langle M_z \rangle$ does not depend on Δx.

sizes for each temperature leads to the values listed in Tab. 8.1.

The cell size dependent spontaneous magnetization $M_{\mathrm{S,cell}}$ is found to decrease with increasing cell size Δx according to the Bloch-like scaling law

$$M_{\mathrm{S,cell}}(\Delta x, T) = M_{\mathrm{S},\infty}(T) + \big(M_{\mathrm{S},0} - M_{\mathrm{S},\infty}(T)\big)\left(\frac{a}{\Delta x}\right)^{3/2} \quad . \tag{8.5}$$

$M_{\mathrm{S},\infty}(T)$ is the experimentally found spontaneous magnetization for large cells and depends on the exchange and anisotropy constants. The exponent 3/2 is typical for simple cubic lattices and slightly changes if other lattice types are considered (see Chap. 10).

Fig. 8.3 shows $M_{\mathrm{S,cell}}$ as a function of the averaging cube size Δx for different temperatures and an external field of $\mu_0 H_{\mathrm{ext}} = 0.1$ T. The reason for a decreasing spontaneous magnetization for an increasing number of atoms within the averaging cell are thermal fluctuations of the magnetic moments. Thus, partial cancellation of the spin components takes place in Eq. (8.4) leading to a smaller $M_{\mathrm{S,cell}}$.

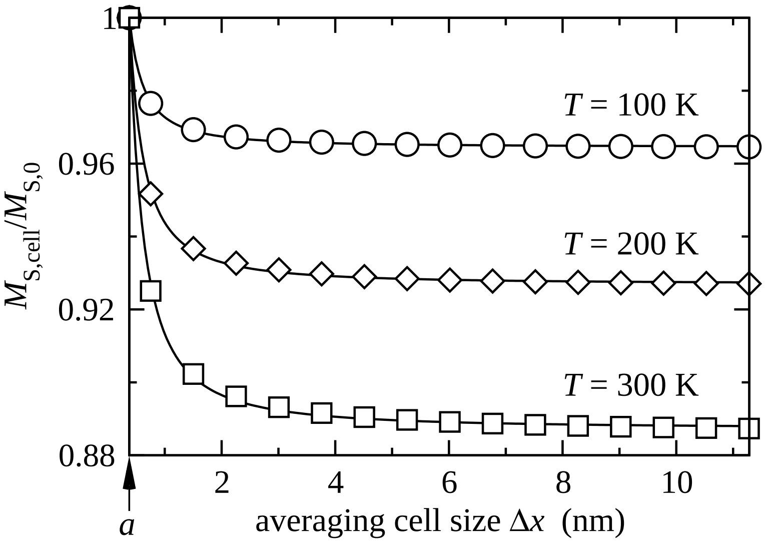

Figure 8.3: Spontaneous magnetization $M_{\mathrm{S,cell}}$ as function of the averaging cell size Δx for different temperatures, resulting from atomistic MC simulations. The graphs are normalized to the atomistic spontaneous magnetization $M_{\mathrm{S,0}}$. The solid lines represent fitting curves according to the Bloch-like scaling law (8.5). $M_{\mathrm{S,cell}}$ decreases with increasing cell size due to thermal fluctuations and finally approaches the experimentally found $M_{\mathrm{S},\infty}$.

The scaling law (8.5) with the exponent 3/2 is found to be valid for a wide range of the exchange constant (at least for $10^{-13}\mathrm{J/m} \leq A \leq 2 \cdot 10^{-11}\mathrm{J/m}$), for arbitrary anisotropy constants, and holds for temperatures up to $T/T_{\mathrm{C}}^{\mathrm{mf}} \approx 0.75$. The effect of the external field strength on $M_{\mathrm{S,cell}}$ is very small. For the chosen material parameters and $T = 300$ K ($T/T_{\mathrm{C}}^{\mathrm{mf}} \approx 0.34$) the difference in $M_{\mathrm{S,cell}}$ between simulations at zero field and 0.5 T is less than 0.1% for $a \leq \Delta x \leq 11$ nm and thus negligible for most cases. This result validates the assumption of a field independent spontaneous magnetization in micromagnetics (see Sec. 4.1).

$M_{\mathrm{S},\infty}$ as function of temperature T is given in Tab. 8.1 and is found to agree well with Bloch's $T^{3/2}$ law [28]

$$\frac{M_{\mathrm{S,0}} - M_{\mathrm{S},\infty}(T)}{M_{\mathrm{S,0}}} \propto (k_{\mathrm{B}}T)^{3/2} \quad . \tag{8.6}$$

T (K)	$\langle M_z \rangle / M_{\mathrm{S},0}$	$M_{\mathrm{S},\infty}/M_{\mathrm{S},0}$
100	0.9643	0.9646
200	0.9265	0.9270
300	0.8872	0.8873
400	0.8431	0.8444
500	0.7957	0.7974
600	0.7428	0.7444

Table 8.1: Mean value $\langle M_z \rangle$ of the magnetization parallel to the field axis and spontaneous magnetization for large cells, $M_{\mathrm{S},\infty}$, for different temperatures ($T_{\mathrm{C}}^{\mathrm{mf}} = 884.4$ K).

The proportionality factor in Eq. (8.6) depends among others on the exchange constant.

8.1.2 Anisotropy Constant

To obtain a scaling law for the uniaxial anisotropy constant, we have a closer look at the anisotropy field

$$H_{\mathrm{ani}} = \frac{2K_1}{\mu_0 M_{\mathrm{S}}} \quad , \tag{8.7}$$

which equals the required external field perpendicular to the easy axis of a Stoner-Wohlfarth particle to find a magnetization vector parallel to $\boldsymbol{H}_{\mathrm{ext}}$ [37]. Demanding cell size independent simulations in the context of anisotropy means that the anisotropy field should not depend on the cell size Δx,

$$H_{\mathrm{ani},0} = \frac{2K_{1,0}}{\mu_0 M_{\mathrm{S},0}} \equiv \frac{2K_{1,\mathrm{cell}}}{\mu_0 M_{\mathrm{S,cell}}} = H_{\mathrm{ani,cell}} \quad , \tag{8.8}$$

yielding

$$K_{1,\mathrm{cell}}(\Delta x, T) = K_{1,0} \, \frac{M_{\mathrm{S,cell}}}{M_{\mathrm{S},0}} \quad . \tag{8.9}$$

Thus, in our coarse-graining procedure the anisotropy constant scales like the spontaneous magnetization $M_{\mathrm{S,cell}}$, Eq. (8.5).

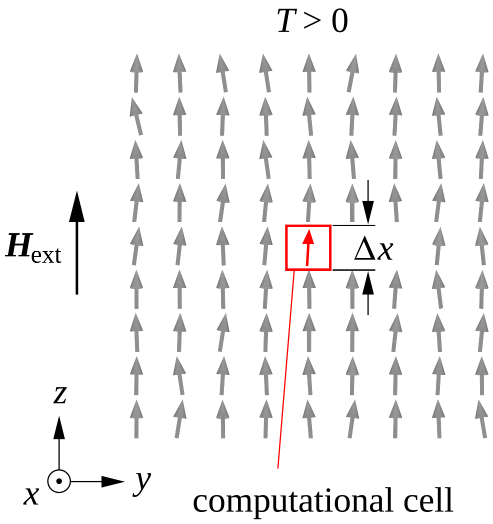

Figure 8.4: For non-atomistic simulations with one magnetic moment per computational cell we suggest to use cell size dependent material parameters, obtained from atomistic MC simulations. With the proper coarse-graining procedure the equilibrium properties of the central magnetic moment should coincide with those of the central averaging cube of same size obtained via atomistic simulations.

8.2 Non-atomistic Simulations

After evaluating the behavior of the spontaneous magnetization as function of cell size, we perform non-atomistic MC and Langevin simulations with an discretization length of $\Delta x = na$, i.e. the atomistic spins within an averaging cube are now replaced by one non-atomistic magnetic moment, see Fig. 8.4. In the expression of the total energy, Eq. (8.2), the atomistic lattice constant a has to be substituted by the discretization length Δx. Again, we look at the averaged magnetization parallel to the field axis, $\langle M_z \rangle$, at equilibrium and investigate the influence of cell size dependent material parameters. For averaging, the same number of MC steps and Langevin time steps as in the previous section are used. To ensure that the properties of the central moment do not depend on the number of spins, a system size of $N^3 = 30^3$ turned out to be sufficient. Again, periodic boundary conditions are applied in all directions.

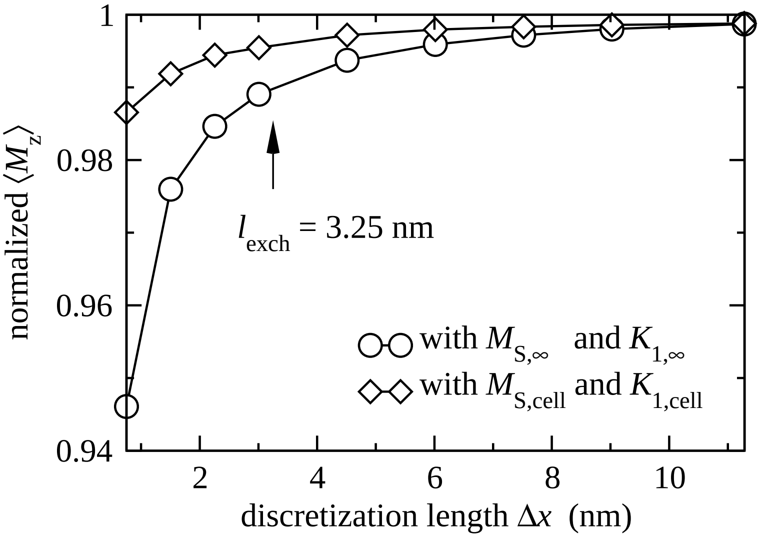

Figure 8.5: Mean value of the magnetization parallel to the field axis as a function of cell size Δx for $T/T_\mathrm{C}^\mathrm{mf} = 0.34$, resulting from non-atomistic stochastic LLG simulations. The curves are normalized to the correct value of $\langle M_z \rangle$ obtained via atomistic MC simulations ($\langle M_z \rangle / M_{\mathrm{S},0} = 0.8872$, see Tab. 8.1). No cell size corrections were used for ○. Simulations with cell size dependent $M_{\mathrm{S,cell}}$ and $K_{1,\mathrm{cell}}$ according to Eq. (8.5) and Eq. (8.9), respectively, resulted in ◇.

The results of our simulations show that the spontaneous magnetization and the anisotropy constant have to be corrected for small cells according to Eq. (8.5) and Eq. (8.9), respectively. Otherwise physical properties, such as the equilibrium magnetization $\langle M_z \rangle$, will depend on the computational cell size Δx.

Fig. 8.5 summarizes the results for $\langle M_z \rangle$ at equilibrium obtained via non-atomistic Langevin simulations with $\alpha = 1$ at $T = 300$ K, normalized to the correct value $\langle M_z \rangle / M_{\mathrm{S},0} = 0.8872$. Since Chap. 7 pointed out an excellent agreement between MC and stochastic LLG simulations at all cell sizes and temperatures, only the results of the LLG simulations are presented in Fig. 8.5. Simulations using the experimentally found values $M_{\mathrm{S},\infty}/M_{\mathrm{S},0} = K_{1,\infty}/K_{1,0} = 0.8873$ for all cell sizes show a systematic deviation for decreasing Δx. At $\Delta x = 0.75$ nm the deviation of $\langle M_z \rangle$ is 5.4% as compared with the correct

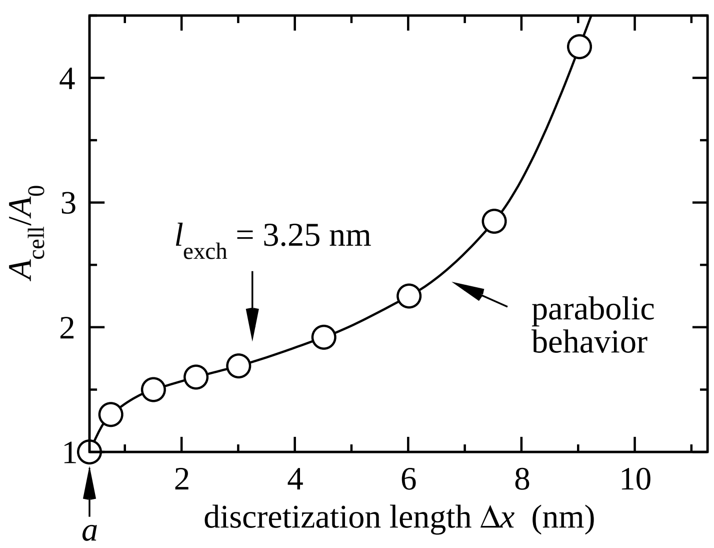

Figure 8.6: Exchange constant A_{cell} as a function of the computational cell size Δx, derived for $T/T_C^{\text{mf}} = 0.34$. The numerical results of A_{cell} reveal an inflection point near the exchange length l_{exch}. Above the exchange length, A_{cell} behaves parabolically, leading to non-vanishing exchange fields $\boldsymbol{H}_{\text{exch}}$ for large cells (Eq. (8.10)).

atomistic result. The use of a cell size dependent spontaneous magnetization and anisotropy sufficiently reduces systematic errors due to different computational cell sizes. The deviation is then only 1.3% even at the very small cell size of $\Delta x = 0.75$ nm. If one applies the atomistic values $M_{S,0}$ and $K_{1,0}$ for all cell sizes, $\langle M_z \rangle$ is too large for all Δx. The difference at $\Delta x = 0.75$ nm is then 6.7% and increases rapidly with increasing cell size. At $\Delta x = 4.5$ nm the error is even 12%.

8.2.1 Exchange Constant

To get rid of the remaining small deviations in Fig. 8.5 it is necessary to use a rescaled exchange constant A_{cell}, which can be derived numerically via the condition of a constant $\langle M_{\text{z}} \rangle$, either with nonatomistic MC or stochastic LLG simulations. Fig. 8.6 shows A_{cell} for $T = 300$ K and an external field of $\mu_0 H_{\text{ext}} = 0.1$ T. A_{cell} increases with increasing cell size and finally behaves

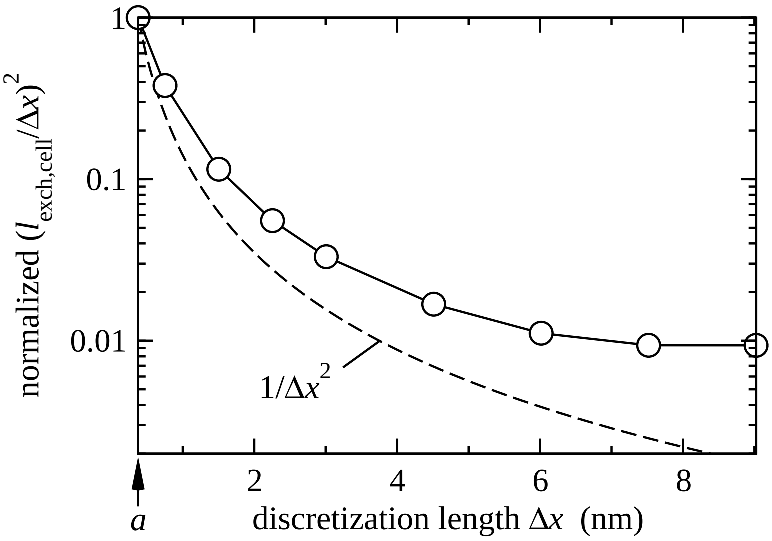

Figure 8.7: Comparison between the cell size dependent prefactor $(l_{\mathrm{exch,cell}}/\Delta x)^2$ of $\boldsymbol{H}_{\mathrm{exch}}$ and $1/\Delta x^2$, both normalized to 1 at $\Delta x = a$. The constant behavior above 7 nm avoids an unphysical disappearance of the ferromagnetic character for large computational cells.

parabolically above the exchange length $l_{\mathrm{exch}} = 3.25$ nm (calculated with the atomistic parameters). This leads to non-vanishing exchange fields

$$\boldsymbol{H}_{\mathrm{exch}} = \frac{2A_{\mathrm{cell}}}{\mu_0 M_{\mathrm{S,cell}} \Delta x^2} \sum_{\nu \in \mathrm{nn}} \boldsymbol{u}^{\nu} \tag{8.10}$$

for large cells because $\boldsymbol{H}_{\mathrm{exch}}$ is proportional to $A_{\mathrm{cell}}/\Delta x^2$.

Additionally, the exchange length also depends on the cell size, $l_{\mathrm{exch}} = l_{\mathrm{exch,cell}}$. With this, Eq. (8.10) reads

$$\boldsymbol{H}_{\mathrm{exch}} = M_{\mathrm{S,cell}} \left(\frac{l_{\mathrm{exch,cell}}}{\Delta x} \right)^2 \sum_{\nu \in \mathrm{nn}} \boldsymbol{u}^{\nu} \quad . \tag{8.11}$$

Fig. 8.7 shows a comparison between $1/\Delta x^2$ and $(l_{\mathrm{exch,cell}}/\Delta x)^2$, both normalized to 1 at $\Delta x = a$. The constant behavior of the prefactor above $\Delta x \approx 7$ nm means, that the exchange length increases proportional to the discretization length and thus preserves the ferromagnetic behavior of the material.

Since the aim of this work is to give corrections for the material parameters for small computational cells, the interesting part of A_{cell} is near and below the inflection point.

8.3 Summary

We suggested a simple coarse-graining procedure for nonzero-temperature micromagnetics:

1. Determine the atomistic spontaneous magnetization $M_{\text{S},0} = M_{\text{S}}(T = 0)$, the experimentally found spontaneous magnetization for large cells $M_{\text{S},\infty}(T)$ at the desired temperature T, and the atomistic lattice constant a.
2. Apply Eq. (8.5) and Eq. (8.9) to calculate the cell size dependent values $M_{\text{S,cell}}$ and $K_{1,\text{cell}}$, respectively, for non-atomistic simulations.
3. If necessary, calculate the cell size dependent exchange constant A_{cell} with non-atomistic MC or LLG simulations via the condition of a constant $\langle M_z \rangle$.

The obtained rescaled material parameters can then be used for any kind of micromagnetic simulations at nonzero-temperatures.

In the next chapter we investigate the influence of our coarse-graining procedure on the switching time of small particles.

Chapter 9

Relaxation Times

The obtained scaling laws for the spontaneous magnetization M_S, the anisotropy constant K_1, and the exchange constant A were derived from equilibrium magnetization properties and represent statistical averages over a large number of Monte Carlo steps. Thus, it is a priori not justified to use the results of the previous chapter for highly dynamic processes such as magnetization switching. The simulation results in this chapter point out that our coarse-graining procedure is also able to improve numerical results of dynamic behavior.

9.1 Geometry and Material Parameters

We perform stochastic LLG simulations of small cubic particles with uniaxial anisotropy and investigate the dependence of the averaged relaxation time on the number of exchange coupled subcubes or discretization length Δx, respectively. Both, simulations with and without dipole interaction are considered.

The simulation setup is shown in Fig. 9.1. The material parameters are the same as in the last chapter: $\mu_0 M_{\mathrm{S},0} = 1.76$ T, $A_0 = 1.3 \cdot 10^{-11}$ J/m, $K_{1,0} = 4.5 \cdot 10^5$ J/m^3, and $a = 0.376$ nm. The edge length of the ferromagnetic particle is 6 nm, the damping constant $\alpha = 1$, and open boundary conditions are applied in all directions. For the stochastic time integration of the Langevin

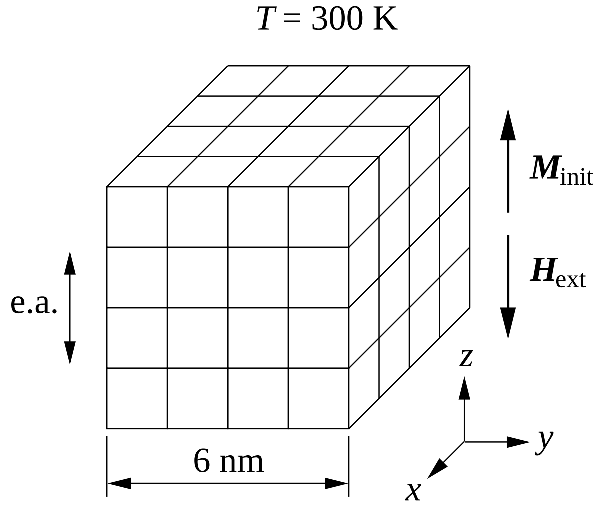

Figure 9.1: Setup of switching simulations.

equation without dipole interaction a time step of $\Delta t = 0.1$ ps is sufficient, whereas $\Delta t = 0.01$ ps turned out to be necessary for the simulations with dipole interaction. The initial magnetization points upwards parallel to the z-axis and the anisotropy direction. At an external field of $H/H_{\mathrm{ani},0} = -0.84$ ($\mu_0 H_{\mathrm{ani},0} = 0.64$ T), applied in the negative z-direction, thermal activation drives the magnetization out of the z-axis and finally causes the particle to switch. For each cell size 2000 switching events were used to calculate an averaged switching time.

9.2 Results and Discussion

The results of the switching simulations without dipole interaction for $T = 300$ K are shown in Fig. 9.2. The relaxation time as a function of the discretization length is found to decrease with decreasing Δx when cell size independent material parameters are used, such as the atomistic material parameters $M_{\mathrm{S},0}$, $K_{1,0}$ and A_0. Fig. 9.2 points out that the results can be improved by applying the previously derived scaling laws for the parameters $M_{\mathrm{S,cell}}$, $K_{1,\mathrm{cell}}$ and A_{cell}. Then, the switching time remains almost constant.

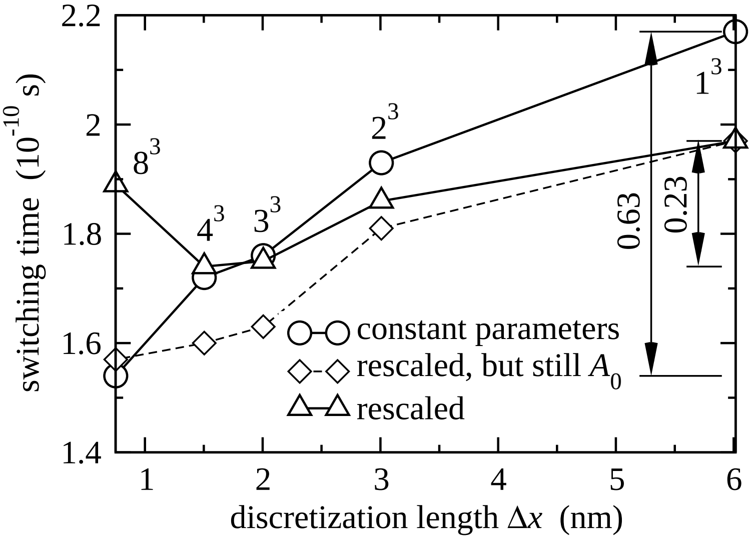

Figure 9.2: Switching times as a function of the computational cell size Δx at $T = 300$ K and without dipole interaction. The numbers in the diagram indicate the number of subcubes. Simulations with the constant system parameters $M_{\mathrm{S},0}$, $K_{1,0}$, and A_0 resulted in a decreasing switching time for decreasing cell size. This behavior can be improved by using cell size dependent material parameters. Then, the difference between the lowest and highest switching times reduces from 63 ps to 23 ps. Scaling of M_{S} and K_1 but still using A_0 resulted in the dashed curve. Standard deviations are always smaller than the symbol size.

The simulation results also show that, contrary to equilibrium properties as discussed in the previous section, the scaling of the exchange constant has a strong impact on dynamic processes and thus on the relaxation time. Scaling of M_{S} and K_1 but still using A_0 resulted in the dashed curve in Fig. 9.2.

However, the results for the switching time increase for very small cell sizes, which indicates that high frequency spin waves may slow down thermally induced switching. Simulations with $\Delta x = a = 0.376$ nm (16^3 subcubes) resulted in switching times being about 2.5 times larger than those of Fig. 9.2. Anyway, stochastic LLG simulations on an atomistic level are a special case and should be handled carefully.

Fig. 9.3 summarizes the results for the same system but with dipole interac-

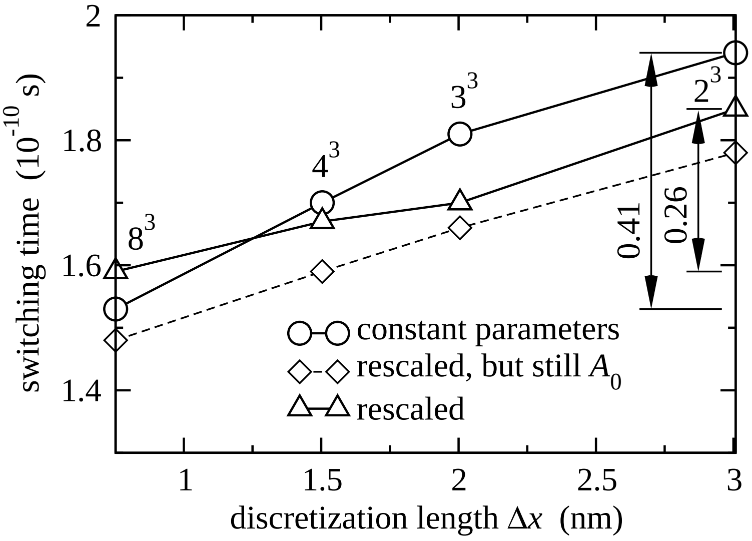

Figure 9.3: Switching times as a function of the computational cell size Δx at $T = 300$ K and with dipole interaction. The constant parameters $M_{\mathrm{S},0}$, $K_{1,0}$, and A_0 again resulted in a decreasing switching time for decreasing cell size. The cell size dependent parameters improve the behavior.

tion. The case of just one magnetic moment representing the whole magnetic system was excluded in this diagram since the strayfield does not affect the result. Decreasing switching times with decreasing discretization length can be observed. The cell-size dependent parameters again improve the results.

Chapter 10

Cubic Crystal Lattices

For simplicity reasons we introduced our coarse-graining method for simple cubic lattices and obtained scaling laws for the spontaneous magnetization and the anisotropy constant directly from atomistic MC simulations. Nonatomistic simulations suggested to use cell size dependent exchange constants at least when dynamic properties are of interest.

However, simple cubic lattices with an atom (or ion) at each vertex are very rare. The alpha phase of polonium is the only known example among the elements under normal conditions [3]. The other two cubic Bravais lattices – the face-centered cubic (fcc) and the body-centered cubic (bcc) lattices – are much more important. An enormous variety of solids crystallize in these structures. Typical elements with a monatomic bcc crystal structure are for instance Cr and α-Fe, with a monatomic fcc lattice Ni, Pt, and β-Co.

In this chapter we focus on bcc and fcc lattices and extract scaling laws from atomistic MC simulations for these lattice types. Other important elements for magnetic applications (e.g. α-Co) crystallize in hexagonal forms, but cannot be considered with the simple data structure of our MC program.

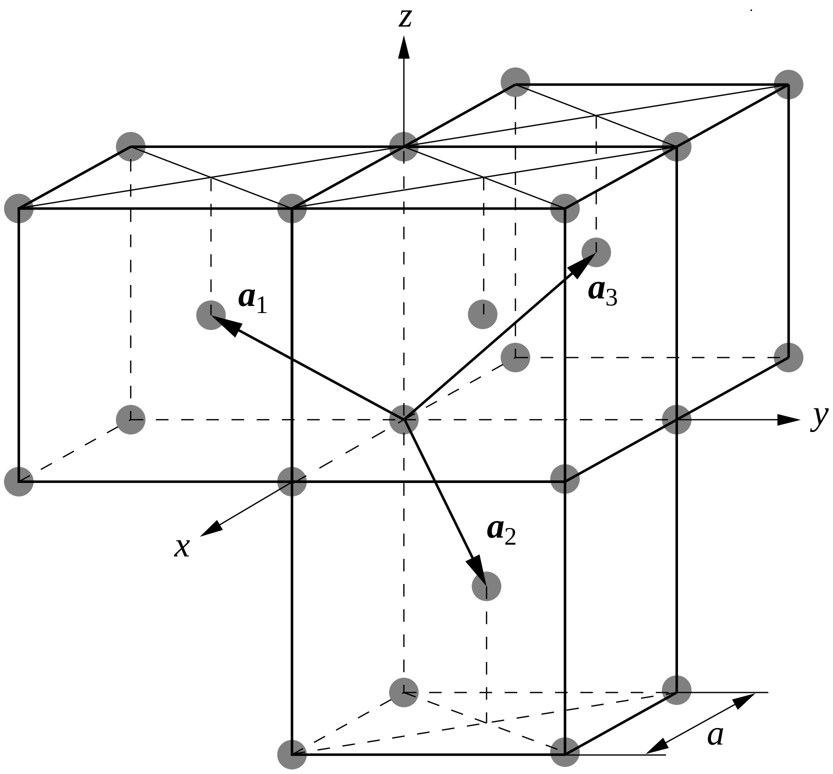

Figure 10.1: Body-centered cubic (bcc) Bravais lattice. The set $\{\boldsymbol{a}_1, \boldsymbol{a}_2, \boldsymbol{a}_3\}$ defines the primitive unit cell, whereas the conventional cubic unit cell is described by $\{a\hat{\boldsymbol{x}}, a\hat{\boldsymbol{y}}, a\hat{\boldsymbol{z}}\}$.

10.1 General Aspects

The body-centered cubic lattice is formed by adding an additional site to the simple cubic lattice at the center of each cube, see Fig. 10.1, whereas the face-centered cubic lattice shows an additional point in the center of each square face, Fig. 10.2. The coordination number 6 for simple cubic lattices consequently changes to 8 for bcc and 12 for fcc, respectively. Usually, the cubic non-primitive unit cell (*conventional unit cell*) is described by the orthogonal set of vectors $\{a\hat{\boldsymbol{x}}, a\hat{\boldsymbol{y}}, a\hat{\boldsymbol{z}}\}$, where a denotes the edge of the cubic unit cell. The conventional unit cell is often preferred because the cubic symmetry is reflected explicitly. The primitive cell, defined by $\{\boldsymbol{a}_1, \boldsymbol{a}_2, \boldsymbol{a}_3\}$ (see Fig. 10.1 and Fig. 10.2), contains precisely one lattice point, and the volume is the

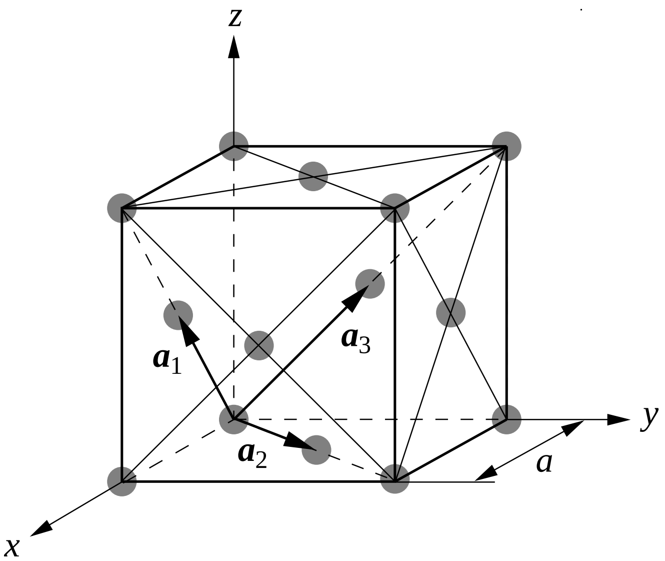

Figure 10.2: Face-centered cubic (fcc) Bravais lattice. The vectors $\{\boldsymbol{a}_1, \boldsymbol{a}_2, \boldsymbol{a}_3\}$ describe the primitive unit cell, whereas the conventional cubic unit cell is defined by $\{a\hat{\boldsymbol{x}}, a\hat{\boldsymbol{y}}, a\hat{\boldsymbol{z}}\}$.

volume per atom or lattice site,

$$v_{\mathrm{at}} = \left| \boldsymbol{a}_1 \cdot (\boldsymbol{a}_2 \times \boldsymbol{a}_3) \right| = \frac{a^3}{c} \quad . \tag{10.1}$$

The volume of the cubic unit cell is c-times larger than v_{at}, where c is the number of atoms in the cubic unit cell. $c = 1$, 2, 4 for simple cubic, bcc, and fcc lattices, respectively.

10.2 Geometry and Material Parameters

The atomistic MC simulations of bcc and fcc materials are performed in the same way as in Sec. 8.1. Following the discussion in Sec. 8.1, considering $c \neq 1$, and again neglecting dipole interactions, we arrive at the total energy

$$\begin{aligned} c\,E &= -A_0\,a\sum_{\mu=1}^{N'}\sum_{\nu\in\mathrm{nn}}\boldsymbol{u}^\mu\cdot\boldsymbol{u}^\nu + K_{1,0}\,a^3\sum_{\mu=1}^{N'}\left(1-(\hat{\boldsymbol{z}}\cdot\boldsymbol{u})^2\right) \\ &\quad -\mu_0 M_{\mathrm{S},0}\,a^3 H_{\mathrm{ext}}\hat{\boldsymbol{z}}\cdot\sum_{\mu=1}^{N'}\boldsymbol{u}^\mu \quad , \end{aligned} \tag{10.2}$$

where N' now denotes the *total* number of spins. The system size is set to $(60\,a)^3$, and periodic boundary conditions are applied in all directions. For the calculation of the equilibrium properties $\langle M_z\rangle$ and $M_{\mathrm{S,cell}}$ (see Eq. (8.3) and Eq. (8.4)) a central averaging cube is used with the maximum edge length of $30\,a$. Again, we discard the first 10^4 MC steps and use the next 10^5 steps for averaging.

Contrary to the primitive cubic lattice, the relation between the edge length of the averaging cube and the number of spins in one direction within the cube is not linear for bcc and fcc lattices. Thus, we extract the equilibrium values as function of the number of spins within the averaging cube, n', and subsequently relate them with the discretization length $\Delta x = (n' v_{\mathrm{at}})^{1/3}$ of (nonatomistic) finite difference simulations. Consequently, $\Delta x_{\mathrm{at}} = v_{\mathrm{at}}^{1/3}$ denotes the edge length of a cube with the same volume as the primitive unit cell. The question is if there is still a scaling law for $M_{\mathrm{S,cell}}$ of the form

$$M_{\mathrm{S,cell}}(\Delta x, T) = M_{\mathrm{S},\infty}(T) + \left(M_{\mathrm{S},0} - M_{\mathrm{S},\infty}(T)\right)\left(\frac{\Delta x_{\mathrm{at}}}{\Delta x}\right)^q \quad . \tag{10.3}$$

The bcc material parameters are chosen as $\mu_0 M_{\mathrm{S},0} = 2.15$ T and $A_0 = 2.5\cdot 10^{-11}$ J/m, which are those of α-Fe [52], though measured at room temperature. The lattice constant of α-Fe is found to be $a = 2.87$ Å [46]. The fcc material parameters are $\mu_0 M_{\mathrm{S},0} = 0.603$ T and $A_0 = 2.5\cdot 10^{-11}$ J/m and correspond to those of Ni [41] (again measured at room temperature), which has a lattice constant of $a = 3.52$ Å [46]. Both materials are exposed to an external field of 0.1 T parallel to the z-axis. Since the anisotropy term does not influence

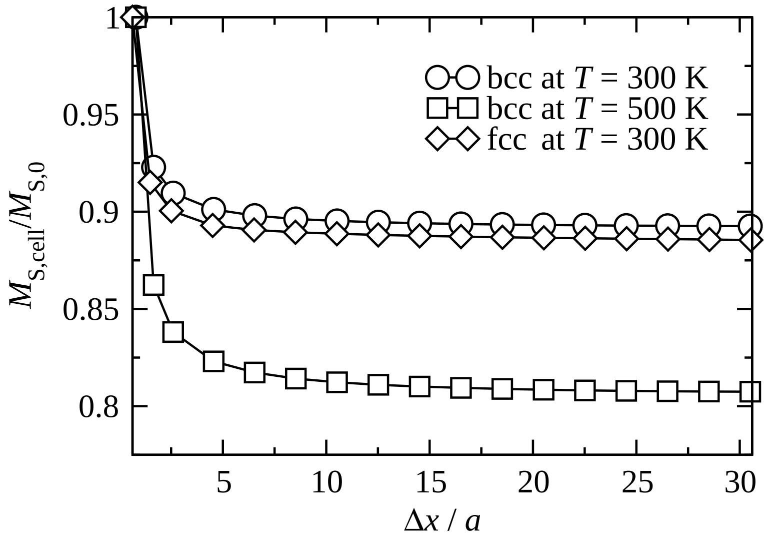

Figure 10.3: Spontaneous magnetization as function of $\Delta x/a$ for bcc (a = 2.87 Å) and fcc (a = 3.52 Å) materials, resulting from atomistic MC simulations. A fit according to the Bloch-like scaling law (8.5) does not give reasonable results. The solid lines in the diagram are guides for the eyes only.

Structure	q	$\langle M_z\rangle/M_{S,0}$	$M_{S,\infty}/M_{S,0}$
bcc at $T = 300$ K	1.60	0.8916	0.8925
bcc at $T = 500$ K	1.58	0.8065	0.8073
fcc at $T = 300$ K	1.55	0.8858	0.8861

Table 10.1: Results of atomistic MC simulations for bcc (α-Fe) and fcc (Ni) materials.

the form of the scaling law for the spontaneous magnetization, we neglect anisotropy for both materials. Moreover, the scaling law for the anisotropy constant is already given in Eq. (8.9).

10.3 Results and Discussion

Fig. 10.3 shows the spontaneous magnetization as function of $\Delta x/a$. If one tries to fit the data according to the Bloch-like scaling law (8.5) of the form $y = a_0 + (1 - a_0)(a/\Delta x)^{3/2}$, no reasonable results can be obtained. It is necessary to

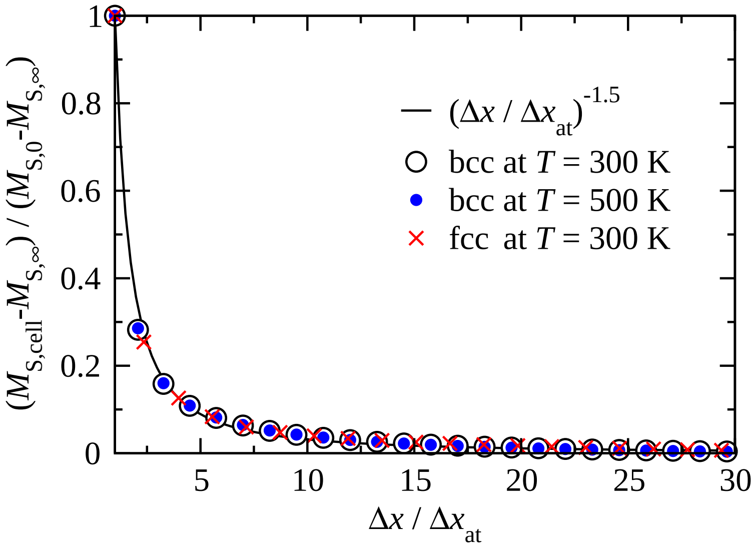

Figure 10.4: Normalized spontaneous magnetization as function of the averaging cell size $\Delta x/\Delta x_{\mathrm{at}}$ for bcc ($\Delta x_{\mathrm{at}} = 2.28$ Å) and fcc ($\Delta x_{\mathrm{at}} = 2.22$ Å) materials, resulting from atomistic MC simulations. The fitting curve $(\Delta x/\Delta x_{\mathrm{at}})^{-1.5}$ is a good approximation for any kind of cubic unit cell.

calculate Δx_{at} first and make use of the modified scaling law (10.3). For this case, the results are given in Tab. 10.1. As for simple cubic lattices, $\langle M_z \rangle$ does not depend on the averaging cell size. The values after taking the average over all cell sizes are listed in the table. The exponent q in the scaling law Eq. (10.3) takes the values 1.60 for bcc at $T = 300$ K, 1.58 for bcc at $T = 500$ K, and 1.55 for fcc at $T = 300$ K, respectively. However, the difference between a fitting curve with q and the exponent 1.5 is negligible for all cases. This can be seen in Fig. 10.4, where $(M_{\mathrm{S,cell}} - M_{\mathrm{S},\infty})/(M_{\mathrm{S},0} - M_{\mathrm{S},\infty})$ versus $\Delta x/\Delta x_{\mathrm{at}}$ is plotted and reveals a universal behavior. The fitting curve $(\Delta x/\Delta x_{\mathrm{at}})^{-1.5}$ is reasonable for all three examples. Since $\Delta x_{\mathrm{at}} = (a^3/c)^{1/3}$ appears in the scaling law (10.3), the universal fitting curve in Fig. 10.4 does not mean that the behavior of the spontaneous magnetization is independent of the crystal structure.

The results of nonatomistic MC simulations for bcc α-Fe at $T = 300$ K are shown in Fig. 10.5. In order to extract $\langle M_z \rangle$ of the central magnetic moment

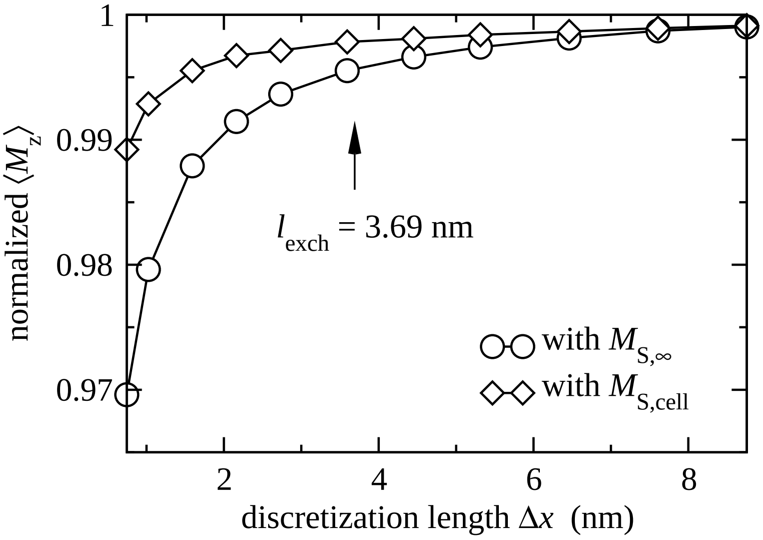

Figure 10.5: Mean value $\langle M_z \rangle$ for α-Fe as a function of discretization length Δx for $T = 300$ K, resulting from nonatomistic MC simulations. The curves are normalized to the correct value of $\mu_0 \langle M_z \rangle = 1.9170$ T obtained via atomistic MC simulations. No cell size corrections were used for ○. Simulations with the cell size dependent spontaneous magnetization $M_{\mathrm{S,cell}}$ from Fig. 10.4 resulted in ◇. The atomistic parameters give an exchange length of $l_{\mathrm{exch}} = 3.69$ nm.

after equilibration, we simulated a system of 30^3 moments localized on a regular cubic lattice with lattice spacing Δx. Using the cell size independent value $M_{\mathrm{S},\infty}$ for all discretization lengths Δx again reveals a decreasing magnetization parallel to the external field, $\langle M_z \rangle$. $M_{\mathrm{S,cell}}$ of Fig. 10.4 strongly improves the behavior (about a factor of 3 at $\Delta x = 1$ nm). The remaining difference can be attributed to a cell size dependent exchange constant, A_{cell}, following from nonatomistic MC simulations (see Sec. 8.2).

10.4 Summary

In this chapter, we looked at the behavior of the spontaneous magnetization $M_{\mathrm{S,cell}}$ as function of the discretization length for bcc and fcc lattices. The Bloch-like scaling law in the modified form of Eq. (10.3) with the exponent

$q = 3/2$ turned out to be a good approximation for bcc and fcc lattices. Thus, we can generalize the suggested coarse-graining procedure of Sec. 8 for any kind of cubic lattice:

1. Determine the atomistic spontaneous magnetization $M_{\mathrm{S},0} = M_{\mathrm{S}}(T = 0)$, the experimentally found spontaneous magnetization for large cells $M_{\mathrm{S},\infty}(T)$ at the desired temperature T, the crystal structure, and the atomistic *cubic* lattice constant a.
2. Calculate the volume $v_{\mathrm{at}} = a^3/c$ of the primitive unit cell ($c = 1$, 2, 4 for simple cubic, bcc, and fcc lattices, respectively) and $\Delta x_{\mathrm{at}} = v_{\mathrm{at}}^{1/3}$.
3. Apply Eq. (10.3) with $q = 3/2$ and Eq. (8.9) to calculate the cell size dependent values $M_{\mathrm{S,cell}}$ and $K_{1,\mathrm{cell}}$, respectively, for nonatomistic simulations.
4. If necessary, calculate the cell size dependent exchange constant A_{cell} with nonatomistic MC or LLG simulations via the condition of a constant $\langle M_z \rangle$.

The cell size dependent material parameters sufficiently improve numerical results of micromagnetic simulations at nonzero-temperatures. Though, the same scaling law for the spontaneous magnetization can be used for simple cubic, bcc, and fcc lattices, the crystal structure enters as Δx_{at}.

Appendix A

Dirac Delta Function

The Dirac δ is a generalized function and can be defined as

$$\delta(x) = \lim_{a\to 0} \frac{1}{2a}\big(\Theta(x+a) - \Theta(x-a)\big) \quad , \tag{A.1}$$

with the Heavyside function

$$\Theta(x) = \begin{cases} 0 & \text{for} \quad x < 0\,, \\ 1 & \text{for} \quad x > 0\,. \end{cases} \tag{A.2}$$

Throughout this chapter the variables x, y and the parameters a, b are real.

The function $\delta(f(x,y))$ can be written as

$$\delta(f(x,y)) = \sum_i \frac{\delta(x - x_i(y))}{\left|\frac{\partial f(x,y)}{\partial x}\right|_{x=x_i(y)}} \quad , \tag{A.3}$$

where the sum is carried out over all real roots $x_i(y)$ of $f(x_i, y) = 0$.

The often used introduction of the δ function via

$$\int_a^b \mathrm{d}x\, \delta(x - x')\, f(x) = f(x')\big[\Theta(b - x') - \Theta(a - x')\big] \tag{A.4}$$

is valid for any continuous function $f(x)$.

Appendix B

Kramers-Moyal Coefficients

The one-dimensional Kramers-Moyal coefficients

$$K^{(n)}(x,t) = \frac{1}{n!} \lim_{\tau\to 0} \frac{1}{\tau} \left\langle \, (\xi(t+\tau) - \xi(t))^n \, \right\rangle \Big|_{\xi(t)=x} \tag{B.1}$$

are calculated for the Langevin equation of the stochastic variable $\xi(t)$,

$$\dot{\xi} = h(\xi,t) + g(\xi,t)\,\eta(t) \quad , \tag{B.2}$$

with the *Markovian* Langevin force $\eta(t)$,

$$\langle \eta(t) \rangle = 0 \qquad \text{and} \qquad \langle \eta(t)\eta(t') \rangle = 2\,\delta(t-t') \quad . \tag{B.3}$$

A generalization for d dimensions is more or less straightforward and can be found in Ref. [48].

We start our derivation with the integration of Eq. (B.2) over a small time interval $[t, t+\tau]$ with the value of the stochastic variable $\xi(t) = x$:

$$\xi(t+\tau) - x = \int_t^{t+\tau} \mathrm{d}t' \big(h(\xi,t') + g(\xi,t')\,\eta(t') \big) \quad . \tag{B.4}$$

The Taylor expansions of h and g read

$$\begin{aligned} h(\xi(t'),t') &= h(x+\xi(t')-x,t') = \\ &= h(x,t') + h_x(x,t')\,(\xi(t')-x) + \ldots && \text{(B.5)} \\ g(\xi(t'),t') &= g(x,t') + g_x(x,t')\,(\xi(t')-x) + \ldots \quad . && \text{(B.6)} \end{aligned}$$

To keep the notation simple, we used $h_x \equiv \partial h/\partial x$ just in the context of the following derivation.

Using Eq. (B.5) and Eq. (B.6) iteratively in Eq. (B.4), we find

$$\begin{aligned} \xi(t+\tau) - x \;=\; & \int_t^{t+\tau} \mathrm{d}t' h(x,t') + \int_t^{t+\tau} \mathrm{d}t' h_x(x,t') \int_t^{t'} \mathrm{d}t'' h(x,t'') + \\ & + \int_t^{t+\tau} \mathrm{d}t' h(x,t') \int_t^{t'} \mathrm{d}t'' g(x,t'')\,\eta(t'') + \ldots + \\ & + \int_t^{t+\tau} \mathrm{d}t' g(x,t')\,\eta(t') + \int_t^{t+\tau} \mathrm{d}t' g_x(x,t')\,\eta(t') \int_t^{t'} \mathrm{d}t'' h(x,t'') + \\ & + \int_t^{t+\tau} \mathrm{d}t' g_x(x,t')\,\eta(t') \int_t^{t'} \mathrm{d}t'' g(x,t'')\,\eta(t'') + \ldots \quad . \qquad \text{(B.7)} \end{aligned}$$

Taking the average of Eq. (B.7) and utilizing $\langle \eta(t) \rangle = 0$ and Eq. (A.1), we obtain

$$\begin{aligned} \langle \xi(t+\tau) - x \rangle \;=\; & \int_t^{t+\tau} \mathrm{d}t' h(x,t') + \int_t^{t+\tau} \mathrm{d}t' h_x(x,t') \int_t^{t'} \mathrm{d}t'' h(x,t'') + \ldots + \\ & + \int_t^{t+\tau} \mathrm{d}t' g_x(x,t') \underbrace{\int_t^{t'} \mathrm{d}t'' g(x,t'') \underbrace{\langle \eta(t')\eta(t'') \rangle}_{2\,\delta(t'-t'')}}_{2\,g(x,t')\,\Theta(t'-t')} + \ldots \quad . \qquad \text{(B.8)} \end{aligned}$$

The common definition $\Theta(0) = 1/2$ leads to the Stratonovich interpretation (see Sec. 6.3.2) of the stochastic differential equation (B.2) and is equivalent to any *symmetric* representation of the δ function around the origin (like Eq. (A.1)). In this thesis we always use the Stratonovich interpretation of stochastic integrals. Hence, we get

$$\begin{aligned} \langle \xi(t+\tau) - x \rangle &= \int_t^{t+\tau} \mathrm{d}t' h(x,t') + \int_t^{t+\tau} \mathrm{d}t' h_x(x,t') \int_t^{t'} \mathrm{d}t'' h(x,t'') + \ldots + \\ &\quad + \int_t^{t+\tau} \mathrm{d}t' g(x,t')\, g_x(x,t') + \ldots \quad . \end{aligned} \tag{B.9}$$

The first Kramers-Moyal coefficient can now be obtained by multiplying Eq. (B.9) with τ^{-1} and performing $\tau \to 0$:

$$K^{(1)}(x,t) = h(x,t) + g(x,t) \frac{\partial}{\partial x} g(x,t) \quad . \tag{B.10}$$

What happened to the other integrals in Eq. (B.9) in the limit $\tau \to 0$? Any other term in Eq. (B.9) without $\eta(t)$ contains at least two integrals and thus is at least proportional to τ^2. So, these terms vanish for $\tau \to 0$. Terms with the random force $\eta(t)$ and not given explicitly in Eq. (B.9) contain products of $[\eta(t')\eta(t'') \ldots \eta(t^{(n)})]$ with $n \geq 3$. The averages of these products are multitime correlation functions of $\eta(t)$. Since the Langevin forces are assumed to be Gaussian with zero mean, they obey Isserlis's theorem [16]

$$\langle \eta(t')\eta(t'') \ldots \eta(t^{(n)}) \rangle = \begin{cases} 0 & \text{for } n \text{ odd,} \\ \sum \prod_{i<j} \langle \eta(t^{(i)}) \eta(t^{(j)}) \rangle & \text{for } n \text{ even,} \end{cases} \tag{B.11}$$

where the sum runs over all distinct products of pairs $\langle \eta(t^{(i)}) \eta(t^{(j)}) \rangle$, each formed by selecting $n/2$ pairs of $\{t', \ldots, t^{(n)}\}$. With Eq. (B.3), Eq. (B.11) represents a sum over terms each with $n/2$ functions $\delta(t^{(i)} - t^{(j)})$. The n-fold integrals in Eq. (B.9) are thus proportional to $\tau^{n/2}$ and vanish for $\tau \to 0$.

With the same arguments we find for the other coefficients in Stratonovich interpretation

$$\begin{aligned} K^{(2)}(x,t) &= \frac{1}{2} \lim_{\tau \to 0} \frac{1}{\tau} \int_t^{t+\tau} \mathrm{d}t' g(x,t') \int_t^{t'} \mathrm{d}t'' g(x,t'') 2\delta(t'-t'') = \\ &= g^2(x,t) \quad , \end{aligned} \tag{B.12}$$

$$K^{(n)}(x,t) = 0 \ , \quad \forall n \geq 3 \quad . \tag{B.13}$$

Appendix C

Algorithm Tests

The algorithms for stochastic Landau-Lifshitz-Gilbert and Metropolis Monte Carlo simulations have been checked via test cases with well-known solutions. In the following a useful selection of test cases for micromagnetic codes is presented. When examples of simulation results are given, they were obtained in equilibrium. In particular, in the MC simulations the first 10^4 MC steps were discarded and the next 10^5 steps were used for averaging, whereas $2 \cdot 10^6$ time steps were executed for the Langevin simulations and the first 10^5 steps were excluded from averaging. For the stochastic LLG simulations, a damping constant of $\alpha = 1$ has been chosen.

C.1 Paramagnetism

The simplest case is a single (classical) magnetic moment in an external field $\boldsymbol{H}_{\text{ext}} = H_{\text{ext}}\hat{\boldsymbol{z}}$ at a fixed temperature T. The total energy is the Zeeman energy (see Eq. (3.18)) and reads

$$E = -vJ_{\text{S}}H_{\text{ext}}\cos\theta \quad , \tag{C.1}$$

where θ denotes the angle between the moment $\boldsymbol{u}$ and the z-axis. The probability to find the magnetic moment at an angle θ is proportional to Boltzmann's

T (K)		$\langle u_z \rangle$	
	exact	MC	LLG
50	0.9306	0.9295	0.9301
100	0.8612	0.8618	0.8615
150	0.7919	0.7923	0.7921

Table C.1: Results for a single magnetic moment in an external field.

factor $\exp(-\beta E)$, with $\beta = (k_{\mathrm{B}}T)^{-1}$.

After equilibration, the averaged magnetization parallel to the external field is given by

$$\langle u_z \rangle \equiv \langle \cos\theta \rangle = \frac{\int_0^\pi \mathrm{d}\theta \, \sin\theta \cos\theta \exp(\zeta\cos\theta)}{\int_0^\pi \mathrm{d}\theta \, \sin\theta \exp(\zeta\cos\theta)} = \coth\zeta - \frac{1}{\zeta} \quad , \tag{C.2}$$

where we used $\zeta = \beta v J_{\mathrm{S}} H_{\mathrm{ext}}$. The mean values of the other components vanish due to symmetry reasons.

Some results for $J_{\mathrm{S}} = 1$ T, $\mu_0 H_{\mathrm{ext}} = 0.1$ T, and $v = 125$ nm^3 are compared in Tab. C.1 for different temperatures and reveal a good agreement between the analytical values and those obtained from MC and stochastic LLG simulations.

C.2 Stoner-Wohlfarth Particle

In the Stoner-Wohlfarth model, small magnetic particles are approximated by rigid magnetic moments [37]. This is equivalent to coherent rotation, where exchange interaction keeps magnetic moments parallel during reversal.

The energy of a Stoner-Wohlfarth particle with uniaxial anisotropy parallel to the z-axis in an external field $\boldsymbol{H}_{\mathrm{ext}} = H_{\mathrm{ext}}\hat{\boldsymbol{z}}$ reads

$$E = -K_1 v \cos^2\theta - v J_{\mathrm{S}} H_{\mathrm{ext}} \cos\theta \quad , \tag{C.3}$$

where θ again denotes the angle between the magnetization vector and the z-axis. In equilibrium, the average magnetization $\langle u_z \rangle$ can be calculated nu-

T (K)	$\langle u_z \rangle$		
	exact	MC	LLG
100	0.9742	0.9743	0.9740
200	0.9470	0.9465	0.9467
300	0.9180	0.9181	0.9178

Table C.2: Results for a Stoner-Wohlfarth particle in an external field.

merically as

$$\langle u_z \rangle = \frac{\int_0^\pi \mathrm{d}\theta\ \sin\theta\cos\theta\exp(\xi\cos^2\theta + \zeta\cos\theta)}{\int_0^\pi \mathrm{d}\theta\ \sin\theta\exp(\xi\cos^2\theta + \zeta\cos\theta)} \quad , \tag{C.4}$$

where $\xi = \beta K_1 v$ and $\zeta = \beta v J_{\mathrm{S}} H_{\mathrm{ext}}$.

Tab. C.2 presents some results for $J_{\mathrm{S}} = 1$ T, $K_1 = 1{\cdot}10^5$ J/m^3, $v = 125\,\mathrm{nm}^3$, and an external field of $\mu_0 H_{\mathrm{ext}} = 0.3$ T. The simulation results agree very well with the exact values obtained using `Mathematica`.

C.3 Exchange Coupled Moments

In general, no analytic solutions exist for exchange coupled moments. However, one can consider special cases for which solutions are known and allow for verification of correct implementation. To check the MC code on an atomistic level for simple cubic, bcc, and fcc lattices, we can assume all spins but one fixed parallel to the z-axis. Then, the total energy of exchange coupled spins in an external field $\boldsymbol{H}_{\mathrm{ext}} = H_{\mathrm{ext}}\hat{\boldsymbol{z}}$ reads (see Eq. (10.2))

$$E = -\frac{1}{c}\left(2zAa + J_{\mathrm{S}}a^3 H_{\mathrm{ext}}\right)\cos\theta' \quad . \tag{C.5}$$

Constant energy terms have been omitted. z denotes the number of nearest neighbors, a the edge length of the cubic unit cell, and θ' is the angle between the external field and the only free spin, $\boldsymbol{u}'$. Going back to Eq. (C.2), the

T (K)	crystal	$\langle u'_z \rangle$	
		exact	MC
10	simple	0.9617	0.9618
	bcc	0.9426	0.9422
	fcc	0.9234	0.9232
30	simple	0.8852	0.8855
	bcc	0.8277	0.8274
	fcc	0.7704	0.7701

Table C.3: Results for exchange coupled spins in an external field obtained via atomistic MC simulations.

solution for the averaged magnetization can be found as

$$\langle u'_z \rangle \equiv \langle \cos\theta \rangle = \coth\zeta - \frac{1}{\zeta} \quad , \tag{C.6}$$

with

$$\zeta = \frac{\beta}{c}\left(2zAa + J_{\mathrm{S}} a^3 H_{\mathrm{ext}}\right) \quad . \tag{C.7}$$

For this test case, the same material parameters were used for simple cubic ($z = 6$, $c = 1$), bcc ($z = 8$, $c = 2$), and fcc ($z = 12$, $c = 4$) lattices: $J_{\mathrm{S}} = 1$ T, $A = 1 \cdot 10^{-12}$ J/m, and $a = 3$ Å. The spins were exposed to an external field of $\mu_0 H_{\mathrm{ext}} = 0.3$ T. Tab. C.3 shows some results compared with the exact values.

Choosing different directions for the fixed spins is an easy way to check whether the right nearest neighbors contribute to the exchange energy.

Appendix D

Monte Carlo Program

The Metropolis Monte Carlo program has been implemented in `ANSI-C`. All array sizes are defined in the main program before compiling the code:

```
#define n            60
#define navstart     2
#define navend       30
#define navstepsize  2
```

For simple cubic lattices, `n` is the number of cubic unit cells in x-, y-, and z-direction, `navstart` and `navend` denote the start and end size of the central averaging box, respectively, and `navstepsize` is the step size of the averaging cube size. Body-centered (bcc) and face-centered (fcc) cubic lattices are build up by considering only the required spins on a regular cubic lattice. Thus, for bcc and fcc lattices, `n` denotes the number of lattice points of a regular cubic lattice in one direction, which are necessary to build the desired bcc or fcc lattice, respectively. This applies analogously to the other values listed above.

For the initialization of the simulation, all parameters are read from the file `parameter.ini`, listed in Tab. D.1. Only a few parameters need further explanations: The MC program calculates averaged quantities for different temperatures, starting at the temperature `tempfinal/tempsteps` and ending with `tempfinal`. The case $T = 0$ is not simulated automatically. If one is interested in the zero-temperature configuration (e.g. for systems with strayfield interaction), one has to set `tempfinal = 0`. The averaging procedure starts after the number of MC steps specified by the value `start`. Running averages are saved every `savemag`. If `writemagconfig = 1`, the magnetization configuration is saved every `savemag` in a format readable by `MicroAVS`.

```
# 0 = open bound. cond., 1 = periodic bound. cond.       #
pbc = 1
# 0 = no dipole interaction                              #
dipolefield = 0
# 1 = spins parallel z-axis, 0 = random spin directions  #
coldstart = 1
# 0 = simple cubic, 1 = bcc, 2 = fcc                     #
structure = 2
# Spontaneous polarization in [T]                        #
Js = 1.0
# exchange constant in [J/m]                             #
exchangeconstant = 1e-12
# Anisotropy constant in [J/m^3]                         #
K = 1e5
# lattice constant of CUBIC unit cell, in [m]            #
a = 3e-10
# B field VALUE in [T]                                   #
Bfield = 0.1
# B DIRECTION in cartesian coordinates                   #
Bextx = 0.0
Bexty = 0.0
Bextz = 1.0
# tempinitial = 0 K, but not calculated automatically    #
tempfinal = 10.0
tempsteps = 1
# n^3*anzMonte = total number of trial steps             #
anzMonte = 110000
# start averaging after # Monte steps                    #
start = 10000
# save magn. configuration and averages every savemag    #
savemag = 1000
# 1 = write magnetization configuration every savemag    #
writemagconfig = 0
```

Table D.1: Initialization file `parameter.ini`.

List of Figures

1.1 Number of atoms in the computational cell and the required spontaneous magnetization for micromagnetic simulations as function of the discretization length. 16
1.2 Illustration of the coarse-graining procedure. 17

5.1 Transition probability for the heat bath algorithm. 47
5.2 Trial step in the heat bath algorithm. 49
5.3 Comparison between adaptive cone method and completely random trial steps. 51

6.1 Illustration of the LLG equation 54

7.1 Magnetization parallel to the external field axis as a function of the discretization length Δx at $T = 300$ K without strayfield interaction. 72
7.2 Comparison of $\langle M_z \rangle$ as a function of Δx between stochastic LLG simulations with and without strayfield interaction at $T = 300$ K. 73

8.1 Setup of the atomistic MC simulations. 78
8.2 $\langle M_z \rangle$ as function of the averaging cube size Δx. 79
8.3 Spontaneous magnetization $M_{\mathrm{S,cell}}$ as function of the averaging cell size Δx for different temperatures. 80
8.4 Central non-atomistic magnetic moment. 82
8.5 $\langle M_z \rangle$ with and without cell size corrections for $T/T_{\mathrm{C}}^{\mathrm{mf}} = 0.34$. . 83
8.6 A_{cell} as function of Δx for $T/T_{\mathrm{C}}^{\mathrm{mf}} = 0.34$. 84

8.7 Comparison between the cell size dependent prefactor $(l_{\text{exch,cell}}/\Delta x)^2$ of $\boldsymbol{H}_{\text{exch}}$ and $1/\Delta x^2$. 85

9.1 Setup of switching simulations. 88
9.2 Switching times as a function of the computational cell size Δx at $T = 300$ K and without dipole interaction. 89
9.3 Switching times as a function of the computational cell size Δx at $T = 300$ K and with dipole interaction. 90

10.1 Body-centered cubic Bravais lattice. 92
10.2 Face-centered cubic Bravais lattice. 93
10.3 Spontaneous magnetization as function of $\Delta x/a$ for bcc and fcc materials. 95
10.4 Normalized spontaneous magnetization as function of the averaging cell size $\Delta x/\Delta x_{\text{at}}$ for bcc and fcc materials. 96
10.5 $\langle M_z \rangle$ versus discretization length Δx, with and without cell size corrections for α-Fe at $T = 300$ K. 97

List of Tables

8.1 Mean value $\langle M_z \rangle$ and spontaneous magnetization for large cells, $M_{\mathrm{S},\infty}$, for different temperatures. 81

10.1 Results of atomistic MC simulations for bcc (α-Fe) and fcc (Ni) materials. 95

C.1 Results for a single magnetic moment in an external field. 104
C.2 Results for a Stoner-Wohlfarth particle in an external field. . . . 105
C.3 Results for exchange coupled spins in an external field obtained via atomistic MC simulations. 106

D.1 Initialization file `parameter.ini`. 109

Bibliography

[1] A. Aharoni, "Magnetostatic Energy Calculations," *IEEE Trans. Magn.*, vol. 27, no. 4, pp. 3539–3547, 1991.

[2] A. Aharoni, *Introduction to the Theory of Ferromagnetism.* New York: Oxford University Press, 1996.

[3] N.W. Ashcroft and N.D. Mermin, *Solid State Physics.* Philadelphia: Saunders College, 1976.

[4] S. Batra, W. Scholz, and T. Roscamp, "Effect of thermal fluctuation field on the noise performance of a perpendicular recording system," *J. Appl. Phys.*, 2005, submitted.

[5] D.V. Berkov and N.L. Gorn, "Micromagnetic simulations using Langevin dynamics studying thermal field correlations," *J. Magn. Magn. Mat.*, vol. 267, pp. 687–689, 2004.

[6] D.V. Berkov and N.L. Gorn, "Transition from the macrospin to chaotic behavior by a spin-torque driven magnetization precession of a square nanoelement," *Phys. Rev. B*, vol. 71, pp. 052403–1–4, 2005.

[7] D.V. Berkov and N.L. Gorn, "Stochastic dynamic simulations of fast remagnetization processes: recent advances and applications," *J. Magn. Magn. Mat.*, vol. 290-291, pp. 442–448, 2005.

[8] G. Bertotti, *Hysteresis in Magnetism.* New York: Academic Press, 1998.

[9] K. Binder, *Monte Carlo Methods in Statistical Physics*. Berlin, Heidelberg: Springer, 1979.

[10] K. Binder and D. Stauffer, *Applications of the Monte Carlo Method in Statistical Physics*, Berlin, Heidelberg: Springer, 1984.

[11] W.F. Brown, Jr., *Micromagnetics*. New York: Interscience, 1963.

[12] W.F. Brown, Jr., "Thermal Fluctuations of a Single-Domain Particle," *Phys. Rev.*, vol. 130, no. 5, pp. 1677–1686, 1963.

[13] S.H. Charap, P.-L. Lu, Y. He, "Thermal stability of recorded information at high densities," *IEEE Trans. Magn.*, vol. 33, no. 1, pp. 978–983, 1997.

[14] O. Chubykalo, U. Nowak, R. Smirnov-Rueda, M.A. Wongsam, R.W. Chantrell, J.M. Gonzalez, "Monte Carlo technique with a quantified time step: Application to the motion of magnetic moments," *Phys. Rev. B*, vol. 67, p. 64422–1–10, 2003.

[15] O. Chubykalo, R. Smirnov-Rueda, J.M. Gonzalez, M.A. Wongsam, R.W. Chantrell, U. Nowak, "Brownian dynamics approach to interacting magnetic moments," *J. Magn. Magn. Mat.*, vol. 266, pp. 28–35, 2003.

[16] W.T. Coffey, Yu.P. Kalmykov, J.T. Waldron, *The Langevin Equation*. Singapore: World Scientific Publishing, 1996.

[17] M.D.O. de Meo and S.K. Oh, "Wolff algorithm and anisotropic continuous-spin models: An application to the spin-van der Waals model," *Phys. Rev. B*, vol. 46, pp. 257–260, 1992.

[18] V.V. Dobrovitski, M.I. Katsnelson, B.N. Harmon, "Statistical coarse-graining as an approach to multiscale problems in magnetism," *J. Magn. Magn. Mat.*, vol. 221, pp. L235–L242, 2000.

[19] V.V. Dobrovitski, M.I. Katsnelson, and B.N. Harmon, "Length Scale Coupling for Nonlinear Dynamical Problems in Magnetism," *Phys. Rev. Lett.*, vol. 90, no. 6, pp. 067201–1–4, 2003.

[20] M.J. Donahue and R.D. McMichael, “Exchange energy representations in computational micromagnetics,” *Physica B: Condensed Matter*, vol. 233, pp. 272–278, 1997.

[21] X. Feng and P.B. Visscher, “Coarse-graining Landau-Lifshitz damping,” *J. Appl. Phys.*, vol. 89, no. 11, pp. 6988–6990, 2001.

[22] D.R. Fredkin, W. Chen, and T.R. Koehler, “Hysteresis in random collections of isotropic interacting particles,” *IEEE Trans. Magn.*, vol. 28, no. 5, pp. 2380–2381, 1992.

[23] E.E. Fullerton, D.T. Margulies, M.E. Schabes, M. Carey, B. Gurney, A. Moser, M. Best, G. Zeltzer, K. Rubin, H. Rosen, M. Doerner, “Antiferromagnetically coupled magnetic media layers for thermally stable high-density recording,” *Appl. Phys. Lett.*, vol. 77, pp. 3806–3808, 2000.

[24] J.L. García-Palacios and F.J. Lázaro, “Langevin-dynamics study of the dynamical properties of small magnetic particles,” *Phys. Rev. B*, vol. 58, no. 22, pp. 14937–14958, 1998.

[25] C.W. Gardiner, *Handbook of Stochastic Methods.* Berlin, Heidelberg: Springer, 2nd ed., 1985.

[26] T.L. Gilbert, Armour Research Foundation Project, Project No. A059, Supplementary Report, 1956.

[27] G. Grinstein and R.H. Koch, “Coarse Graining in Micromagnetics,” *Phys. Rev. Lett.*, vol. 90, no. 20, pp. 207201–1–4, 2003.

[28] K.-H. Hellwege, *Einführung in die Festkörperphysik.* Berlin, Heidelberg: Springer, 1976.

[29] D.W. Heermann, *Computer Simulation Methods in Theoretical Physics.* Berlin, Heidelberg: Springer, 1986.

[30] O. Heinonen and H.S. Cho, “Thermal Magnetic Noise in Tunneling Readers,” *IEEE Trans. Magn.*, vol. 40, no. 4, pp. 2227–2232, 2004.

[31] D. Hinzke and U. Nowak, “Magnetic relaxation in a classical spin chain,” *Phys. Rev. B*, vol. 61, no. 10, pp. 6734–6740, 2000.

[32] Hitachi Global Storage, “Technology Announcement,” 2005.
URL: `http://www.hitachigst.com/hdd/research/recording_head/pr/index.html`.

[33] T. Holstein and H. Primakoff, “Field Dependence of the Intrinsic Domain Magnetization of a Ferromagnet,” *Phys. Rev.*, vol. 58, pp. 1098–1113, 1940.

[34] A. Hubert and R. Schäfer, *Magnetic Domains: The Analysis of Magnetic Microstructures.* Berlin, Heidelberg: Springer, 1998.

[35] M. Igarashi, M. Hara, Y. Suzuki, A. Nakamura, and Y. Sugita, “Computer Simulation of Coercive Force and Thermal Viscosity in Perpendicular Recording Media,” *IEEE Trans. Magn.*, vol. 39, no. 5, pp. 2303–2305, 2003.

[36] H. Kronmüller, “Magnetische Eigenschaften fester Körper,” lecture notes, Inst. f. Theoretische u. Angewandte Physik der Universität Stuttgart und Inst. f. Physik am Max-Planck-Institut f. Metallforschung, 1988.

[37] H. Kronmüller and M. Fähnle, *Micromagnetism and the Microstructure of Ferromagnetic Solids.* Cambridge: University Press, 2003.

[38] D.P. Landau and K. Binder, *A Guide to Monte Carlo Simulations in Statistical Physics.* Cambridge: University Press, 2000.

[39] L. Landau and E. Lifshitz, “On the theory of magnetic permeability in ferromagnetic bodies,” *Phys. Z. Sowjetunion*, vol. 8, p. 153, 1935.

[40] A. Lyberatos, D.V. Berkov, and R.W. Chantrell, "A method for the numerical simulation of the thermal magnetization fluctuations in micromagnetics," *J. Phys.: Condens. Matters*, vol. 5, pp. 8911–8920, 1993.

[41] E. Martínez, L. López-Díaz, L. Torres, O. Alejos, "Temperature Dependence of Spontaneous Magnetization Using a Continuous Model," *IEEE Trans. Magn.*, vol. 39, no. 5, pp. 2522–2524, 2003.

[42] E. Martínez, L. López-Díaz, L. Torres, O. Alejos, "On the interpretations of Langevin stochastic equation in different coordinate systems," *Physica B: Condensed Matter*, vol. 343, pp. 252–256, 2004.

[43] N. Metropolis, A.W. Rosenbluth, M.N. Rosenbluth, A.H. Teller, and E. Teller, "Equation of State Calculations by Fast Computing Machines," *J. Chem. Phys.*, vol. 21, no. 6, pp. 1087–1092, 1953.

[44] P. Mohn, *Magnetism in the Solid State, An Introduction.* Berlin: Springer, 2002.

[45] B. Özyilmaz, A.D. Kent, D. Monsma, J.Z. Sun, M.J. Rooks, and R.H. Koch, "Current-Induced Magnetization Reversal in High Magnetic Fields in Co/Cu/Co Nanopillars," *Phys. Rev. Lett.*, vol. 91, pp. 067203–1–4, 2003.

[46] W.B. Pearson, *Handbook of Lattice Spacings and Structures of Metals and Alloys – 2.* Oxford: Pergamon Press, 1967.

[47] W. Rave, K. Ramstöck, A. Hubert, "Corners and nucleation in micromagnetics," *J. Magn. Magn. Mat.*, vol. 183, pp. 329–333, 1998.

[48] H. Risken, *The Fokker-Planck Equation.* Berlin, Heidelberg: Springer, 2nd ed., 1989.

[49] M.E. Schabes and A. Aharoni, "Magnetostatic Interaction Fields for a Three-Dimensional Array of Ferromagnetic Cubes," *IEEE Trans. Magn.*, vol. MAG-23, no. 6, pp. 3882–3888, 1987.

[50] M.E. Schabes and H.N. Bertram,"Magnetization processes in ferromagnetic cubes," *J. Appl. Phys.*, vol. 64, no. 3, pp. 1347–1357, 1988.

[51] W. Scholz, "Micromagnetic Simulation of Thermally Activated Switching in Fine Particles," Diplomarbeit, TU Wien, 1999.
URL: `http://magnet.atp.tuwien.ac.at/scholz/`.

[52] W. Scholz, *Scalable Parallel Micromagnetic Solvers for Magnetic Nanostructures*. Dissertation, TU Wien, 2003.
URL: `http://magnet.atp.tuwien.ac.at/scholz/`.

[53] W. Scholz, S. Batra, "Micromagnetic Simulation of Head Field and Write Bubble Dynamics in Perpendicular Recording," *IEEE Trans. Magn.*, 2005, submitted.

[54] W. Scholz, T. Schrefl, J. Fidler, "Micromagnetic simulation of thermally activated switching in fine particles," *J. Magn. Magn. Mat.*, vol. 233, pp. 296–304, 2001.

[55] P.A. Serena, N. García, and A. Levanyuk, "Monte Carlo calculations on the two-dimensional anisotropic Heisenberg model," *Phys. Rev. B*, vol. 47, no. 9, pp. 5027–5036, 1993.

[56] N. Smith and P. Arnett, "Thermal Magnetization Noise in Spin Valves," *IEEE Trans. Magn.*, vol. 38, no. 1, pp. 32–37, 2002.

[57] V. Tsiantos, W. Scholz, D. Suess, T. Schrefl, J. Fidler , "The effect of the cell size in Langevin micromagnetic simulations," *J. Magn. Magn. Mat.*, vol. 242–245, pp. 999-1001, 2002.

[58] J.-S. Wang, "Clusters in the three-dimensional Ising model with a magnetic field," *Physica A*, vol. 161, no. 2, pp. 249–268, 1989.

[59] X. Wang, H.N. Bertram, E. Boerner, A. Lyberatos, and V.L. Safonov, "Thermal Decay of Interacting Grains in Perpendicular Thin-Film Media," *IEEE Trans. Magn.*, vol. 38, no. 5, pp. 2084–2086, 2002.

[60] M.C. Wang and G.E. Uhlenbeck, "On the Theory of the Brownian Motion II," *Rev. Mod. Phys.*, vol. 17, no. 2 and 3, pp. 323–342, 1945.

[61] D. Weller and A. Moser, "Thermal Effect Limits in Ultrahigh-Density Magnetic Recording," *IEEE Trans. Magn.*, vol. 35, no. 6, pp. 4423–4439, 1999.

[62] U. Wolff, "Collective Monte Carlo Updating for Spin Systems," *Phys. Rev. Lett.*, vol. 62, no. 4, pp. 361–364, 1989.

[63] J.G. Zhu, "Thermal magnetic noise and spectra in spin valve heads," *J. Appl. Phys.*, vol. 91, no. 10, pp. 7273–7275, 2002.

Presentations and Publications

In the following, oral and poster presentations are listed in chronological order. Together with the other members of the working group, numerous joint papers have been published. They are given at the end of this chapter, ordered by the year of publication.

Talks

[1] M. Kirschner, "Micromagnetic calculations of bias field and coercivity of compensated F/AF bilayers," Vienna University of Technology, Institute of Solid State Physics, November 20, 2002, Vienna, Austria.

[2] M. Kirschner, D. Suess, T. Schrefl, J. Fidler, R.L. Stamps, and J.V. Kim, "Exchange bias and training effect in polycrystalline antiferromagnetic/ferromagnetic bilayers," MRS Fall Meeting 2002, December 2-6, 2002, Boston, MA, USA.

[3] M. Kirschner, T. Schrefl, W. Scholz, and D. Suess, "Scaling relations in nonzero-temperature micromagnetics," 9th Joint MMM-Intermag Conference, January 5-9, 2004, Anaheim, CA, USA.

[4] M. Kirschner and F. Dorfbauer, "Vom Magnetkompass zum Terabitspeicher," Scienceweek Vienna, May 8-16, 2004, Vienna, Austria.

[5] M. Kirschner, T. Schrefl, F. Dorfbauer, G. Hrkac, D. Suess, and J. Fidler, "Cell size corrections for nonzero-temperature micromagnetics," 49th

Annual Conference on Magnetism and Magnetic Materials (MMM'04), November 7-11, 2004, Jacksonville, FL, USA.

[6] M. Kirschner, T. Schrefl, G. Hrkac, F. Dorfbauer, D. Suess, and J. Fidler, "Relaxation Times and Cell Size in Nonzero-temperature Micromagnetics," 5th International Symposium on Hysteresis and Micromagnetic Modelling (HMM-2005), May 30 - June 1, 2005, Budapest, Hungary.

[7] M. Kirschner, "Simulation magnetischer Datenspeicherung," University of Veterinary Medicine Vienna, Movement Science Group, November 22, 2005, Vienna, Austria.

[8] M. Kirschner, T. Schrefl, F. Dorfbauer, D. Suess, G. Hrkac, and J. Fidler, "Micromagnetic coarse-graining for different crystal structures," 7th Latin American Workshop on Magnetism, Magnetic Materials and their Applications (LAW3M05), December 12-16, 2005, Reñaca, Chile.

Posters

[1] M. Kirschner, D. Suess, T. Schrefl, J. Fidler, and J.N. Chapman, "Micromagnetic Calculation of Bias Field and Coercivity of Exchange Biased IrMn/NiFe Bilayers," Intermag 2003, March 28 - April 3, 2003, Boston, MA, USA.

[2] M. Kirschner, F. Dorfbauer, G. Hrkac, O. Ertl, P. Speckmayr, T. Schrefl, and D. Suess, "Vom Magnetkompass zum Terabitspeicher – Simulation magnetischer Datenspeicherung," Scienceweek Vienna, May 8-16, 2004, Vienna, Austria.

[3] M. Kirschner, T. Schrefl, F. Dorfbauer, G. Hrkac, D. Suess, and J. Fidler, "Cell size dependencies in nonzero-temperature micromagnetics," Ultrabias Summer School 2004, September 12-16, 2004, Anglet, France.

[4] M. Kirschner, T. Schrefl, F. Dorfbauer, G. Hrkac, D. Suess, and J. Fidler, “Cell size dependencies of relaxation times in nonzero-temperature micromagnetics,” Spring School on Nanomagnetism and Spintronics, May 23 - June 4, 2005, Cargèse, Corsica.

Publications

[1] M. Kirschner, D. Suess, T. Schrefl, J. Fidler, and J.N. Chapman, “Micromagnetic calculation of bias field and coercivity of polycrystalline ferromagnetic/antiferromagnetic layers,” *IEEE Trans. Magn.*, vol. 39, no. 5, pp. 2735–2737, 2003.

[2] D. Suess, M. Kirschner, T. Schrefl, J. Fidler, R.L. Stamps, and J.V. Kim, “Exchange bias of polycrystalline antiferromagnets with perfectly compensated interface,” *Phys. Rev. B*, vol. 67, pp. 54419–1–8, 2003.

[3] D. Suess, M. Kirschner, T. Schrefl, W. Scholz, R. Dittrich, H. Forster, and J. Fidler, “Micromagnetic calculations of bias field and coercivity of compensated ferromagnetic/antiferromagnetic bilayers,” *J. Appl. Phys.*, vol. 93, pp. 8618–8620, 2003.

[4] M. Kirschner, D. Suess, T. Schrefl, J. Fidler, R.L. Stamps, and J.V. Kim, “Exchange bias and training effect in polycrystalline antiferromagnetic/ferromagnetic bilayers,” in *Magnetoelectronics and Magnetic Materials – Novel Phenomena and Advanced Characterization* (S. Zhang, G. Guntherodt, A. Kent, I. Schuller, and T. Shinjo, eds.), MRS proceedings vol. 746, pp. 25–30, 2003.

[5] J. Fidler, T. Schrefl, W. Scholz, D. Suess, R. Dittrich, and M. Kirschner, “Micromagnetic modelling and magnetization processes,” *J. Magn. Magn. Mater.*, vol. 272-276, pp. 641–646, 2004.

[6] J. Fidler, T. Schrefl, W. Scholz, D. Suess, V.D. Tsiantos, R. Dittrich, and

M. Kirschner, “Magnetostatic spin waves in nanoelements,” *Physica B: Condensed Matter*, vol. 343, pp. 200–205, 2004.

[7] G. Hrkac, M. Kirschner, F. Dorfbauer, D. Suess, O. Ertl, J. Fidler, and T. Schrefl, “Three-dimensional micromagnetic finite element simulations including eddy currents,” *J. Appl. Phys*, vol. 97, no. 10, pp. 10E311–1–3, 2005.

[8] M. Kirschner, T. Schrefl, F. Dorfbauer, G. Hrkac, D. Suess, and J. Fidler, “Cell size corrections for nonzero-temperature micromagnetics,” *J. Appl. Phys.*, vol. 97, pp. 10E301–1–3, 2005.

[9] R. Dittrich, T. Schrefl, M. Kirschner, D. Suess, G. Hrkac, F. Dorfbauer, O. Ertl, and J. Fidler, “Thermally Induced Vortex Nucleation in Permalloy Elements,” *IEEE Trans. Magn.*, vol. 41, no. 10, pp. 3592–3594 , 2005.

[10] G. Hrkac, T. Schrefl, O. Ertl, D. Suess, M. Kirschner, F. Dorfbauer, and J. Fidler, “Influence of Eddy Current on Magnetization Processes in Submicrometer Permalloy Structures,” *IEEE Trans. Mag.*, vol. 41, no. 10, pp. 3097–3099, 2005.

[11] T. Schrefl, M.E. Schabes, D. Suess, O. Ertl, M. Kirschner, F. Dorfbauer, G. Hrkac, and J. Fidler, “Partitioning of the Perpendicular Write Field Into Head and SUL Contributions,” *IEEE Trans. Magn.*, vol. 41, no. 10, pp. 3064–3066, 2005.

[12] D. Suess, T. Schrefl, M. Kirschner, G. Hrkac, F. Dorfbauer, O. Ertl, and J. Fidler, “Optimization of Exchange Spring Perpendicular Recording Media,” *IEEE Trans. Magn.*, vol. 41, no. 10, pp. 3166–3168 , 2005.

[13] F. Dorfbauer, T. Schrefl, D. Suess, M. Kirschner, G. Hrkac, and J. Fidler, “Pulsed Inductive Microwave Magnetometer Response Calculated for IrMn/FeNi Bilayers,” *Eur. Phys. J. B*, vol. 45, pp. 267–271, 2005.

[14] F. Dorfbauer, D. Suess, J. McCord, M. Kirschner, T. Schrefl, and J. Fidler, “Micromagnetic simulation of asymmetric magnetization reversal in exchange biased bilayers,” *J. Magn. Magn. Mater.*, vol. 290-291, pp. 754–757, 2005.

[15] D. Suess, T. Schrefl, R. Dittrich, M. Kirschner, F. Dorfbauer, G. Hrkac, and J. Fidler, “Exchange spring recording media for areal densities up to 10 Tbit/in^2,” *J. Magn. Magn. Mat.*, vol. 290-291, pp. 551–554, 2005.

[16] D. Suess, T. Schrefl, S. Fahler, M. Kirschner, G. Hrkac, F. Dorfbauer, and J. Fidler, “Exchange spring media for perpendicular recording,” *Appl. Phys. Lett.*, vol. 87, no. 1, pp. 12504–1–3, 2005.

[17] M. Kirschner, T. Schrefl, G. Hrkac, F. Dorfbauer, D. Suess, and J. Fidler, “Relaxation times and cell size in nonzero-temperature micromagnetics,” *Physica B: Condensed Matter*, 2005, in press.

[18] J. Fidler, T. Schrefl, D. Suess, O. Ertl, M. Kirschner, and G. Hrkac, “Full micromagnetics of recording on patterned media,” *Physica B: Condensed Matter*, 2005, in press.

[19] F. Dorfbauer, T. Schrefl, M. Kirschner, G. Hrkac, D. Suess, O. Ertl, and J. Fidler, “Nano-structure calculation of CoAg core-shell clusters,” *J. Appl. Phys.*, 2005, accepted.

[20] O. Ertl, G. Hrkac, D. Suess, M. Kirschner, F. Dorfbauer, J. Fidler, and T. Schrefl, “Multiscale micromagnetic simulation of GMR read heads,” *J. Appl. Phys.*, 2005, to be published.

Curriculum Vitæ

Markus Kirschner
Angergasse 61
A-7123 Mönchhof

Born	February 22, 1975 in Mönchhof, Austria
Parents	Annemarie and Josef Kirschner
Nationality	Austrian

1981 – 1985	Elementary school in Mönchhof
1985 – 1989	Secondary school in Gols
1989 – 1994	Institution of higher education for precision engineering in Mödling, graduation with excellence
1994 – 1995	Military service in Bruckneudorf
Oct. 1995 – March 2003	Studying physics at the Vienna University of Technology
March 2003	Graduation with excellence
since April 2003	Researcher in the working group of Prof. T. Schrefl and Prof. J. Fidler, working on dissertation

Lebenslauf

Markus Kirschner
Angergasse 61
A-7123 Mönchhof

Geboren am	22. Februar 1975 in Mönchhof, Österreich
Eltern	Annemarie und Josef Kirschner
Staatsbürgerschaft	Österreich

1981 – 1985	Volksschule in Mönchhof
1985 – 1989	Hauptschule in Gols
1989 – 1994	HTL für Feinwerktechnik in Mödling, Matura mit Auszeichnung bestanden
1994 – 1995	Präsenzdienst in Bruckneudorf
Okt. 1995 – März 2003	Studium der Technischen Physik an der Technischen Universität Wien
Februar 2003	Einreichung der Diplomarbeit
März 2003	2. Diplomprüfung mit Auszeichnung bestanden
seit April 2003	Wissenschaftlicher Mitarbeiter in der Arbeitsgruppe von Prof. T. Schrefl und Prof. J. Fidler, Doktoratsstudium an der Technischen Universität Wien